EPSC2018

EXO1 abstracts

EPSC Abstracts
Vol. 12, EPSC2018-23, 2018
European Planetary Science Congress 2018

Exoplanet Characterisation: threshold radii for water-worlds and Neptune-like planets

Michael Lozovsky (1), Ravit Helled (1), Caroline Dorn (1) and Julia Venturini (1)
(1) Center for Theoretical Astrophysics & Cosmology, Institute for Computational Science, University of Zurich, Zurich, Switzerland

Abstract

Upcoming space missions such as CHEOPS, TESS, and PLATO will bring exoplanetary characterisation to the next level with the aim of constraining the planetary composition.

We present a statistical analysis to determine the threshold radii for various compositions of exoplanets with masses up to 20 Earth masses. First, we confirm that most planets with radii larger than 1.6 Earth radius ($R_\oplus$) are not rocky, and must consist of lighter elements, as found by previous studies. We suggest that planets with radii larger than 2.6 $R_\oplus$ cannot be pure-water worlds, and must have atmospheres, presumably, of hydrogen and helium (H-He). We suggest that the threshold from Earth-analogs to Neptune-analogs occurs at ~ 3 $R_\oplus$. We also discuss and present the sensitivity of the results to the assumed envelope's metallicity, the distribution of the elements, the planetary temperature and albedo, and the accuracy of the mass and radius measurement.

EPSC Abstracts
Vol. 12, EPSC2018-93, 2018
European Planetary Science Congress 2018

Interior characterization in multiplanetary systems: Trappist-1

Caroline Dorn (1), Klaus Mosegaard (2) and Simon Grimm (3)
(1) University of Zurich, Institut of Computational Sciences, Switzerland (2) Niels-Bohr-Institute, Copenhagen, Danmark, (3) University of Bern, Center for Space and Habitability, Switzerland

Abstract

There are available data specific to multi-planetary systems which have not yet been considered for interior characterization of planetary interiors. For Trappist, the specific data are the correlations of masses between different planets as derived from TTV analysis. Furthermore, we demonstrate that the rocky interior of planets in a multi-planetary can be preferentially probed by studying the most dense planet being an analogue for a rock-dominated interior.
Our methodology includes a Bayesian inference analysis that uses a Markov chain Monte Carlo scheme. In addition, we develop a new resampling method that allows us to account for the correlations of masses between different planets.

For the interiors of Trappist-1 planets, we find that possible water mass fractions generally range from 0-25%. No clear trends in the amount of water and orbital period are observed. Our results suggest that planetary water budgets originate from the accretion of material with limited bulk volatile content (below 30 %) and from fairly well-mixed regions in the protoplanetary disk that blurred any trend of increasing volatile fraction with orbital period.

1. Introduction

The Trappist-1 planets do not follow a single mass-radius trend, but there is some scatter among the bulk densities of planets. Previously characterized by [4], the most recent and more precise mass and density estimates from [5] provide new insights into the planet bulk compositions. They find that purely rocky interiors are likely for planets c and e, while planets b, d, f, g, and h require envelopes of volatiles. The outer planets f–h have cold enough equilibrium temperatures such that common volatile species CO_2 and H_2O are condensed out. The high bulk density and temperature conditions of planet e may allow for Earth-like surface conditions.

The volatile layers are unlikely to be hydrogen-dominated, since their lifetimes are limited by the large EUV irradiation [1], which is supported by transit spectroscopic observations [3]. Thus, previous atmospheric investigations strongly suggest the presence of terrestrial-type atmospheres.

Here, we quantify the origin of the scatter in bulk densities of the planets and investigate the value of different data types for an improved interior characterization.

2. Method

We employ a Bayesian inference analysis that uses a Markov chain Monte Carlo scheme. In addition, we develop a new resampling method that allows us to account for the correlations of masses between different planets.

Our interior estimates account for the anticipated variability in the compositions and layer thicknesses of a pure iron core, a silicate mantle of general composition, pure-water ice and ocean layers, and terrestrial-type atmospheres, and thermal state of the planets.

The data comprise planetary masses and radii and their correlations, stellar irradiation, and different abundance proxies (i.e., no proxy, a stellar proxy, a proxy based on the most dense planet of the system). In addition, we account for the correlation between the masses of different planets, which has not been consiedered in previous characterization studies.

3. Results

Our results show that there are significant influences on interior estimates given (1) different abundance proxies on rock-forming elements and (2) the correlations of masses between different planets. In comparison, observational uncertainties on mass and radius have only limited influence on interior estimates.

Different abundance proxies can lead to differences in the median predicted water mass fraction that range

from 25% up to 50%. This is because different proxies allow differently dense rocky interiors, which affect the amounts of possible water in order to fit mass and radius.

The improvements gained by accounting for the correlations of masses between different planets are large. For planets b, c, e and h thay vary between 50-70 %, while they range from 0-30% for d, f, and g. The level of improvements depend on the abundance proxies and how compatible they are with the individual measured masses and radii of the planets.

In Figure 1, we show a summary of predicted water mass fractions for all planet that account for the anticipated variability in structure and composition of Super-Earths. For the shown Figure, water mass fractions range up to 20-30% for b and d. Lowest values are found for planet e, but also c and h with few percents of water mass fractions.

There is no clear trend of increasing water mass fraction with orbital period which can be explained with mixing of planetesimals from ice-rich and ice-poor regions of a disk. The fact that the Trappist-1 planets are much more volatile-rich compared to the terrestrial Solar System planets is in line with predictions from planet formation [6].

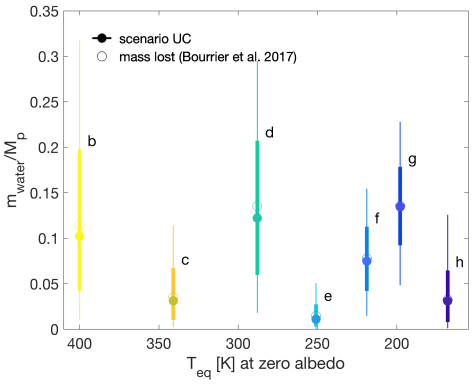

Figure 1: Marginalized water mass fractions as a function of equilibrium temperature T_{eq} (at zero albedo). No obvious trend of increasing water mass fraction with larger orbital distance and thus cooler T_{eq}. For the water mass fractions, the 3th-16th-84th-97th-percentiles are depicted by the thin and thick error bars. How much water mass fraction there could have been after formation (open circles) is calculated by adding the amount of possibly lost water [2] to our inferred median estimates (filled circles).

4. Summary and Conclusions

Trappist-1 planets are not scale-up analogs of each other but have variable bulk densities. Here, we have quantified the origin of this variability, that is mostly due to different amounts of water, but also to some extent the sizes of rocky interiors and the thicknesses of gas envelopes. There is no clear trend of volatile fraction with orbital period. This suggests that accreted planetesimals were sufficiently mixed such as to blur otherwise expected increases of water fraction with distance from the star.

With our study on Trappist-1, we have explored the data types that are specific to multi-planetary systems. Such data will be relevant for the interior characterization of planets in other systems as well, for which our study provides new pathways for an improved interior characterization.

Acknowledgements

This work was supported by the Swiss National Foundation under grant PZ00P2_174028. It was in part carried out within the frame of the National Centre for Competence in Research PlanetS.

References

[1] Bolmont, E., Selsis, F., Owen, J.E., Ribas, I., Raymond, S.N., Leconte, J. and Gillon, M., 2016. MNRAS, 464(3), pp.3728-3741.

[2] Bourrier, V., Ehrenreich, D., Wheatley, P.J., Bolmont, E., Gillon, M., de Wit, J., Burgasser, A.J., Jehin, E., Queloz, D. and Triaud, A.H.M.J., 2017. A& A, 599, p.L3.

[3] de Wit, J., Wakeford, H.R., Lewis, N.K., Delrez, L., Gillon, M., Selsis, F., Leconte, J., Demory, B.O., Bolmont, E., Bourrier, V. and Burgasser, A.J., 2018. Nature Astronomy, 2(3), p.214.

[4] Gillon, M., Triaud, A.H., Demory, B.O., Jehin, E., Agol, E., Deck, K.M., Lederer, S.M., De Wit, J., Burdanov, A., Ingalls, J.G. and Bolmont, E., 2017. Nature, 542(7642), p.456.

[5] Grimm, S.L., Demory, B.O., Gillon, M., Dorn, C., Agol, E., Burdanov, A., Delrez, L., Sestovic, M., Triaud, A.H., Turbet, M. and Bolmont, É., 2018. arXiv preprint arXiv:1802.01377.

[6] Alibert, Y. and Benz, W., 2017. A & A, 598, p.L5.

EPSC Abstracts
Vol. 12, EPSC2018-107-2, 2018
European Planetary Science Congress 2018

Optical indices of organic aerosols for oxidizing atmospheres of Earth-like exoplanets

Lisseth Gavilan (1), Laurent Broch (2), **Nathalie Carrasco** (1), Benjamin Fleury (3), and Ludovic Vettier (1)
(1) LATMOS, Université Versailles St Quentin, UPMC Université Paris 06, CNRS, France, (2) LCP-A2MC, Institut Jean Barriol, Université de Lorraine, France, (3) Jet Propulsion Laboratory, California Institute of Technology, USA (lisseth.gavilan@gmail.com and nathalie.carrasco@uvsq.fr)

Abstract

Photochemical haze is likely produced in most planetary atmospheres. Optical indices are required to evaluate the haze contribution to the climate of a planet. Unfortunately few experimental data exist and most of them have been measured with laboratory analogs of Titan's haze, which can only be a model scenario for totally reduced atmospheres. In the present work we study the optical indices in the UV-Vis range of analogs of planetary organic haze produced with CO_2/CH_4 ratios varying between 1 and 4 in order to provide appropriate optical indices for a large range of Earth-like oxidizing atmospheres. Oxidized analogues are found as much as four times better absorbers in the UV than the reduced ones [1].

1. Introduction

Depending on their optical properties, hazes could impact planetary habitability via UV shielding and surface cooling [2]. Due to the lack of data, models usually incorporate laboratory optical constants of analogues of hazes produced under Titan's reducing conditions.
The aim of this work is provide optical indices of oxidized organic aerosols better appropriate to provide constraints on climate models of Earth-like exoplanets.

2. Method

1.1 Preparation of the analogues

Analogues of photochemical haze are produced using the PAMPRE setup, a 13.56 MHz radiofrequency capacitively coupled plasma reactor [3]. This setup triggers complex organic chemistry mimicking ionospheric chemical conditions at room temperature. The R.F. power source is tuned at 30 W. A low pressure (0.95 mbar) is ensured in the reactor by a 55 sccm gas flow of the reactive gas mixture. Four different gas mixtures are used to simulate increasing oxidizing atmospheric conditions (Table 1). The plasma is produced within a cylindrical plasma box. Bare silicon substrates are placed on the bottom electrode. The plasma is turned on until a thin film is deposited on the substrates.

Table 1: Thickness of the organic films

N_2:CO_2:CH_4	Thickness (nm)
95:0:5	36.02 ± 0.03
90:5:5	78.80 ± 0.05
95:2.5:2.5	79.04 ± 0.04
90:8:2	26.56 ± 0.38

1.2 Analysis

We obtain the thickness (Table 1) and the optical indices by UV-Visible ellipsometry (Figure 1). The measured ellipsometric parameters result from the interaction between light and both the organic film and the Si substrate. We model a multilayer system consisting of the substrate, the organic material and a roughness layer, combining the optical constants of the organic layer and air. The organic thin film is modeled via a Tauc-Lorentz oscillator, applicable to amorphous organic films. In this model, the imaginary part of the permittivity, ε_i, is given by:

$$\varepsilon_i(E) = \begin{cases} \frac{AE_0C(E-E_g)^2}{E((E^2-E_0^2)^2+C^2E^2} , for\ E > E_g \\ 0 \qquad\qquad\qquad\qquad , for\ E \leq E_g \end{cases} \quad (1)$$

, where Eg (eV) is the optical band gap energy, Eo (eV) is the energy position of the major UV absorption peak, A(eV) is related to the strength of this peak, and C (eV) is related to its broadening. The real part of the permittivity, ε_r, is derived from ε_i using the Kramers-Kronig relations:

$$\varepsilon_r(E) = \varepsilon_r(\infty) + \frac{2}{\pi} P \int_{Eg}^{\infty} \frac{\xi \times \varepsilon_i(\xi)}{\xi^2 - E^2} d\xi \quad (2)$$

where $\varepsilon_r(\infty)$ is the high-frequency real permittivity and P is the Cauchy principal value containing the residues of the integral at the poles on the lower half of the complex plane and along the real axis. And for non-magnetic materials, the complex refractive index is : $\bar{\varepsilon} = \bar{n}^2 = (n + ik)^2$

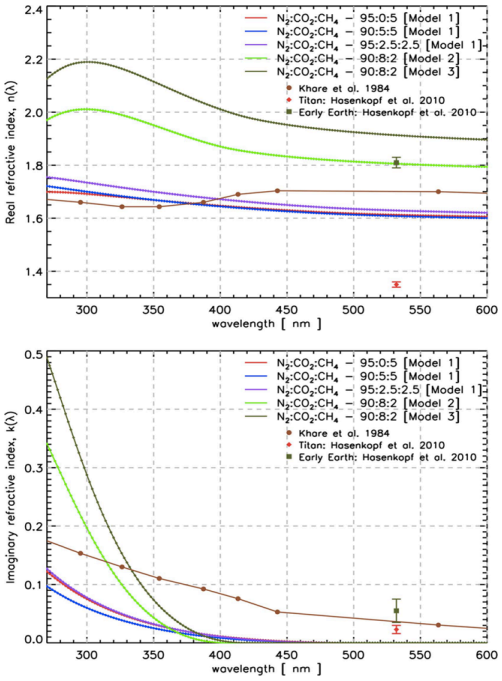

Figure 1: Refractive indices in the UV–visible (270–600 nm) for haze analogues prepared with different mixtures of N_2:CO_2:CH_4. As CO_2/CH_4 increases, the strength of the major UV absorption is significantly increased [1].

3. Summary and Conclusions

This study provides, for the first time, laboratory wavelength-dependent refractive indices of oxidized organic aerosols in the UV–visible range at increasing degrees of oxidation. The analogues produced under oxidizing conditions present a larger band gap than the reduced ones, i.e., their absorption begins in the UV rather than the visible range. Furthermore, oxidized analogues are as much as four times better absorbers in the UV than the reduced ones, at least up to the measured wavelength of 270 nm.

Such indices can be used to refine radiative transfer models of increasingly oxidizing planetary atmospheres including photochemical hazes [4].

Acknowledgements

N.C. and L.G. thank the European Research Council for funding via the ERC PrimChem project (grant agreement No. 636829.)

References

[1] Gavilan L., Broch L., Fleury B., Vettier L. and Carrasco N.: Organic Aerosols in the Presence of CO2 in the Early Earth and Exoplanets: UV–Vis Refractive Indices of Oxidized Tholins, ApJL, Vol. 848, pp. L5, 2017.

[2] Pavlov, A. A., Brown, L. L., & Kasting, J. F.: UV shielding of NH_3 and O_2 by organic hazes in the Archean atmosphere, JGR, 106, 23267, 2001.

[3] Mahjoub, A., Carrasco, N., Dahoo, P.-R., et al. Icarus, 221, 670, 2012.

[4] Forget, F., & Leconte, J.: Possible climates on terrestrial exoplanets, RSPTA, 372, 20130084, 2014.

EPSC Abstracts
Vol. 12, EPSC2018-146-1, 2018
European Planetary Science Congress 2018

Direct imaging of magma oceans in nearby young stellar associations

Irene Bonati (1,2), Tim Lichtenberg (2), Dan J. Bower (3), Miles L. Timpe (4) and Sascha P. Quanz (5)
(1) Earth-Life Science Institute, Tokyo Institute of Technology, Japan (irene.bonati@elsi.jp) (2) Institute of Geophysics, ETH Zürich, Switzerland (3) Center for Space and Habitability, University of Bern, Switzerland (4) Institute for Computational Science, University of Zurich, Switzerland (5) Institute for Particle Physics and Astrophysics, ETH Zürich, Switzerland

Abstract

During their formation and early evolution, terrestrial planets experience repeated global melting events (so-called magma oceans) from interactions with other protoplanets, similar to the Moon-forming giant impact in Earth's history. The detection and characterization of post-collisional afterglows provides direct observational constraints for theoretical models of planet formation, interior and atmospheric dynamics, as well as insights into the origin and diversification of planets in the Solar System and extrasolar systems. Here, we quantitatively assess the observational prospects to detect magma oceans in nearby young stellar associations with future direct imaging facilities. We find that probabilities of detection significantly increase when focusing on young and close stellar targets, and are highest for the β Pictoris association.

1. Introduction

With the advent of a number of imminent ground- and space-based missions, a comprehensive assessment of the potential detectability of bodies in their formation stage is desired. The present study aims to quantify the likelihood of observing magma ocean planets inside ten young stellar associations that are located within 100 pc from the Sun.

The observability of hot molten planets is strongly controlled by the coupled evolution of a magma ocean and its outgassed atmosphere. The accumulation of over-saturated volatiles within the pre-existing atmosphere exerts a thermal blanketing effect that inhibits heat radiation to space and slows down the cooling of the interior. Prolonged solidification timescales increase the probability of detection because a planet remains hotter for longer. However, the presence of dense and optically thick atmospheres can make magma ocean bodies appear less bright, thus hindering the direct observation of planetary surfaces [1].

2. Methods

The probability P_{MO} of detecting at least one magma ocean event in each of the stellar associations is calculated using

$$P_{\mathrm{MO}}(\lambda_{\mathrm{cen}}, \mathrm{d}, \tau_*, \epsilon) = 1 - \prod_{i=1}^{i=n_*} \left(1 - \frac{\bar{n}_{\mathrm{GI,i}} \cdot \Delta t_{\mathrm{obs}_{\bar{\mathrm{R}}},\mathrm{i}}}{\Delta t_{\mathrm{bin,i}}}\right), \quad (1)$$

for a given telescope filter central wavelength λ_{cen}, distance d of the stellar association from the Sun, age of the stellar sample τ_*, and planetary atmospheric emissivity ϵ. n_* is the number of stars of a given spectral type located inside a given stellar association. $\bar{n}_{\mathrm{GI,i}}$ is the number of detectable giant impacts taking place within a specified time interval of planet formation ($\Delta t_{\mathrm{bin,i}}$ = 20 Myr), which accounts for the age of the considered stellar association. $\Delta t_{\mathrm{obs}_{\bar{\mathrm{R}}},\mathrm{i}}$ indicates the time interval within which a magma ocean planet with radius $\bar{R}$ is bright enough to be detected.

The telescope parameters used for the detectability assessment are the inner working angle (IWA) and the sensitivity. A planet is considered as detectable if its angular separation exceeds the instrument's IWA, and if its total flux observed in a specific band is higher than the instrument's sensitivity. We consider two filters each for a space-based interferometer similar to the ESA Darwin concept, and ESO's ground-based Extremely Large Telescope (ELT).

We use the *N*-body code GENGA [2] to constrain the occurrence rate and timing of magma ocean-inducing impacts during terrestrial planet formation around different star types. For every collision we calculate the specific impact energy Q [3] and determine the size of the resulting post-impact body.
The thermal evolution of magma ocean planets is investigated using an energy balance model with self-consistent thermodynamics of melt and solid silicate phases [4]. We track the surface temperature evolution for various planetary sizes using two different models

for the efficiency of heat transport in the atmosphere, namely (1) a gray body, where the insulating effect of the atmosphere is parameterized using an effective emissivity ϵ , and (2) a steam atmosphere parameterization [5].

3. Results

The probabilities of detecting at least one magma ocean planet in young nearby stellar associations (calculated according to Equation 1) within an observation time of 30 hours are shown in Figure 1 for different observation strategies and planetary parameters.

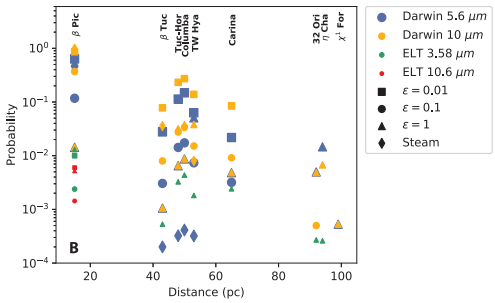

Figure 1: Probability of detecting at least one magma ocean planet in nearby stellar associations for 30 hours integration time with either the Darwin or ELT observing concepts. The colors and shapes refer to different telescope filters and planetary atmospheric emissivities, respectively.

A young stellar age translates into a high number of expected giant impacts. Therefore, the younger a stellar association and the more stars of a given type it contains, the higher the probability of detecting at least one magma ocean planet. Planets with lower emissivities are the most likely to be directly observed due to their long-lived magma oceans, but the atmosphere could be sufficiently dense to prevent the surface from being imaged at all. In contrast, a less dense atmosphere will pose less of a barrier to observing the planetary surface, but it will enable a magma ocean to cool faster, thus lowering the observation likelihood.

In general, ELT/METIS displays only low detection probabilities, even for bodies with negligible atmospheric effects (i.e. high emissivity). Contrarily, due to its higher resolution and sensitivity, a space-based interferometer similar to the ESA Darwin concept is the preferred instrument for magma ocean exploration.

The most promising stellar targets to be explored are β Pictoris, Columba, Tucana-Horologium and TW Hydrae.

4. Summary and Conclusions

Our work provides first-order predictions of the detectability of protoplanetary collision afterglows using performance estimates of next-generation direct imaging instruments, simulations of giant impact occurrence rates during planet formation around different star types, and models of magma ocean cooling for bodies of various sizes and atmospheric emissivities. Overall we find that:

- Target selection favoring young and nearby stellar associations containing a large amount of stars significantly increases the likelihood of detecting a magma ocean planet.
- For sufficiently long integration times to fully exploit the number of planetary systems, the β Pictoris association is best suited for future observations of magma ocean bodies.

These findings motivate the need for a large space-based mid-infrared interferometer alike Darwin for future explorations devoted to the study of the formation and early evolution of planetary bodies.

References

[1] Massol, H., Hamano, K., Tian, F., et al.: Formation and Evolution of Protoatmospheres, Space Sci. Rev. 205, 153–211, 2016.

[2] Grimm, S. L. and Stadel, J. G.: The GENGA code: Gravitational encounters in N-body simulations with GPU acceleration, Astrophys. J. 796, 23–39, 2014.

[3] Leinhardt, Z. M. and Stewart, S. T.: Collisions between Gravity-dominated Bodies. I. Outcome Regimes and Scaling Laws, Astrophys. J. 745, 79–106, 2012.

[4] Bower, D. J., Sanan, P. and Wolf, A. S.: Numerical solution of a non-linear conservation law applicable to the interior dynamics of partially molten planets, Phys. Earth Planet. Inter. 274, 49–62, 2018.

[5] Zahnle, K. J., Kasting, J. F. and Pollack, J. B.: Evolution of a steam atmosphere during Earth's accretion, Icarus 74, 62–97, 1988.

EPSC Abstracts
Vol. 12, EPSC2018-234, 2018
European Planetary Science Congress 2018

GAPS: Results from 5 years of observations

R. Claudi(1), S. Benatti (1), C. Boccato (1), E. Covino (2), S. Desidera (1), R. Gratton (1), A.F. Lanza (3), A. Maggio (4), G.Micela (4), E. Molinari (5), I. Pagano (3), G. Piotto (6), E. Poretti (7,8), R. Smareglia (9), A. Sozzetti (10), and the GAPS Team

(1) INAF - Astronomical Observatory of Padova (riccardo.claudi@inaf.it), (2) INAF - Astronomical Observatory of Capodimonte, (3) INAF - Astrophysical Observatory of Catania, (4) INAF - Astronomical Observatory of Palermo, (5) INAF - Astronomical Observatory of Cagliari, (6) University of Padova, Dep. of Physics and Astronomy, (7) INAF - TNG, Fundación Galileo Galilei, (8) INAF Astronomical Observatory of Brera, Italy, (9) INAF - Astronomical Observatory of Trieste; (10) INAF - Astronomical Observatory of Torino

The "Global Architecture of Planetary Systems" (GAPS) Project is the result of a collaboration among part of the Italian exoplanetary community that exploited the great capabilities of the HARPS–N instrument. It gathers more than 60 astronomers from several institutes of the Italian National Institute for Astrophysics (INAF) and Italian Universities (Padova, Torino and Milano). A technical and scientific support is also provided by a few collaborators from European and American Institutions. The main purpose of GAPS is the study and the characterization of the architectural properties of planetary systems through the radial velocity technique, by analyzing the distributions of planetary parameters and their correlations with those of the host star. The opportunity to extend our knowledge of the planetary systems will help to understand the most debated aspects of the exoplanet research, such as their formation and evolution. The GAPS observing programme started in September 2012. Since then $\sim$ 2500 observing hours were allocated and about 7000 spectra have been collected for the targets of our sample ($\sim$ 300 stars). For 16 interesting objects we have obtained 90 or more RV data points. The GAPS observations are performed with HARPS–N, the twin instrument in the northern hemisphere of HARPS at the 3.6m ESO–La Silla telescope. These two spectrographs are fiber–fed and work in the the visible range ($400 - 600$ nm) with a resolution of 114,000. They represent the state of the art for the measure of high precision radial velocities: thanks to the simultaneous calibration technique [1] and the extreme instrumental stability, ensured by a series of control systems, they can reach a RV accuracy better than 1 m s^{-1}. In the framework of the GAPS project, HARPS-N spectra are also supported by a coordinated photometric monitoring, in particular for M dwarf stars, performed through the APACHE (Astronomical Observatory of the Autonomous Region of the Aosta Valley, [2]) and EXORAP1 (Serra la Nave Observatory) surveys, from the INAF–Astrophysical Observatory of Asiago and by a number of amateur astronomers. Thanks to the wide expertise of the GAPS members (high-resolution spectroscopy, stellar activity and pulsations, crowded stellar environments, planetary systems formation, planetary dynamics, data handling) our data are carefully analyzed and discussed within the community, aiming to produce scientific results with a quality as high as possible.

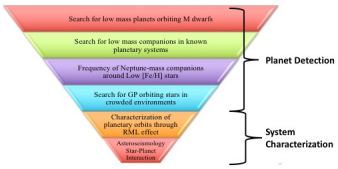

Figure 1: The scientific objectives and the six sub–programs of GAPS subdivided in the two main branches, planet detection and system characterization

We have developed robust RV data analysis tools (DE-MCMC, Gaussian processes) which are in use to analyze RV data affected by astrophysical noise and to enable the detection of very small amplitude planetary signals. These tools showed their effectiveness also in the international context, as in the "RV challenge" experiment (see [3]) and in the collaboration with the HARPS-N GTO program, allowing a preliminary mass estimate for the first transiting habitable-

zone Super-Earth (in a multiple system) around the M0 dwarf K2-3 [4]. The scientific objectives of GAPS, which are pursued by six sub-programs focused on different type of stars, can be separated into two main aspects: planet discovery and planet characterization (see Fig. 1). Several interesting results were published up to now and even more papers are in preparation or close to the submission. A number of planet candidates has been identified but in some cases we need more data for their confirmation, so we plan further observations. After five years of HARPS-N observations and analysis we have developed an optimized observing strategy and new analysis tools, in particular for those objects which require many data and specific treatment of the RV time series. Anyway, new perspectives are foreseen for GAPS, since GIARPS is now available at TNG with high impact on the exoplanetary research. In fact GIARPS will combine HARPS-N and GIANO-B, the high resolution spectrograph of TNG in the near infrared, providing simultaneous observations in the visible and in the near infrared bands, see [5]for details. The extension of the wavelength range will open to the GAPS community new scenarios and objectives in the study of the extrasolar planets.

Acknowledgements

Authors would like to thank the support by INAF through *Progetti Premiali* funding scheme of the Italian Ministry of Education, University, and Research.

References

[1] C.Lovis & D.Fischer 2010 Radial Velocity Techniques for Exoplanets pp. 27 - 53,Ed.Seager, S. University of Arizona Press Tucson, AZ.

[2] Sozzetti, A., et al. 2013 The APACHE Project, Hot Planets and Cool Stars, ed. R. Saglia, EPJ Web of Conferences 47, id. 03006.

[3] X. Dumusque 2017 Radial Velocity Fitting Challenge. I. Simulating the data set including realistic stellar radial-velocity signals, A&A, 598, 133.

[4] I. Crossfield et al. 2015 A Nearby M Star with Three Transiting Super-Earths Discovered by K2, ApJ, 804, 10.

[5] Claudi, R., Benatti, S., Carleo, I. et al. Eur. Phys. J. Plus (2017) 132: 364.

EPSC Abstracts
Vol. 12, EPSC2018-241, 2018
European Planetary Science Congress 2018

Effective induction heating inside exoplanets orbiting strongly magnetized M dwarfs

Kristina Kislyakova (1,2), Lena Noack(3), Colin Johnstone (1), Luca Fossati (2), Helmut Lammer (1), Manuel Güdel (1), and the PATH team
(1) University of Vienna, Department of Astrophysics, Vienna, Austria, (2) Space Research Institute, Austrian Academy of Sciences, Graz, Austria, (3) Freie Universität Berlin, Berlin, Germany

Abstract

We suggest electromagnetic induction heating as an energy source inside terrestrial planets orbiting late M dwarfs with strong magnetic fields. Induction heating arises due to varying magnetic field flux penetrating the planet. We show that for close-in planets, induction heating can be stronger than the tidal heating occurring inside Jupiter's satellite Io; namely, it can generate a surface heat flux exceeding $2\,\mathrm{W\,m^{-2}}$. An internal heating source of such magnitude can lead to extreme volcanic activity on the planet's surface, possibly also to internal local magma oceans, and to the formation of a plasma torus around the star aligned with the planetary orbit.

1. Introduction

Many M dwarfs have been observed to host strong dipole-dominated magnetic fields of a few kG and more [1]. Induction heating arises when a changing magnetic field induces currents in a conducting medium which then dissipate to heat the body, mostly within an upper layer called the skin depth. For induction heating to be substantial, the planetary orbit has to be inclined with respect to the stellar rotation and dipole axes, or (if the planet orbits in the stellar equatorial plane) the stellar dipole axis has to be inclined with respect to the rotation axis (Fig. 1). In this case, stellar magnetic field penetrating the planet varies periodically, which leads to generation of eddy currents in the conducting planetary mantle. Under these conditions, induction heating can be substantial.

2. Methods

In our model, the planet is assumed to be a sphere made up of concentric layers; each layer has a uniform conductivity which is different for different layers. We solve the induction equation in every layer and calculate the magnetic field strength and current. Knowing the current and conductivity, we find the energy release within each layer (see [2], for details). We assume by default an Earth-like mantle conductivity profile, but in the papers we have also considered a case of a molten mantle with increased conductivity. After calculating the heating, we model its influence on interiors and estimate the increase in volcanic activity using the code CHIC [4].

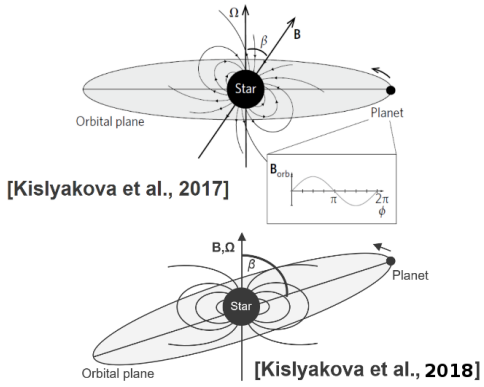

Figure 1: Sketch of the induction heating mechanism. The planet continuously experiences magnetic flux changes in its interior along its orbital motion. The change of the magnetic field arises due to the planetary orbital motion, stellar rotation, and/or stellar dipole tilt. The change of the magnetic flux penetrating the planet generates eddy currents which dissipate and heat the planetary mantle [2, 3].

3. Results

Fig. 2 presents an example calculation of induction heating inside and Earth-sized Earth-mass planet or-

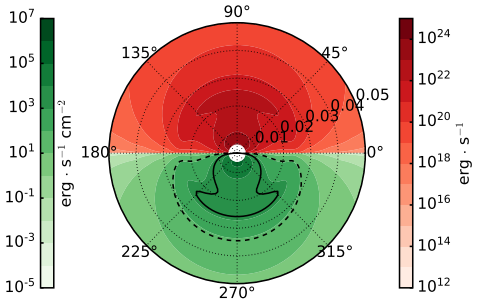

Figure 2: Total energy release inside an Earth-radius and Earth-mass planet (upper half, in red) and surface heat flux (lower half, in green) as a function of distance to WX UMa (concentric dotted rings) and orbital inclination. The solid and dashed black lines mark the surface heat fluxes of 2×10^{3} erg cm^{-2} s^{-1}, which corresponds to the surface heat flux on Io due to tidal heating, and 80 erg cm^{-2} s^{-1}, which corresponds to the total heat flux of modern Earth [3].

biting WX UMa on an inclined orbit, a 0.12 $M_{\odot}$ star with a dipole-dominated magnetic field of 7.3 kG [1]. There is a region close to the star where the surface heat flux due to induction heating exceeds 2×10^{3} erg s^{-1} cm^{-2} (2 W m^{-2}) by up to two orders of magnitude. This value corresponds to Io's heat flux induced by tidal heating, which makes this Jovian satellite the most volcanically active body in the solar system. Even at larger orbital distances, induction heating is still more powerful than the modern Earth energy release due to radioactive decay.

4. Summary and Conclusions

We show that for stellar magnetic fields above 2-3 kG, at some orbital distances energy release due to induction heating is so high that it exceeds the surface heat flux of Io, the most volcanically active body in the solar system. Energy release of such magnitude can lead to the formation of a magma ocean beneath the solid surface. Induction heating is strong also for planets with a molten mantle. Induction heating is the strongest close to the star, but it can be substantial even as far as in the habitable zone of an M dwarf, leading to increased levels of volcanic activity and potentially influencing the conditions for habitability on planets, for instance, in the TRAPPIST-1 system [3]. Therefore, it is likely that the planets orbiting magnetized M dwarfs may experience extreme volcanism and the possible formation of a plasma torus along their orbits, which may be observable in the strong far-ultraviolet OI triplet at about 1304 Åby Hubble Space Telescope or especially by a telecope of a new generation such as LUVOIR. This heating, together with the tidal heating, can be a very powerful energy source for rocky planets orbiting strongly magnetized M dwarfs and should be taken into account among other heating sources when addressing the interior evolution of such planets.

Acknowledgements

We acknowledge the support by the Austria Science Fund (FWF) NFN project S116-N16 and the subprojects S11607-N16 and S11604-N16.

References

[1] Shulyak, D., Reiners, A., Engeln, A., et al: Strong dipole magnetic fields in fast rotating fully convective stars, Nature Astronomy, Vol. 1, id. 0184, 2017.

[2] Kislyakova, K.G., Noack, L., Johnstone, C.P., et al.: Magma oceans and enhanced volcanism on TRAPPIST-1 planets due to induction heating, Nature Astronomy, Vol. 1, pp. 878-885, 2017.

[3] Kislyakova, K.G., Fossati, L., Johnstone, C.P., et al.: Effective induction heating around strongly magnetized stars, ApJ, Vol. 858, p. 105, 2018.

[4] Noack, L., Rivoldini, A., and Van Hoolst, T.: Modeling the Evolution of Terrestrial and Water-rich Planets and Moons, International Journal on Advances in Systems and Measurements, Vol. 9 no 1&2, 2016.

EPSC Abstracts
Vol. 12, EPSC2018-244, 2018
European Planetary Science Congress 2018

Possible discovery of two Mini-Neptune type planets around a dim K-star

Mahesh Herath (1, 2), Tobias C. Hinse (3), Saraj Gunesekera (2), Chandana Jayaratne (1)
(1) University of Colombo, Sri Lanka, (2) Arthur C Clark Institute for Modern Technologies, Sri Lanka, (3) Korea Astronomy and Space Science Institute, Republic of Korea.
(mherath2@gmail.com)

Abstract

We report the detection of two planets around EPIC 212737443, a magnitude 14.4 star using photometric data from the Kepler-K2 mission. By using multi-band photometric measurements to get a Spectral Energy Distribution (SED), the star was determined to have temperature of 4500±50 K, an effective surface gravity of logg = 4.5±0.25, a metallicity of [Fe/H] = 0, which is evidence that this is a K-type star. The planets have orbital periods of 13.60 and 65.60 days with transit depths of approximately 1000 ppm each. The radii of the two planets (2.18±0.04 R_{earth} and 2.42±0.04 R_{earth}) and their estimated masses imply that they are Mini-Neptune type worlds, though further measurements are required to constrain their masses. An RV follow-up study of these planets would be crucial for determining the exact density and mass of these planets as they lie in the transition region between Super-Earth's and Mini-Neptunes. The outer planet may reside in the habitable zone of the host star and both planets are possible candidates for follow-up studies with the JWST for atmospheric studies.

1. Introduction

EPIC 212737443 was observed during Campaign 6 of the K2 mission between July 13, 2015 and September 30, 2015. The light curve was obtained from the K2 archives hosted by the Mikulski Archive for Space Telescopes (MAST). We measured the mid-transit time for each individual transit event using the Kwee-Woerden technique. A total of six transits for the inner and two transits for the outer planet were identified and a linear ephemeris was determined (Table 1).

1.1 K2 photometry and transit vetting

Due to a malfunction in the reaction wheels of the Kepler spacecraft, the light curve contained position dependent and time dependent (mostly due to stellar variability) systematic trends. We used the *K2SC* correction algorithm (Aigrain et al 2016) which uses a Gaussian Process regression model to separate and remove the trends. Then a Box Least Square (BLS) algorithm was used to find transit signals followed by the fitting of Mandel & Agol (2002) transit models to determine if there are differences in the odd-even transits, and if there are any secondary eclipses. After finding transits with periods of 13.60 and 65.60 days, it was determined that the transits do not have odd-even depth variations or secondary eclipses. This mostly rules out the possibility that the transits are binary stellar companions. For the inner planet no significant transit-timing variations beyond the ephemeris uncertainty were found during the time period of the data.

2. Stellar characterization and additional observations

We also attempted to infer atmospheric properties of the host star via spectral energy distribution fitting. The VOSA/SED tool was utilized. For this we acquired intermediate- and broad-band photometric data from various sky-survey archive databases including WISE and 2MASS data. We probed several atmospheric models. The BT-SETTL CIFIST model provided an optimum description of the data revealing an effective temperature of 4500±50 K, logg = 4.5±0.25 and [Fe/H] = 0 for a solar abundance in metallicity. The stellar radius of 0.57 R_{sun} was taken from Huber et al (2016) which did a spectroscopic survey of K2 targets. Additionally we have acquired Lucky Imaging data using the two-instrument EMCCD cameras at the Danish 1.54m telescope (ESO/La Silla). A preliminary but close to certain investigation of the photometry revealed that no nearby companions are present.

3. MCMC fitting, orbital stability and a preliminary mass

We re-extracted the transits for each planet candidate and fit them with a Monte Carlo Markov Chain (MCMC). We used the *emcee* package (Foreman-Mackay et al. 2013) to fit the model light curves produced by the *PyTransit* package (Parviainen et al 2015), which uses the Mandel & Agol algorithm. We supersampled the data by a factor of 10 and adjusted for the K2 long cadence time of 29.5 minutes. The MCMC was implemented with 10 variables including the limb darkening parameters for which we used the triangular sampling as suggested by Kipping (2013). We ran 60,000 chains with 150 walkers and a burn-in of 200 chains. The final parameters and their errors can be seen in Table 1. We estimated the mass of each planet

using the mass-radius relationship proposed by Weiss & Marcy (2014), which is given here as Equation 1. The masses were found to be 5.54 M_{Earth} and 6.11 M_{Earth} respectively. As a final investigation we numerically integrated the orbits of the two-planet system over 10^7 years using a symplectic algorithm within the MERCURY (Chambers 1999) orbit integration package. Initial circular orbits were assumed. We find an overall orbital stability with small perturbations in the orbital elements. The system is found not to be locked within a specific mean-motion resonance.

4. Figures

Figures 1&2: The best fit curves with the observed data for each planet in EPIC 212737443. Planet a (blue) with 13.60 days and Planet b (Green) with 65.60 days.

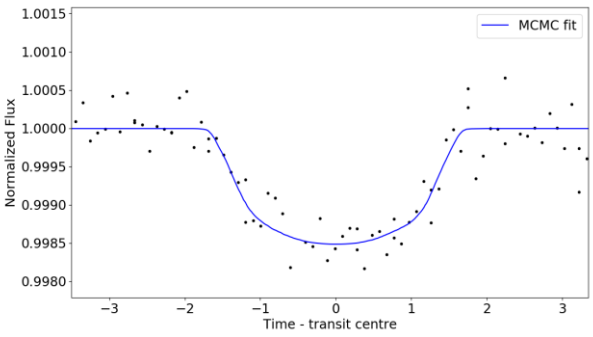

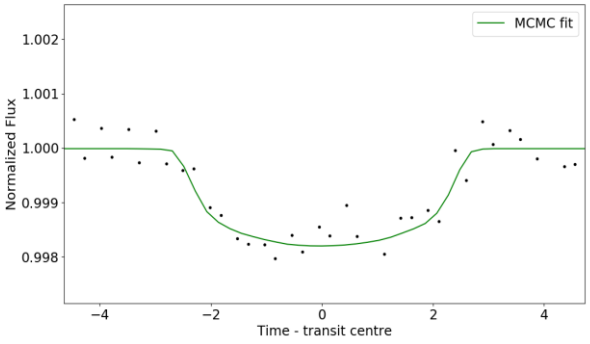

5. Equations

$$\frac{M_p}{M_s} = 2.69\left(\frac{R_p}{R_s}\right)^{0.93} \qquad (1)$$

6. Tables

Table 1: Parameters measured through MCMC fitting for the planets in EPIC 212737443

	Planet a	Planet b
Epoch (BJD)	2457221.35	2457227.80
Period (days)	13.602±0.0004	65.601±0.0002
R_p/R_{star}	0.035±0.0005	0.039±0.0005
Impact param.	0.42±0.05	0.44±0.06
a/R_{star} (scaled)	32.4±0.30	90±0.60
eccentricity	0.002±0.0006	0.004±0.0003
Radius (R_{Earth})	2.18±0.04	2.42±0.04

7. Summary and Conclusions

We have provided observational evidence for the possible detection of a transiting two-planet system EPIC 212737443. The transit signals seem to be in accordance with other planetary systems detected from the K2 mission. We have attempted to characterize the host star via SED modelling determining it to be a K-type star. The planetary architecture points towards a non-resonant and stable configuration. This is partially supported by non-significant timing variations of the inner planet. The masses measured by using the Weiss & Marcy relation show that the two planets are within the mass range of Super-Earth's but the radii imply they are not quite dense enough. This puts them firmly in the boundary between Super-Earth's and Mini-Neptunes. Future photometric and spectroscopic follow-up observations will provide a more detailed characterization of the two planets. Studying this system would be particularly important in order to study the transition region between Super-Earth's and Mini-Neptunes and to better constrain our understanding of planet formation.

References

[1] S. Aigrain, H. Parviainen, B. J. S. Pope, "*K2SC: Flexible systematics correction and detrending of K2 light curves using Gaussian Process regression*", MNRAS, Vol. 000, pp. 1-14, 2016.

[2] David M. Kipping, "*Binning is sinning: morphological light-curve distortions due to finite integration time*", MNRAS, Vol. 000, 1-14, 2010.

[3] Lauren M. Weiss & Geoffrey W. Marcy, "*The mass-radius relationship for 65 exoplanets smaller than 4 Earth radii*", ApJ Letters, 30 January 2013.

[4] Daniel Huber, Stephen T. Bryson, Michael R. Haas, Thomas Barclay, Geert Barentsen, Steve B. Howell, Sanjib Sharma, Dennis Stello, Susan E. Thompson, "*The K2 Ecliptic Plane Input Catalogue (EPIC) and stellar classifications of 138,600 targets in campaigns 1–8*", APJs, arXiv:1512.0264, 2016.

EPSC Abstracts
Vol. 12, EPSC2018-253-1, 2018
European Planetary Science Congress 2018

Impact of exomoons in flux and polarization phase curves of starlight reflected by exoplanets

J. Berzosa Molina⋆, L. Rossi, and D. M. Stam
Faculty of Aerospace Engineering, Delft University of Technology, Delft, The Netherlands (j.berzosamolina@gmail.com)
⋆Now at GMV AD, Isaac Newton 11, 28760 Tres Cantos, Spain

Abstract

While the search for exoplanets harvests an increasing interest, the times of exomoon detection and characterization are still to come. As those found in our Solar System, exomoons are potential candidates for hosting extraterrestrial life and/or granting their parent exoplanet with the required habitability conditions. Moreover, seizing and characterizing the orbit and properties of these companions is the keystone of a more exhaustive exoplanet characterization and a comprehensive understanding of planetary system formation mechanisms.

We show that measuring the flux and polarization of starlight reflected by a planet–moon system could potentially lead to the characterization of the lunar albedo, size and orbital parameters of its orbit around the planet.

1. Introduction

The capabilities of current and future instruments (e.g. SPHERE, GPI, EPICS) to perform high contrast direct imaging of exoplanets both through spectroscopy and polarimetry is about to open the prospect of extra–solar research by using an unexploited technique: measuring the state of polarization of starlight reflected by extra-solar bodies.

Previous studies have already modelled the phase light curves and polarization signals of exoplanets [12, 10] showing that polarimetry enhances the contrast between the exoplanet and its star. The spectral and temporal dependence of the polarization is also related to the properties of the planet and can be used to characterise the surface or atmosphere [5, 11].

We decided to investigate the effect of an exomoon on the reflected flux and polarization of a planet. In this line, we modeled phase curves of an unresolved Earth–Moon–like system including the transits and eclipses between the moon and the planet.

2. Numerical model

We describe the flux and polarization of starlight reflected by a spatially unresolved planet–moon system by a Stokes vector [4] computed using PyMieDAP [9], an adding-doubling radiative transfer algorithm [3], assuming the starlight is unpolarized [6]. Our model planet has a Lambertian depolarizing surface with horizontally homogeneous atmospheric layers filled with gas and/or aerosol particles on top, and our model moon has a Lambertian depolarizing surface without atmosphere.

The computed Stokes vectors at a certain epoch are a function of: (1) the atmosphere and surface properties of the bodies (e.g. radius and albedo), (2) the relative body–star–observer position, (3) the position of the moon around the planet. The latter is defined as a Keplerian orbit in the framework of a 'nested two-body' problem [8, 7] and will determine, in last instance, the duration, latency and shape of light curves during mutual events (see Fig. 1).

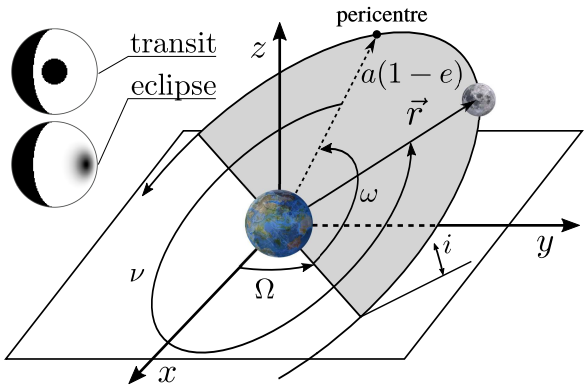

Figure 1: Geometry of the generic exomoon orbit around an exoplanet as a function of the lunar orbital parameters a, e, i, ν, Ω, ω. Top–left: example of modelled transit–eclipse events.

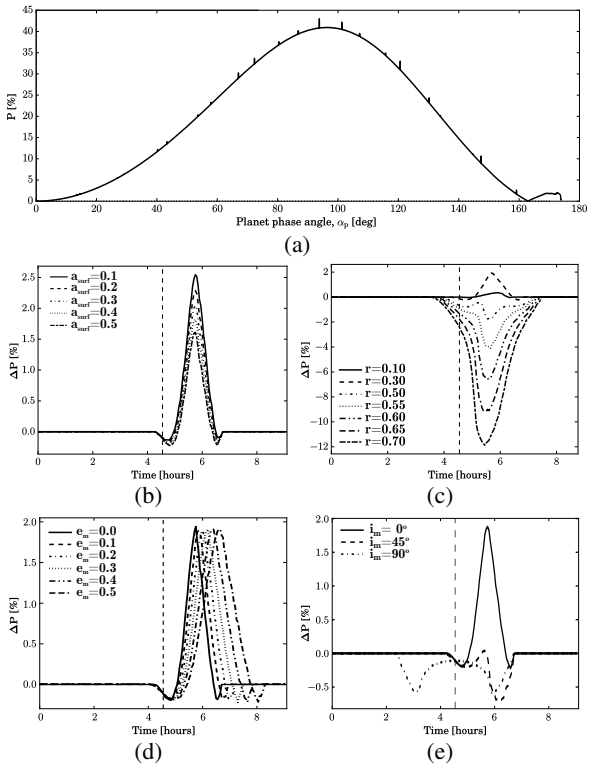

Figure 2: Degree of polarization phase curve (a), as well as change in degree of polarization, ΔP, during a lunar transit in front of the planet at $\alpha \approx 100°$ as a function of (a) lunar albedo $\mathrm{a_{surf}}$, (b) moon–to–planet ratio r, (c) moon orbit eccentricity $\mathrm{e_m}$, and (d) moon orbit inclination $\mathrm{i_m}$.

3. Discussion and results

Our results (submitted to A&A) show that the moon modulates the observed signal, both in flux and in polarization, revealing its presence [2, 1]. In particular, the variation of the degree of polarization is found to be maximum at phase angles close to 90° (see Fig. 2a). In fact, face–on coplanar systems will always display these events at a phase angle of 90°, making these moons easier to be detected.

We also analyzed whether exomoon characterization can be performed via the measurement of reflected starlight. We identify four different phenomena when varying the moon used in our simulations on the degree of polarization P (see Fig. 2): (1) change in duration of mutual events with i and e, (2) change in time interval between events with a and e, (3) change in curve's shape with i and R_m, (4) change in curve's amplitude with R_m and lunar albedo. These phenomena, and in particular the change in curve's shape, are strongly coupled with the surface and atmosphere properties of both the planet and moon along their disks, what might lead to batch fitting–like algorithms for exomoon characterization.

4. Conclusion

The outcome of our simulations reveal a strong correlation between the studied lunar properties (i.e. lunar radius and albedo) and moon orbit parameters (i.e. eccentricity, inclination and semi–major axis) and the shape, duration, and magnitude of the flux and degree of polarization variations of the reflected starlight of a extra–solar planet–moon system experiencing mutual transit and eclipse events at any phase angle.

With the foreseeable future arrival of very–high precision polarimeters, such correspondence could potentially lead to a detailed characterization of exomoons via polarimetry techniques.

References

[1] Berzosa Molina, J., Stam, D. M. and Rossi, L.: Traces of exomoons in flux and polarization signals of starlight reflected by exoplanets, in EPSC17, vol. 11, 2017.

[2] Berzosa Molina, J., Stam, D. M. and Rossi, L.: Traces of exomoons in flux and polarization phase curves of starlight reflected by exoplanets, (submitted) A&A, 2018.

[3] de Haan, J. F., Bosma, P. B. and Hovenier, J. W.: The adding method for multiple scattering calculations of polarized light, A&A 183, 371-391, 1987.

[4] Hansen, J. E. and Travis, L. D.: Light scattering in planetary atmospheres, Space Sci. Rev. 16, 527-610, 1974.

[5] Karalidi, T., Stam, D. M. and Hovenier, J. W.: Looking for the rainbow on exoplanets covered by liquid and icy water clouds, A&A 548, A90, 2012.

[6] Kemp, J. C., Henson, G. D., Steiner, C. T. and Powell, E. R.: The optical polarization of the Sun measured at a sensitivity of parts in ten million, Nature, 326, 270-273, 1987.

[7] Kipping, D. M.: How to weigh a star using a moon, MNRAS: Letters, Oxford University Press, 409, L119-L123, 2010.

[8] Kipping, D. M.: Transit Timing Effects Due to an Exomoon (in The Transits of Extrasolar Planets with Moons), Springer Berlin Heidelberg, 2011.

[9] Rossi, L., Berzosa Molina, J. and Stam, D. M.: PyMieDAP: a Python–Fortran tool to compute fluxes and polarization signals of (exo)planets, ArXiv 1804.08357, 2018.

[10] Seager, S., Whitney, B. A. and Sasselov, D. D.: Photometric Light Curves and Polarization of Close-in Extrasolar Giant Planets, ApJ 540, 504, 2000.

[11] Stam, D. M.: Spectropolarimetric signatures of Earth-like extrasolar planets, A&A, 482, 989-1007, 2008.

[12] Stam, D. M., Hovenier, J. W. and Waters, L. B. F. M.: Using polarimetry to detect and characterize Jupiter-like extrasolar planets, A&A, 428, 663-672, 2004.

EPSC Abstracts
Vol. 12, EPSC2018-266, 2018
European Planetary Science Congress 2018

ExoAI: Deep learning in exoplanet spectroscopy

Ingo Waldmann (1), Tiziano Zingales (1)
(1) Dept. Physics & Astronomy, University College London, Gower Street, London, WC1E 6BT, UK (ingo@star.ucl.ac.uk)
(2) INAF – Observatorio Astronomico di Palermo, Piazza del Parlamento 1, 90134 Palermo, Italy

Abstract

The field of exoplanetary spectroscopy is as fast moving as it is new. Analysing currently available observations of exoplanetary atmospheres often invoke large and correlated parameter spaces that can be difficult to map or constrain. This is true for both: the data analysis of observations as well as the theoretical modelling of their atmospheres. Modelling both sets of correlations in data and modelling is key to understanding the nature of exoplanet atmospheres.

In recent years, bayesian atmospheric retrieval algorithms have become the norm in exoplanet characterization.
Traditional atmospheric retrievals are limited by the sampling time required to fully map the likelihood space of the solution. Such large sampling processes do consequently require the atmospheric forward model to be fast, and hence simplistic. Whilst simple forward models are sufficient for the resolution and signal-to-noise of currently available Hubble data, this will not be the case in the era of JWST or Ariel. Though, more complex forward models require more computation time, making them the paramount bottleneck of next generation atmospheric retrievals.

In this talk I will discuss how these improvements in deep learning can be applied to solve correlations in the models as well as speeding up the statistical sampling.

By designing deep neural networks, we can significantly speed up data analysis and interpretation and allow our current models to 'learn from experience'. Such AI driven systems will help to resolve model correlations, and allow us to incorporate complex forward models in the atmospheric retrieval of extrasolar planets.

EPSC Abstracts
Vol. 12, EPSC2018-343, 2018
European Planetary Science Congress 2018

Atmospheric Retrieval using Deep Learning

T. Zingales (1,2) and I. Waldmann (1)
(1) University College London, London, United Kingdom (2) INAF - Osservatorio Astronomico di Palermo, Palermo, Italy
(tiziano.zingales.15@ucl.ac.uk)

Abstract

Atmospheric retrievals on exoplanets involve usually computationally intensive Bayesian methods. The choice of the fitting parameters bounds are often leaded by physical constraints and and the user experience. We introduce ExoGAN, a new generation artificial intelligence able to recognise molecular features, abundances and atmospheric physical parameters using unsupervised learning. ExoGAN will return a probability distribution for each parameters that can be used either as a final atmospheric analysis or as prior distribution for a subsequent Bayesian model.

1. Introduction

Artificial Intelligence has been used extensively in the last few years in many different fields. The use of Artificial Neural Networks in Astrophysics is a relatively young but the growing interest of the scientific community towards this tool will increase dramatically within the next decade. Independently on the research field, Neural Networks can be used to understand and describe relatively complex structures and behaviour in a wide variety of dataset. Waldmann (2016) is a pioneering work who apply a deep-belief neural network (DBN) to recognize the atmospheric features on an exoplanetary transmission spectrum. Rodriguez et al. (2018) developed a tool able learn models that can efficiently generate new, physically realistic realizations of the cosmic web using generative networks. In the exoplanetary field, and more in general, in the astrophysics field, the use of GANs is still a new method able to solve computationally intensive problems. In our work we suggest a more advanced and up-to-date unsupervised algorithm to understand and reliably reproduce the atmosphere of an exoplanets. In particular we used a Deep Convolutional Generative Adversarial Network (DCGAN) introduced for the first time by Goodfellow et al. (2014). We introduce ExoGAN, a DCGAN able to recognise spectral feature from exoplanetary spectra and return a detailed chemical and physical analysis in a completely new way, reducing the computational time from several hours to a few minutes.

2. What is a DCGAN

A GAN has two different neural networks competing each other and learning how to reproduce realistic synthetic data from an input dataset. A Deep Convolutional GAN (DCGAN) is a GAN which uses batch normalisation, it is made of two all-convolutional networks, uses the Adam Optimizer and the leaky ReLU activation function (Xu et al., 2015; Radford et al., 2015).

3. The training

A good training set is crucial to teach ExoGAN how to generate a realistic transmission spectrum. GANs are general methods, recently they have been applied to several serious problems, such as semi-supervised learning, stabilizing sequence learning methods for speech and language, and 3D modelling (Denton et al., 2015; Radford et al., 2015; Salimans et al., 2016; Lamb et al., 2016; Wu et al., 2016). However, they still remain remarkably difficult to train, with most current papers dedicated to heuristically finding stable architectures (Arjovsky and Bottou, 2017). We use a training set of 10 million of spectra varying 7 different parameters: H_2O, CO_2, CH_4 and CO abundances, the mass of the planet M_p, the radius R_p and the temperature T_p. In order to stretch as much as possible every feature we divide the input spectrum into several different bins as shown in Fig 1 We normalised each of these spectra between 0 and 1 and, to optimise the efficiency of our GAN to recognise the features and the correlations between the parameters we normalised each parameters as following (see Fig 2)

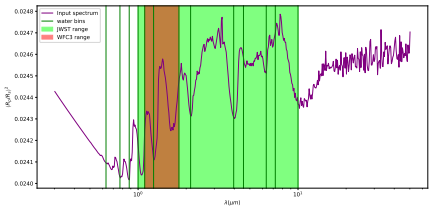

Figure 1: Spectral binning used in this work. The green vertical line are represent the bin edges according to some water features. the Red area is the wavelength range related the the Hubble WFC3 camera and the lime area is that of the JWST.

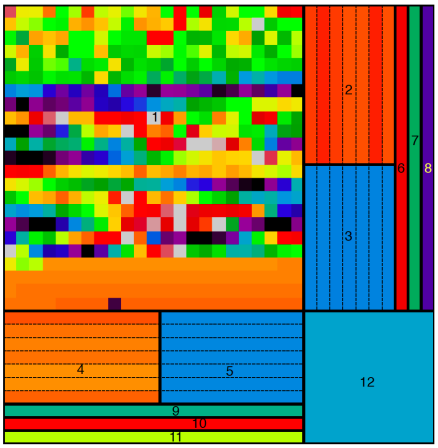

Figure 2: Normalised spectrum. Each area is dedicated to a particular atmospheric characteristic: Area **1** is the spectrum between 1μm and 50μm at resolution 100 normalised between 0 and 1 in each spectral bin. From area **2** to **5** give information about the normalisation factors used in the different section of the spectrum, clear and dark area give, respectively, information about the maximum values and the minimum values. In areas from **6** to **8** there are, respectively, CO_2, CO and CH_4 abundances. Areas **9** to **11** are, respectively M_p, R_p and T_p. Area **12** gives information on the H_2O abundance.

3.1. Method - Generative Adversarial Networks

GANs are classified as unsupervised learning algorithms. In our work we use it to recognise spectral features from exoplanetary spectra. The very same net, nevertheless, can be used to detect the characteristics of an image (Goodfellow, 2017; Creswell et al., 2018). GANs consist of two neural network facing each other and learning how to reproduce a realistic synthetic data from an input dataset. The two essential parts of a GAN are de Discriminator and the Generator nets (Fig 3).

4. The training

In order to update the weights related to the two neural nets we need to differentiate this function with respect to the discriminator and the generator. Concerning the generator training, the gradient of the first term with respect to the generator is zero (the generator does not appear there) so only the second term is relevant. Assuming that the discriminator does a really good job in discriminating the real and the fake images, it means that $D(G(z))$ is very close to zero, the slope of the cost function at point 0 is also very close to zero and the θ_g has no chance to improve and change. It means that in this case the network does not learn anything from the training set. For the generator, a possible solution to this problem could be, instead of targeting the value 0 for fake images, looking at the value 1 target (real images), it means that we are trying to minimise the negative expected value of $\log D(G(z))$ and so we can use as a cost function for the generator:

$$J^{(G)} = \mathbb{E}_{\mathbf{z}\sim p_z}[\log(D(G(z)))] \tag{1}$$

This new solution works because the term $\log D(\text{anyimage})$ corresponds to a target of value 1 in the binary cross-entropy and the other term is irrelevant because its derivative in the gradient descent is zero. For each number of training iteration and for k steps, defining as m as the batch size of or set, we update the discriminator by ascending its stochastic gradient (Goodfellow et al., 2014):

$$\nabla_{\theta_d}\frac{1}{n}\sum_{i=1}^{n}\left[\log D\left(\mathbf{x}^{(i)}\right)+\log\left(1-\log D\left(G\left(\mathbf{z}^{(i)}\right)\right)\right)\right] \tag{2}$$

At the same time we update the generator by de-

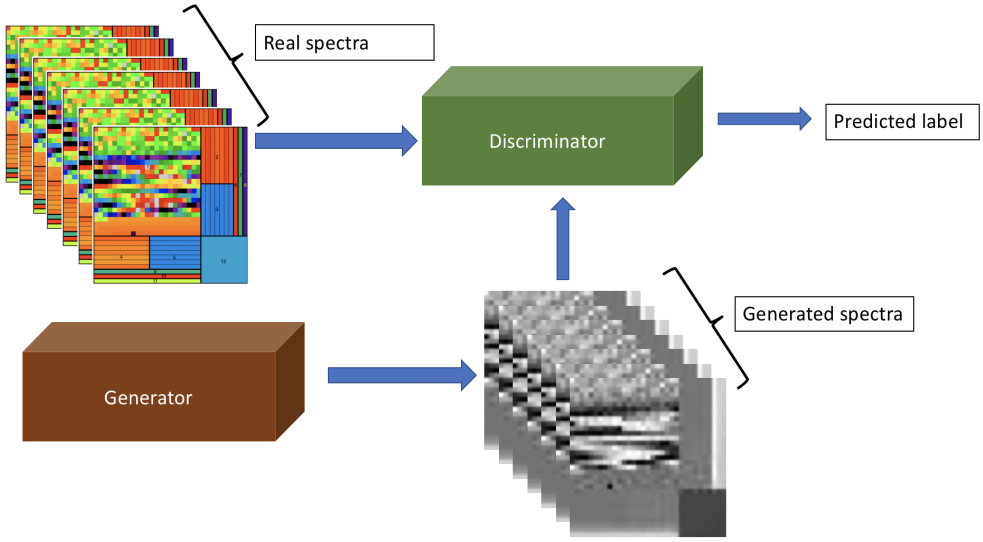

Figure 3: ExoGANscheme. From right to left, The generator reproduce a realistic spectral sample that is seen by the discriminator. The discriminator network is the only one who have access to the real dataset. By analysing both the generated sample and the real one it tries to understand whether the generator is able to reproduce a perfectly realistic spectral sample or not.

scending its stochastic gradient:

$$\nabla_{\theta_d} \frac{1}{n} \sum_{i=1}^{n} \log \left(1 - \log D \left(G \left(\mathbf{z}^{(i)}\right)\right)\right) \quad (3)$$

5. Image reconstruction

Atmospheric Retrievals are often computing intensive and they need to be done by fitting many parameters. A Bayesian model on exoplanetary atmosphere parameters are done using non-informative (flat) priors within a range of values. These ranges are often fixed according to physical constraint and, once one have experience on exoplanetary atmosphere, user experience. The use of Artificial Neural network can replace the user experience with a more sofisticated and completely unsupervised tool. The use of ExoGAN, trained on a huge dataset of exoplanetary atmospheres models can help the retrieval code to have better constraint, get rid of the solutions that are likely not to give any acceptable solution and accelerate the computing analysis. In order to find the best $\hat{z}$ we define two loss functions for an arbitrary $\hat{z} \sim p_z$: the contextual loss and the perceptual loss:

$$\mathcal{L}_{contextual}(z) = \| M \odot G(z) - M \odot y \|_1 \quad (4)$$

with $\| x \|_1 = \Sigma_i |x_i|$ for some vector x.

$$\mathcal{L}_{perceptual}(z) = \log\left(1 - D(G(z))\right) \quad (5)$$

We find $\hat{z}$ defining a combination of the two losses:

$$\mathcal{L} = \mathcal{L}_{contextual}(z) + \lambda \mathcal{L}_{perceptual}(z) \quad (6)$$

where λ is a hyper-parameter which control how important is the contextual loss compared to the perceptual. At this point $\hat{z}$ is defined as:

$$\hat{z} = \arg\min_z \mathcal{L}(z). \quad (7)$$

The best reconstructed image defined in **??** is the one that uses the $\hat{z}$ defined in 7. In Fig 4 we show the three phase associated to a prediction. We see that the input parameters are masked and reproduced by a pre-trained ExoGAN.

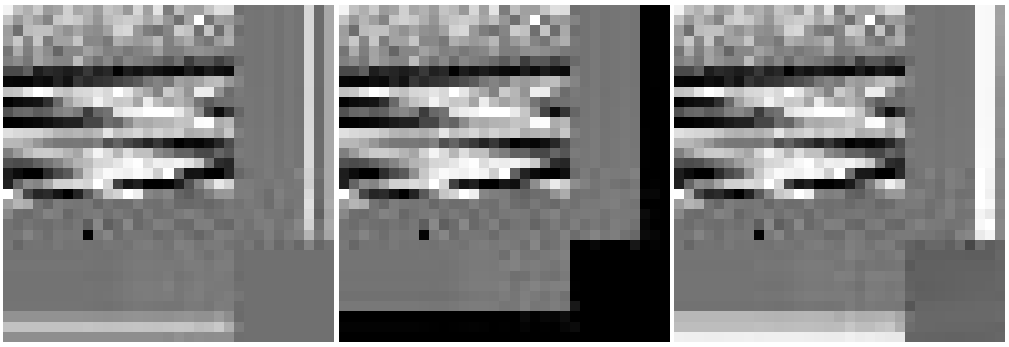

Figure 4: On the **left** we find the input spectrum together with the parameters pixels. In the **centre** there is the masked spectrum which is fed to the ExoGAN and on the **right** we find the predicted spectrum with the best pixels parameters.

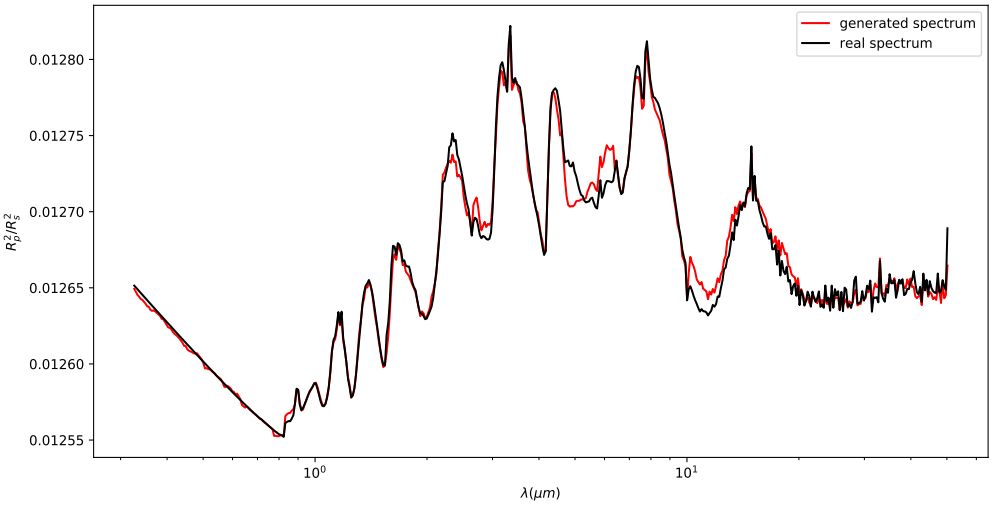

Figure 5: Feature recognition of ExoGAN. The black line is the input spectrum and the red one is the best generated one. ExoGAN recognised all the features of the input spectrum associating to it the parameters that can generate it with a classical model.

6. Results on Test set

Test set parameters			
Variable	accuracy	$\tilde{\chi}^2$ (1σ)	$\tilde{\chi}^2$ (2σ)
CO	50.2%	5.83	1.46
$CO2$	85.3%	0.85	0.21
$H2O$	79.6%	2.64	0.66
$CH4$	68.8%	0.46	0.11
Rp	98.4%	0.03	0.01
Mp	71.8%	1.59	0.40
Tp	75.5%	2.41	0.60

Table 1: Accuracies and $\tilde{\chi}^2$ associated to each parameters for 1000 test spectra. The 2 column represent the absolute accuracy of the prediction without taking into account the error bar of the prediction. The 2nd and 3rd column are the $\tilde{\chi}^2$ calculated, respectively, using one σ and 2 σ prediction errors.

7. Summary and Conclusions

We demonstrated how the use of a DCGAN can help the spectral retrieval of exoplanetary atmosphere. DCGAN in our work are 210% faster than a Bayesian analysis on the same spectrum. The output parameters distribution can be used either as a final solution or as an input prior distribution for a more efficient Bayesian modelling.

Acknowledgements

T. Z. is supported by the European Research Council ERC projects *ExoLights* (617119) and from INAF trough the "Progetti Premiali" funding scheme of the Italian Ministry of Education, University, and Research.

References

Arjovsky, M. and Bottou, L. (2017). Towards Principled Methods for Training Generative Adversarial Networks. *ArXiv e-prints*.

Creswell, A., White, T., Dumoulin, V., Arulkumaran, K., Sengupta, B., and Bharath, A. A. (2018). Generative Adversarial Networks: An Overview. *IEEE Signal Processing Magazine*, 35:53–65.

Denton, E., Chintala, S., Szlam, A., and Fergus, R. (2015). Deep Generative Image Models using a Laplacian Pyramid of Adversarial Networks. *ArXiv e-prints*.

Goodfellow, I. (2017). NIPS 2016 Tutorial: Generative Adversarial Networks. *ArXiv e-prints*.

Goodfellow, I. J., Pouget-Abadie, J., Mirza, M., Xu, B., Warde-Farley, D., Ozair, S., Courville, A., and Bengio, Y. (2014). Generative Adversarial Networks. *ArXiv e-prints*.

Lamb, A., Dumoulin, V., and Courville, A. (2016). Discriminative Regularization for Generative Models. *ArXiv e-prints*.

Radford, A., Metz, L., and Chintala, S. (2015). Unsupervised Representation Learning with Deep Convolutional Generative Adversarial Networks. *ArXiv e-prints*.

Rodriguez, A. C., Kacprzak, T., Lucchi, A., Amara, A., Sgier, R., Fluri, J., Hofmann, T., and Réfrégier, A. (2018). Fast Cosmic Web Simulations with Generative Adversarial Networks. *ArXiv e-prints*.

Salimans, T., Goodfellow, I., Zaremba, W., Cheung, V., Radford, A., and Chen, X. (2016). Improved Techniques for Training GANs. *ArXiv e-prints*.

Waldmann, I. P. (2016). Dreaming of Atmospheres. *ApJ*, 820:107.

Wu, Y., Schuster, M., Chen, Z., Le, Q. V., Norouzi, M., Macherey, W., Krikun, M., Cao, Y., Gao, Q., Macherey, K., Klingner, J., Shah, A., Johnson, M., Liu, X., Kaiser, Ł., Gouws, S., Kato, Y., Kudo, T., Kazawa, H., Stevens, K., Kurian, G., Patil, N., Wang, W., Young, C., Smith, J., Riesa, J., Rudnick, A., Vinyals, O., Corrado, G., Hughes, M., and Dean, J. (2016). Google's Neural Machine Translation System: Bridging the Gap between Human and Machine Translation. *ArXiv e-prints*.

Xu, B., Wang, N., Chen, T., and Li, M. (2015). Empirical Evaluation of Rectified Activations in Convolutional Network. *ArXiv e-prints*.

EPSC Abstracts
Vol. 12, EPSC2018-359, 2018
European Planetary Science Congress 2018

On integrating light-curve modelling with atmospheric retrieval techniques

K.H. Yip, I.P. Waldmann , A. Tsiaras and G. Tinetti
Department of Physics and Astronomy ,University College London, Gower Street,WC1E 6BT London, United Kingdom

Abstract

Characterising exoplanet atmosphere has been one of the major frontier in the field in recent decade. Thanks to many novel atmospheric retrieval techniques, we have detected a number of molecules that lives within various kinds of exoplanets' atmospheres, some of which are vital for life to exist. In the next decade, space missions such as JWST, ARIEL and PLATO will deliver measurements with unprecedented precision and completeness in terms of wavelength coverage. It is thus important for us to upgrade our current retrieval techniques in order to allow optimal exploitation of future instruments.

Contemporary atmospheric retrieval technique has focused on retrieving atmospheric components based on a planet's transmission spectrum, which was independently derived from fitting raw light-curves at different wavelengths. The process essentially compresses an entire light-curve into a single data point on a transmission spectrum, the compression inevitably affects uncertainty estimation and lowers the information gain. A way forward is to include geometric information of a light-curve within the atmospheric retrieval process. We demonstrated this concept by integrating Tau-REx, a fully Bayesian atmospheric retrieval framework , with PyLightcurve, a light-curve modelling routine.

This new approach provides 2 major advantages over the current approach, 1. A statistically more rigorous and more realistic estimation of the uncertainties involved in each retrieved parameters compared to the conventional approach. 2. The possibility to probe, for the first time, the correlation between various light-curve related parameters to atmospheric components. In this conference I will discuss the implication of these advantages using synthetic and actual observed data from Wide Field Camera 3 and the need for a dedicated end-to-end retrieval process that rigorously accounts for the uncertainties propagated from observation data all the way to atmospheric components.

EPSC Abstracts
Vol. 12, EPSC2018-373, 2018
European Planetary Science Congress 2018

Haze layer from reflection spectra of Titan-like exoplanets

P. Rannou (1), R.A. West (2)
(1) GSMA, Université de Reims Champagne-Ardenne, FRANCE (2) Jet Propulsion Laboratory, Pasadena, CA, UNITED-STATES

Abstract

Most of the studies about detection of exoplanetary atmospheres concern tangential transmission at the limb of the planets. This corresponding to the geometry of primary transit observations. However, the reflection planet spectra contains useful and specific information that would complete observation of primary transit. In this work we perform a study to determine in which extent we can obtain information about the haze layer of an atmosphere which is basically unknown. To perform tests, we use the atmosphere of Titan, which is a quite simple case with a spectrum dominated by haze and methane only.

1. Retrieval with a Titan-like planet

In a first part of the work, we study the relationhip, at very high resolution and in a narrow wavelength interval (each absorption line must be resolved), between a synthetic spectrum of intensity, the depth of the haze column that is probed and the outgoing intensity. To do so we use an atmosphere description relevant for Titan, then with a specific vertical profile of haze and of methane. The atmosphere is essentially composed of nitrogen, without spectral features, and bounded at 1.44 bar by a solid surface. For the methane, with use methane lines computed from ab-initio calculation

With this work, we show that the amount of haze probe at a given wavelength could approximatively be described by the outgoing intensity. If we connect the altitude where the integrated gas opacity reach 1 (defining a depth level) and the intensity profile, we can produce a vertical profile that is a good proxy of the haze vertical profile. The advantage is that we do not need to know the properties of the scatterers. The drawback is that this profile is proportional to the real opacity, but is not normalized. It can be used to quickly assess the existence of a haze.

2. Retrieval with an unknown planet

In a second step, we evaluated what kind of information could be retrieved from an atmosphere for which we know almost nothing. In this second step, we use synthetic spectra as in the first step, but we now ignore most of the information about the planet. The only informations which are supposed to be known are the average temperature of the atmosphere, the gravity, the size of the planet (to assume that we correctly know the geometric albedo) and the existence of gaseous methane.

We built a database of methane adsorption as a function of the wavelength and temperature and started to retrieve the haze properties, from intensity spectra, using the restricted information we have. We made tests with synthetic spectra, at wavelengths between 1 and 2.5 μm, at different spectral resolution and with a real spectrum of VIMS.

We find that we are able to retrieve a valuable vertical profile of the haze proxy, we are able to retrieve the spectral behaviour of the haze and as well a degraded information about the temperature profile. On the other hand, the existence of a surface is not unambigous defined and could be confused with a global deck of cloud.

3. Retrieval with an unknown planet

The next steps for this work will consist in ***1)*** implementing other gases to define if we can detect and define a more complex composition ***2)*** improve the retrieval of the haze layer with a better description of the gas vertical opacity ***3)*** Use other test planet and define if we can detect horizontal in-homogeneity in non-resolved planets.

EPSC Abstracts
Vol. 12, EPSC2018-391-1, 2018
European Planetary Science Congress 2018

Investigating cloud cover variability on Earth-like exoplanets using polarimetry

Loïc Rossi (1,2), Ashwyn Groot (1), Thomas Fauchez (3) and Daphne M. Stam (1)
(1) Faculty of Aerospace Engineering, TU Delft, The Netherlands (l.c.g.rossi@tudelft.nl); (2) LATMOS, Guyancourt, France; (3) Climate and Radiation Laboratory, NASA Goddard Space Flight Center, Greenbelt, Maryland, USA

Abstract

Because clouds scatter and absorb incident radiation, they play crucial roles in the radiative balance, the atmospheric chemistry, climate, and thus the habitability of a planet. Clouds usually affect the planet's observables. We investigate here the effect of partial and variable cloud coverage on the light that is reflected by an Earth-like exoplanet, exploring not only the total flux but also the linearly and circularly polarized fluxes.

1. Introduction

Clouds can have a strong effect on the thermal balance of an exoplanetary atmosphere and thus on the presence of liquid water on the surface, and therefore on the habitability [3, 9]. They also affect the appearance of absorption bands [8, 1] and transit spectra [4]. Finally, they could hide surface biomarkers, such as chlorophyll and/or the so-called red edge [7].

Polarimetry has proven to be an effective way to characterize the properties of a planetary atmosphere. In particular, the degree and direction of polarization will change with phase angle, depending on the micro- and macro-physical properties of the atmosphere and the clouds, and an underlying surface. A famous example is the derivation that the clouds of Venus [2] consist of 1μm, sulfuric acid solution droplets from disk–integrated linear polarization observations.

In this study, we discuss the effect of horizontally inhomogeneous cloud covers on the flux and polarization of light reflected by an Earth-like exoplanet.

2. Modeling Earth-like exoplanets

Our radiative transfer computations are performed using PyMieDAP, a Python–Fortran doubling–adding code that we created and made available online[1] [5] The model planetary atmosphere is locally plane–parallel, and vertically divided in homogeneous layers filled with gas, and one of them, optionally, also containing cloud particles. The planetary disk as seen by the observer is divided into a grid of square pixels. For each pixel we compute with the reflected total and polarized fluxes, allowing us to study both disk-resolved and disk-integrated signals. Each pixel can be assigned a different model atmosphere such that we can study the effects of different cloud coverage maps on the reflected signals.

Here, we use three types of coverage: sub-solar clouds, polar clouds, and patchy clouds. For each type we vary the fraction of cloud cover F_c for the whole planet. We use Earth- or Venus-like clouds consisting of water or sulfuric acid solution particles [5, 6].

3. Results

3.1. Linear polarization

As can be seen in Fig. 1, sub-solar clouds show a distinct phase curve pattern in the disk–integrated polarization signal, with a clear transition when the cloud rotated out of the observer's view. The polar cusps and patchy cloud coverages show similar patterns, but the variability in the position of the patches yields a more variable polarization signal than with polar clouds. The variability shown by the patchy clouds is related to the amount of clouds, and could be used for a rough estimate of F_c. Note that the variability will influence the derivation of mixing ratios of gaseous absorbers [1] and is thus a parameter of interest when trying to identify biomarkers such as the amount of oxygen.

At phase angles where the rainbow is visible, its strength is not affected by the type and amount of coverage, potentially allowing to use it to derive cloud particle sizes (the composition and particle shape are known). Finally, at short wavelengths (UV-blue) the polarization phase curves for planets with different cloud coverages are similar, as they are dominated by

[1] `http://gitlab.com/loic.cg.rossi/pymiedap` under a GNU GPL license

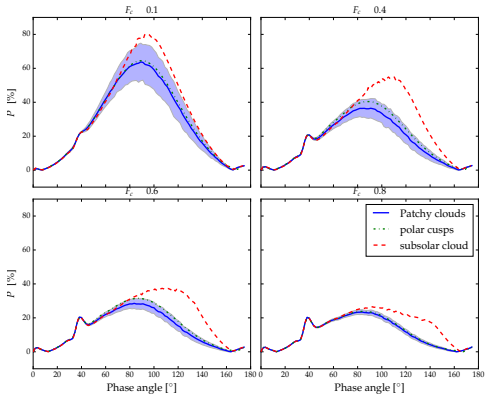

Figure 1: Comparison of the degree of linear polarization at $\lambda = 500$ nm for different cloud coverage types for $F_c = 0.1$, 0.4, 0.6, and 0.8. The cloud-top pressure p_c is 800 mb. Solid lines and shaded areas show the average and the variability over 300 patchy cloud patterns, respectively.

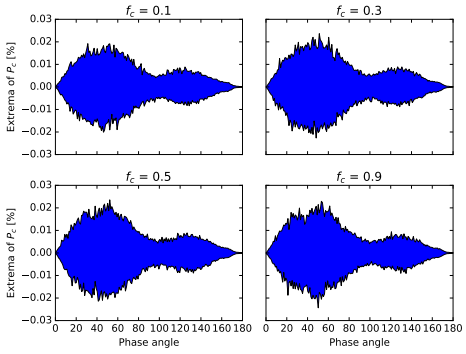

Figure 2: Maximum values of the degree of circular polarization P_c computed for 300 cloud patterns as a function of the phase angle, for different cloud coverage fractions F_c for Earth–like cloud particles.

the contribution of Rayleigh scattering by gas above the clouds. This suggests that at these wavelengths, assuming purely gaseous atmospheres is a reasonable approximation, which would allow to derive orbital parameters from a planetary system using polarimetry.

3.2. Circular polarization

The disk–integrated circular polarization of a planet with a horizontally homogeneous atmosphere is zero, since both hemispheres would produce polarization of the same value but with opposite signs. We therefore investigate the effect of patchy cloud covers on the disk–integrated degree of circular polarization P_c of Earth- and Venus-like planets.

Our simulations (Fig. 2) show that while an increase of the amount of cloud cover, F_c, increases P_c (since Rayleigh scattering doesn't generate circular polarization), it also increases the global symmetry of the cloud cover and therefore leads to a decrease of P_c. The highest values for P_c occur when F_c is about 40% to 50%. Note that the absolute values of P_c are very small anyway (smaller than 0.02%) and therefore likely below the current and (near) future exoplanet detection capabilities.

3.3. A realistic model Earth

To go beyond the ideal cases discussed above, we used MODIS observations to simulate the flux and polarization signals of a model Earth with realistic cloud coverage. The preliminary results show the importance of including the spatial and temporal variability of both the surface and cloud cover on the observed signals. It also appears to be possible to retrieve information about the diurnal rotation or seasonal effects, in line with previous studies based on total flux signals only.

4. Summary and Conclusions

We investigated the effect of cloud variability on the polarization of light reflected by Earth-like and Venus-like planets. Polarimetry should allow to distinguish different sorts of cloud coverage and could help to determine the amount of clouds. A multi-wavelength approach should help to reduce degeneracies when deriving orbital parameters from polarization signals.

References

[1] Fauchez, T., Rossi, L. and Stam, D. M. 2017, ApJ, 842, 41

[2] Hansen, J. E. and Hovenier, J. W., 1974, J. Atmos. Sci., 31, 1137

[3] Kitzmann, D., Patzer, A. B. C, von Paris, P., et al. 2010, A&A, 511, A66

[4] Line, M. R. and Parmentier, V. 2016, ApJ, 820, 78

[5] Rossi, L., Bersoza-Molina, J., Stam, D. M., A&A, in press

[6] Rossi, L. and Stam, D. M., A&A, in press

[7] Tinetti, G., Meadows, V. S., Crisp, D., et al. 2006, Astrobiol., 6, 881

[8] Vasquez, M., Schreier, F., Gimeno Garcia, S. et al. 2013, A&A, 577, A46

[9] Yang, J., Cowan, N. B., & Abbot, D. S., 2013, ApJ, 771, L45

EPSC Abstracts
Vol. 12, EPSC2018-410, 2018
European Planetary Science Congress 2018

Characterizing super-Mercuries via state-of-the-art interior models

B. Brugger, O. Mousis, and M. Deleuil
Aix Marseille Univ, CNRS, LAM, Laboratoire d'Astrophysique de Marseille, Marseille, France (bastien.brugger@lam.fr)

Abstract

In the solar system, Mercury appears as a peculiar body, both on its physical parameters (low mass and highest uncompressed density) and its composition, making it unique among terrestrial planets. It is namely characterized by an enrichment in iron compared to solar abundances, and by reducing chemical conditions, yielding different formation materials than on the Earth or other terrestrial bodies [1]. Observations from the MESSENGER data, coupled to laboratory experiments and models of internal structure allowed to converge towards a precise characterization of Mercury [2, 3]. Beyond the general enrichment in iron of the planet, the general view that Mercury stores a significant fraction of silicon in its core (rather than sulfur, which restrains to the mantle) starts to be widely accepted.

Exoplanets resembling Mercury are identified from their high inferred bulk density. In this work, we investigate the internal structure and composition of a set of exoplanets that potentially present the same characteristics as Mercury (see Figure 1). We use the model of planetary interiors from [4], designed for terrestrial planets up to a few Earth masses, that we improve with finer core and mantle descriptions. This allows us to study planetary compositions that, in our solar system, are specific to Mercury. Current studies of these potential "super-Mercuries" only characterize such bodies as iron-rich planets, with a metallic core made either of pure iron or of an iron-sulfur mixture [5]. By considering the incorporation of silicon in the core of these exoplanets, we aim at determining how similar to Mercury they are, according to their measured fundamental parameters.

We thus show that, as for Mercury, the presence of silicon in the core of these planets allows them to present a bulk Fe/Si ratio closer to the stellar value, compared to the case with an Si-free core. In that latter case, the planetary Fe/Si ratio can reach ∼7 times the stellar value. In contrast, an Si-rich core lowers both Mg/Si and S/Si ratios of the exoplanets, because the silicate mantle only represents a small fraction of their mass. These deviations from the stellar abundances could be consequences of a particular formation mechanism of Mercury-like bodies, not only specific to our solar system. With a constantly increasing number of super-Mercuries, statistical studies on this family of exoplanets could allow to distinguish between the different formation scenarios invoked for Mercury. If Mercury-like bodies are common among exoplanets, the giant impact scenario [6] might not be the most favorable scenario, compared to a possible volatilization of the silicate mantle.

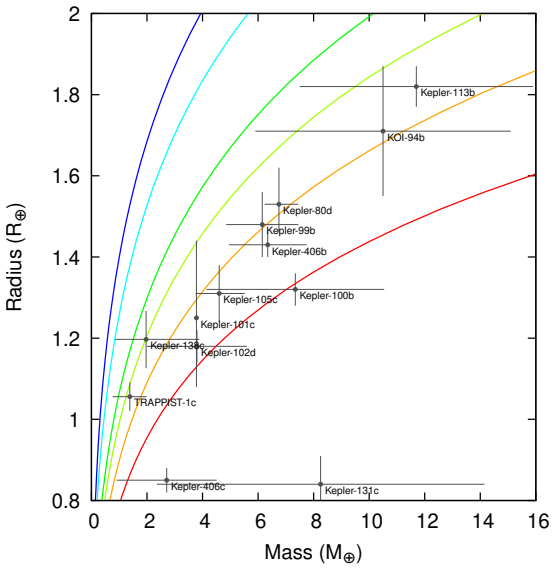

Figure 1: Position of potential super-Mercuries in the mass-radius diagram. The curves are mass-radius relations computed for a given set of planetary compositions (from top to bottom: 100% water, 50% water-50% silicate mantle, 100% silicate mantle, Earth-like, Mercury-like, and 100% metallic core).

Acknowledgements

The project leading to this publication has received funding from Excellence Initiative of Aix-Marseille University - A*MIDEX, a French "Investissements d'Avenir" program. O.M. and M.D. acknowledge support from CNES.

References

[1] Nittler, L. R., Starr, R. D., Weider, S. Z., et al. 2011, Science, 333, 1847

[2] Hauck, S. A., Margot, J.-L., Solomon, S. C., et al. 2013, Journal of Geophysical Research (Planets), 118, 1204

[3] Brugger, B., Mousis, O., Deleuil, M., & Deschamps, F. *In prep.*

[4] Brugger, B., Mousis, O., Deleuil, M., & Deschamps, F. 2017, ApJ, 850, 93

[5] Santerne, A., Brugger, B., Armstrong, D. J., et al. 2018, Nature Astronomy, 2, 393

[6] Benz, W., Anic, A., Horner, J., et al. 2007, Space Science Reviews, 132, 189

EPSC Abstracts
Vol. 12, EPSC2018-467, 2018
European Planetary Science Congress 2018

A comparison of exoplanet retrieval tools

Joanna K. Barstow (1), Ryan Garland (2), Michael R. Line (3), Marco Rocchetto (1), and Ingo P. Waldmann (1)
(1) Department of Physics and Astronomy, University College London, UK (2) Atmospheric, Oceanic and Planetary Physics, University of Oxford, UK (3) School of Earth and Space Exploration, Arizona State University, Arizona, USA
(j.eberhardt@ucl.ac.uk)

Abstract

In recent years, spectroscopic observations of transiting exoplanets have begun to uncover information about their atmospheres including atmospheric structure and composition, and indications of the presence of clouds. Spectral retrieval is the leading technique for interpretation of exoplanet transmission spectra. Whilst several atmospheric models and retrieval algorithms have been successfully employed, as yet the different model suites have mostly been used in isolation and so it is unknown whether results from each are comparable. As we approach the launch of the *James Webb Space Telescope* in 2020, and looking further ahead to the recently-selected *ARIEL* mission, we are entering a new data-rich era in the field of exoplanet atmospheres and so it is important that the tools that will be used to interpret these data are properly verified. We here present a comparative study of three retrieval code suites: *TauREX*; *NEMESIS*; and *CHIMERA*, and demonstrate that they produce comparable results for both forward and retrieval models.

1. Introduction

The launch of the *James Webb Space Telescope* (*JWST*) in 2020 will provide transit and eclipse spectra of exoplanets with unprecedented signal-to-noise and spectral resolution, increasing our capacity for comparative exoplanet science. *ARIEL*, to be launched in 2028, will perform the first atmospheric census of exoplanet atmospheres. For the first time, progress is likely to be be limited by model completeness and robustness rather than data quality, and meaningful comparison between results obtained by different teams will require careful benchmarking of the tools used in interpretation.

Exoplanet retrieval algorithms generate (usually 1-D) forward models of exoplanet atmospheres, then iteratively solve the inverse problem to find the best fitting model solution to the observed data. This technique has been used extensively (e.g. [5, 6, 1, 7]) and is acknowledged to be an efficient and reliable method for constraining exoplanet atmospheres from transmission and eclipse spectra. Whilst all retrieval codes follow the same basic structure, there is substantial variation in both the forward model set up and the method used to solve the inverse problem, leading to the possibility that two different retrieval codes may provide vastly different solutions to the same dataset (e.g. the four analysis of WASP-63b presented by [3]).

To test the robustness of the retrieval approach to this sort of issue we here present a comparison of three different retrieval codes, all of which have been previously used to analyse transmission spectra of exoplanets. *NEMESIS* was originally an optimal estimation retrieval algorithm developed for solar system planets [2], which was expanded to include exoplanets [4] and has recently been upgraded to incorporate a nested sampling algorithm. *TauREX* [8] and *CHIMERA* [5] were both developed for application to exoplanet spectra and also use a nested sampling algorithm.

2. Forward model comparison

The first step of the retrieval comparison was to check that the forward models in each case showed reasonable agreement. We compared output transmission spectra for simple model atmospheres including only a single spectrally active gas, with isothermal temperature profiles. We then moved on to comparing more realistic planet models, including simple clouds and combinations of spectrally active gases. An example is shown in Figure 1; this planet is a super Earth with a cloud-free H_2-dominated atmosphere and an isothermal temperature of 400 K. Trace species in the atmosphere include NH_3, CH_4, and H_2O. An excellent agreement was obtained between the three forward models.

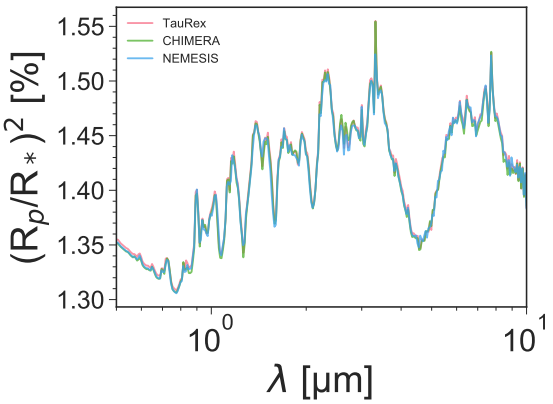

Figure 1: Synthetic transmission spectra for the same model planet generated by each of the three retrieval codes.

3. Retrieval comparison

We take the more realistic model planets such as the case discussed in Section 2 and bin the spectra down to a resolution of R=100 over the wavelength range of 0.5–10 μm. These spectra are cross-retrieved between the three algorithms to assess whether spectra generated with one model can be accurately retrieved using the others. We test error bars at 30, 60 and 100 ppm, with no noise added directly to the spectra to avoid outliers within a noise draw introducing bias into our results. We find that in the majority of cases the cross retrievals produce the correct result, demonstrating that our retrieval codes have been successfully benchmarked against each other.

4. Summary and Conclusions

Benchmarking of forward model and retrieval codes is an important preparatory step for the interpretation of exoplanet spectra obtained with *JWST* and *ARIEL*. We have shown that comparable output can be obtained using retrieval codes with different development histories and parameterizations, and hope this will encourage future efforts in this area.

Acknowledgements

JKB is supported by a Royal Astronomical Society Research Fellowship. IW is supported by European Research Council Starter Grant ExoAI.

References

[1] Barstow, J. K., Aigrain, S., Irwin, P. G. J., & Sing, D. K. 2017, The Astrophysical Journal, 834, 50

[2] Irwin, P. G. J., Teanby, N. A., de Kok, R., et al. 2008, Journal of Quantitative Spectorscopy and Radiative Transfer, 109, 1136

[3] Kilpatrick, B. M., Cubillos, P. E., Stevenson, K. B., et al. 2017, ArXiv e-prints, arXiv:1704.07421

[4] Lee, J.-M., Fletcher, L. N., & Irwin, P. G. J. 2012, Monthly Notices of the Royal Astronomical Society, 420, 170

[5] Line, M. R., Wolf, A. S., Zhang, X., et al. 2013, The Astrophysical Journal, 775, 137

[6] Madhusudhan, N., Crouzet, N., McCullough, P. R., Deming, D., & Hedges, C. 2014, ApJL, 791, L9

[7] Tsiaras, A., Waldmann, I. P., Zingales, T., et al. 2017, ArXiv e-prints, arXiv:1704.05413

[8] Waldmann, I. P., Tinetti, G., Rocchetto, M., et al. 2015, The Astophysical Journal, 802, 107

EPSC Abstracts
Vol. 12, EPSC2018-483, 2018
European Planetary Science Congress 2018

First results of ESA's OGS multi-band observations of extra-solar planets

Ana Maria Heras (1), **Anamarija Stankov (1)**, Stefanie Rätz (2), Goran Pilbratt (1), Louis Dubois (1), Philippe Gondoin (1), Rita Schulz (1), Pierre Ferruit (1), Giovanna Giardino (1), Kate Isaak (1)
(1) European Space Agency, ESTEC, Noordwijk, The Netherlands (Anamarija.Stankov@esa.int)
(2) Institute for Astronomy and Astrophysics Tübingen (IAAT), Eberhard-Karls-Universität Tübingen, Tübingen, Germany

Abstract

We present first results of the analysis of multiwavelength broad-band photometry observations of planetary transits undertaken with the OGS spectrograph in autumn 2017 and spring 2018.

1. Introduction

The ESA Optical Ground Station (OGS) is a 1-m telescope located at the Teide Observatory, Tenerife. It is equipped with a spectrograph with capabilities for imaging and broad-band spectrometry by using filters, as well as dispersive spectroscopy.

Figure 1: View of the Spectrograph mounted on the OGS telescope, showing the liquid N cooling system.

Since the first commissioning run in February 2015, several observation campaigns of exoplanet transits, with a typical duration of one to two weeks, have been undertaken.

This is a follow-up of the exoplanet transit observations that have been performed in 2015-16 and where in total 20 exoplanet transits were observed.

2. Exoplanet transit observations (2017-2018 campaigns)

The main objectives of these observations were to check the feasibility and scientific capability of the spectrograph at the OGS for quasi-simultaneous multi-band photometry of planetary transits.

Photometry of planetary transits in several visible wavelength bands can provide a first view on the nature of the planetary atmosphere. It also allows to determine the planet and orbit parameters with high precision by removing the effect of the stellar activity from the transit profile. This kind of observations also complement spectroscopic observations in the infrared. In a cloudless atmosphere, visible multiwavelength observations allow for measuring the Rayleigh slope of the planet's reflected light, and therefore to derive the atmosphere mean molecular weight [1].

The data reduction and analysis is currently ongoing and results will be presented in this poster.

3. References

[1] Benneke, B, and Seager, S.: Atmospheric Retrieval for Super-Earths: Uniquely Constraining the Atmospheric Composition with Transmission Spectroscopy, ApJ 753, 100, 2012

EPSC Abstracts
Vol. 12, EPSC2018-500, 2018
European Planetary Science Congress 2018

SHINE, the SPHERE High-Contrast Imaging Survey for Exoplanets

M. Langlois (1,2), for the **SHINE Team [3]**
(1) CRAL, UMR 5574, CNRS, Université de Lyon, Ecole Normale Supérieure de Lyon, F-69364 Lyon Cedex 07, France
(2) Aix Marseille Université, CNRS, LAM (Laboratoire d'Astrophysique de Marseille) UMR 7326, 13388 Marseille, France

Abstract

The SHINE survey for SPHERE High-contrast ImagiNg survey for Exoplanets, is a large direct imaging near-infrared survey of 600 young, nearby stars carried out in the context of the SPHERE consortium Guaranteed Time Observations representing 200 nights spread between 2015 and 2020. Our scientific goals are to characterize known planetary systems (architecture, orbit, stability, luminosity, atmosphere), to search for new planetary systems using SPHERE's unprecedented performances, finally to determine the occurrence and orbital and mass function properties of the wide-orbit, giant planet population as a function of the stellar host mass and age.

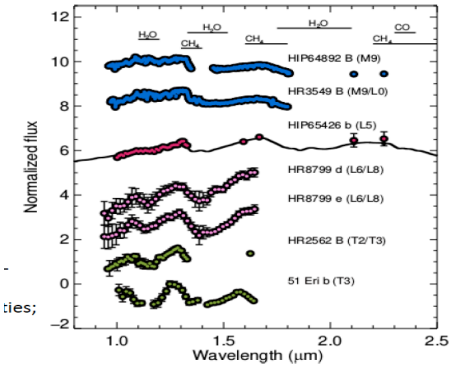

Figure 1: SHINE survey exoplanets/Brown Dwarfs characterization

In this talk, after summarizing the SHINE strategy and current performances after almost 4 years of operation, I will review the breakthrough results obtained so far including the discoveries of new exoplanet/BD companions and disks, the study of young planetary system architecture and stability, the fine characterization of the physical properties and atmospheres of the lightest and coolest Jovian exoplanets imaged to date, and finally the survey completeness and the constraints set on the occurrence and the formation of giant planets beyond 5-10au.

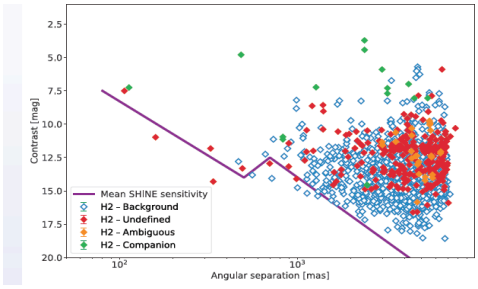

Figure 2: SHINE survey detection limits, candidate companions contrast and classification using astrometry and color-magnitude diagram rejection (Langlois, In prep.)

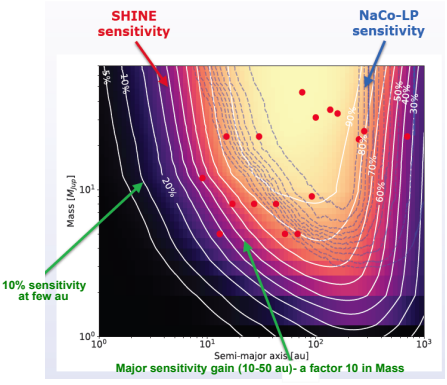

Figure 3: QMESS (Bonavita, 2013) average detection probability for SHINE using observed targets (Vigan, In prep.)

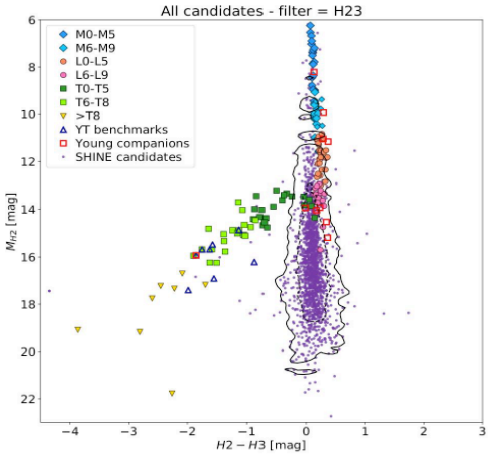

Figure 4: Color-magnitude diagram including all SHINE candidates and example of known systems.

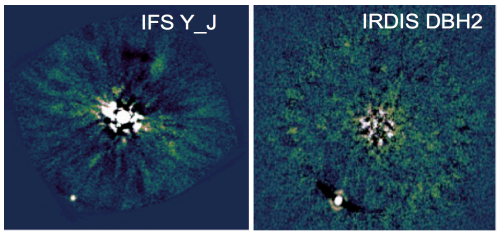

Figure 5: Illustration of the SHINE high contrast capability – Images of the newly discovered exoplanetary HIP65426 b (Chauvin et al. 2017).

Conclusions

The SHINE program is a large high-contrast near-infrared survey of more than 600 young, nearby stars. Aiming at searching for and characterizing new planetary systems using VLT/SPHERE, it achieves unprecedented high-contrast and high-angular resolution capabilities which bring fine characterization of the physical properties and atmospheres of Jovian exoplanets and new statistical constraints on the occurrence and orbital properties of the giant planet population at large orbits as a function of the stellar host mass and age.

Acknowledgements

We acknowledge financial support from the Programme National de Planétologie (PNP) and the Programme National de Physique Stellaire (PNPS) of CNRS-INSU. This work has made use of the SPHERE Data Centre, jointly operated by OSUG/IPAG (Grenoble), PYTHEAS/LAM/CESAM (Marseille), OCA/Lagrange (Nice) and Observtoire de Paris/LESIA (Paris). We thank P. Delorme and E. Lagadec (SPHERE Data Centre) for their efficient help during the data reduction process. SPHERE is an instrument designed and built by a consortium consisting of IPAG (Grenoble, France), MPIA (Heidelberg, Germany), LAM (Marseille, France), LESIA (Paris, France), Laboratoire Lagrange (Nice, France), INAF–Osservatorio di Padova (Italy), Observatoire de Genève (Switzerland), ETH Zurich (Switzerland), NOVA (Netherlands), ONERA (France) and ASTRON (Netherlands) in collaboration with ESO. SPHERE was funded by ESO, with additional contributions from CNRS (France), MPIA (Germany), INAF (Italy), FINES (Switzerland) and NOVA (Netherlands). SPHERE also received funding from the European Commission Sixth and Seventh Framework Programmes as part of the Optical Infrared Coordination Network for Astronomy (OPTICON) under grant number RII3-Ct-2004-001566 for FP6 (2004–2008), grant number 226604 for FP7 (2009–2012) and grant number 312430 for FP7 (2013–2016).

References

[1] M. Bonavita, E. J. W. de Mooij and R. Jayawardhana, Publications of the Astronomical Society of the Pacific, Vol. 125, No. 929 (July 2013), pp. 849-856

[2] Chauvin , G. et al. 2017, A&A 605, L9 (2017)

[3] Langlois et al. (in prep) - SHINE survey observations, reduction and analysis, detection performances & early-results

[4] Vigan et al. (in prep)- SHINE First constraints on the population of young giant exoplanets from the early statistical sample

[5] SHINE Team: G. Chauvin, S. Desidera, M. Bonnefoy, A. Cheetham, M. Feldt, R. Gratton, A.-M. Lagrange, M. Langlois, M. Meyer, A. Vigan, B. Biller, A. Boccaletti, M. Bonavita, S. Daemgen, P. Delorme, V. D'Orazi, R. Galicher, J. Hagelberg, M. Janson, H. Le Coroller, R. Ligi, A.-L. Maire, S. Messina, A. Mueller, S. Perretti, M. Samland, E. Sissa, C, A. Zurlo + the SPHERE consortium

EPSC Abstracts
Vol. 12, EPSC2018-628, 2018
European Planetary Science Congress 2018

Detectability of Atmospheric Features of Terrestrial Planets in the Habitable Zone around M-dwarfs

Fabian Wunderlich (1), Mareike Godolt(1), John Lee Grenfell (2), Steffen Städt (3), Heike Rauer (1,2,4), Stefanie Gebauer (2), Franz Schreier (3) and Pascal Hedelt (3)
(1) Zentrum für Astronomie und Astrophysik, Technische Universität Berlin, Hardenbergstraße 36, 10623 Berlin (fabian.wunderlich@tu-berlin.de), (2) Institut für Planetenforschung, Deutsches Zentrum für Luft- und Raumfahrt, Rutherfordstraße 2, Berlin, Germany, (3) Institut für Methodik der Fernerkundung, Deutsches Zentrum für Luft- und Raumfahrt, Oberpfaffenhofen-Wessling, Germany, (4) Institut für Geologische Wissenschaften, Freie Universität Berlin, Malteserstr. 74-100, Berlin, Germany

Abstract

Small extrasolar planets around M-dwarfs are prime targets in the search for habitable surface conditions and biosignatures with current and near-future telescopes like JWST and E-ELT. For the characterization of their atmosphere, model calculations are needed to predict and interpret potential planetary conditions. Especially the UV Spectral Energy Distribution (SED) is crucial for the photochemical processes in the atmosphere which would e.g. impact the signals from a potential biosphere or cause false positive biosignatures. Here we investigate the atmospheric conditions and spectral appearance of virtual Earth-like exoplanets in the Habitable Zone (HZ) of different observed M-dwarf stars. As input for our coupled one-dimensional climate-chemistry-model we use spectra of 10 observed M1V to M5.5V stars, which differ in the UV SED by several orders of magnitude. With a line-by-line radiative transfer model we calculate synthetic emission and transmission spectra using the resulting atmospheric composition and temperature profiles. We furthermore discuss which biomarker and bioindicator absorption bands are potentially detectable by space-borne JWST or the ground-based E-ELT. Due to weak stellar UV emissions at wavelengths higher than 0.2 μm, planets orbiting M-stars show an increase in the abundance of certain biomarkers and bioindicators (CH_4, H_2O, N_2O) compared to the Earth around the Sun. Therefore the transmission spectra show strong absorption features for these species. The ozone profiles show a high dependency on the UV radiation below 0.2 μm. High UVC radiation can increase the ozone mixing ratio in the stratosphere by several orders of magnitude in comparison to a low UVC environment. The profiles of many biosignatures however lack a strong dependency on the stellar spectral type, hence planets around cool and warm M-dwarfs can have a similar chemical composition if their SED show minor differences in the UV. To investigate the impact of these photochemical responses upon the spectroscopic detectability of absorption bands with JWST and E-ELT we calculate Signal-to-Noise-Ratios (SNR) including photon and instrument noise for all the modelled atmospheric scenarios. We show that for transmission spectra even higher abundances of e.g. O_3 or CH_4 produce a small SNR for warmer M-dwarfs because of the lower ratio between planetary and stellar radius.

EPSC Abstracts
Vol. 12, EPSC2018-669, 2018
European Planetary Science Congress 2018

New Insights into Cosmic Ray induced Biosignature Chemistry in Earth-like Atmospheres

Markus Scheucher (1), Lee Grenfell (2), Mareike Godolt (1), Franz Schreier (3) and Heike Rauer (2)
(1) Zentrum für Astronomie und Astrophysik, Technische Universität Berlin, 10623 Berlin, Germany (scheucher@tu-berlin.de)
(2) Institut für Planetenforschung, Deutsches Zentrum für Luft- und Raumfahrt, 12489 Berlin, Germany
(3) Institut für Methodik der Fernerkundung, Deutsches Zentrum für Luft- und Raumfahrt, 82234 Oberpfaffenhofen, Germany

Abstract

With the recent discoveries of terrestrial planets around active M-dwarfs, better understanding of atmospheric responses to the stellar environment becomes of high importance. Destruction processes which mask the possible presence of life are getting large attention in the exoplanet community.
We investigate the habitability and potential biosignatures of planets having Earth-like (N_2-O_2 dominated) atmospheres orbiting in the habitable zone of the M-dwarf star AD Leo. Such atmospheres are strongly bombarded by high energetic particles which can create showers of secondary particles down to the surface. We apply our cloud-free 1D climate chemistry model to study the influence of key particle shower parameters and chemical efficiencies of NOx and HOx production from cosmic rays. We determine thereby the effect of stellar radiation and cosmic rays upon atmospheric composition, temperature, and spectral appearance. Results suggest that despite strong stratospheric O_3 destruction by cosmic rays, smog O_3 can significantly build up in the lower atmosphere of our modeled planet around AD Leo. We discuss the importance of the Sun's higher UVB flux compared to AD Leo to keep tropospheric O_3 abundances from building up on Earth. N_2O abundances first decrease with increasing flaring energies due to O_3 loss hence stronger photolytic destruction by UV. This decrease in abundance weakens however for the strongest flaring cases because a sink reaction for N_2O with excited oxygen becomes weaker. CH_4 is removed mainly by atomic chlorine in the upper atmosphere for strong flaring cases and not via removal with hydroxyl as is otherwise usually the case. Cosmic rays lead to lower CH_4 abundances which weakens the role of CH_4 in heating the middle atmosphere so that H_2O absorption can play a more important role. Our results additionally underline the importance of HNO_3 as a possible marker for strong stellar particle showers, which is especially apparent in the forward-modeled transmission spectra of our virtual Earth-like planet around AD Leo.

Summary

In a nutshell, uncertainty in the efficiencies of abiotic NOx and HOx production from cosmic rays in our model significantly influences biosignature abundances and their spectral appearances during transits of our modeled Earth-like planets around the M-dwarf star AD Leo.

EPSC Abstracts
Vol. 12, EPSC2018-681, 2018
European Planetary Science Congress 2018

Model Atmospheres for Volatile-Rich Hot Rocky Planets

Roxana E. Lupu (1,2), Bruce Fegley (3), Mark Marley (2) and Katharina Lodders (3)
(1) BAER Institute, California, USA, (2) NASA Ames Research Center, California, USA (roxana.e.lupu@nasa.gov), (3) Washington University in St. Louis, Missouri, USA

Abstract

We are building a versatile set of self-consistent atmospheric models to calculate the structure, composition, and spectra of hot rocky exoplanets in short period orbits. To date, more than 100 such hot rocky exoplanets have been confirmed, and they will form the majority of small planets in close-in orbits to be discovered by the TESS and Kepler K2 missions. These hot worlds offer the best opportunity to characterize rocky exoplanets with current and future instruments. We are using a fully non-grey radiative-convective atmospheric structure code with cloud formation combined with a self-consistent treatment of gas chemistry above the magma ocean. Being in equilibrium with the surface, the vaporized rock material can be a good tracer of the bulk composition of the planet. We are investigating both volatile-poor and volatile-rich compositions, with the volatile-poor ranging from completely depleted, to water-free (Venus-like), to containing only sulfur and halogens (Io-like). To properly account for these exotic compositions and thermodynamic regimes, we are working on a self-consistent treatment of vertical mixing, condensation, and non-ideal gas behavior. We present our preliminary results for the atmospheric structure of volatile-rich hot rocky as a function of planet-star distance. Our models will inform follow-up observations with JWST and ground-based instruments, aid the interpretation of transit and eclipse spectra, and provide a better understanding of volatile behavior in these atmospheres.

1.Introduction and Methods

Hot rocky planets in short and ultra-short orbits will offer us the first opportunities to characterize rocky planets outside our Solar System. Such targets will be scheduled among the first transit and eclipse observations for JWST. However, we currently lack a reliable set of models to guide the planning of such observations and help their interpretation.

1.1 Ultra-Short period planets

Ultra-short period (USP) planets have orbital periods of the order of a day or less [1]. They undergo strong irradiation from the host star. Their atmosphere is thought to be the result of evaporation from the hot surface and stellar processing. A few such rocky planets have measured masses and radii, which are consistent with a rocky composition, as shown in Table 1.

Table 1: USP planets with measured masses and radii

Planet	p (days)	a (AU)	Mass (M_{Earth})	Radius (R_{Earth})
Kepler 78b	0.36	0.01	1.87	1.2
Kepler 10b	0.84	0.0168	3.72	1.47
Corot 7b	0.85	0.0172	4.73	1.585
K2-106b	0.57	0.0116	8.36	1.52
HD 3167b	0.96	0.0182	5.02	1.575
K2-131b	0.37	0.0100	6.5	1.81
WASP-47e	0.79	0.0173	6.83	1.81
55 Cnc e	0.74	0.0154	6.4	1.92
K2-141b	0.28	0.0073	5.08	1.51

1.2 Equilibrium Chemistry

We are investigating a range of compositions from volatile rich to volatile poor. In the volatile-rich limit we started with the compositions of bulk silicate Earth (BSE) and continental crust (CC) from [3], and solar abundances for comparison purposes. The equilibrium abundances take into account condensation and gas-rock equilibrium. Work on other compositions, such as Venus-like and Io-like is in progress. Preliminary work shows that the atmospheres of Io-like planets will be dominated by SO2 and sulfur-bearing hazes and condensates. The inclusion of clouds and hazes in these models will be essential for reproducing these atmospheres.

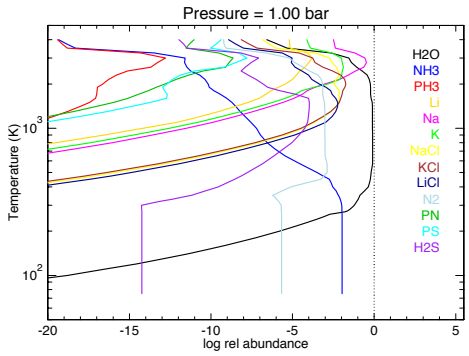

Figure 1: Plot of the most abundant species as a function of temperature at 1 bar pressure for the bulk silicate earth composition, assuming equilibrium chemistry.

1.2 Molecular Opacities

We have vastly increased our already large opacity database by adding new molecules with line lists computed by the ExoMol group. These are: AlO, CS, CaO, KCl, LiH, NaCl, PO, PS, CH, CN, CP, NH, NaH, PN, ScH, and TiH. For our conditions, the most important will be NaCl and KCl. The H2O and CH4 opacities are shown for comparison.

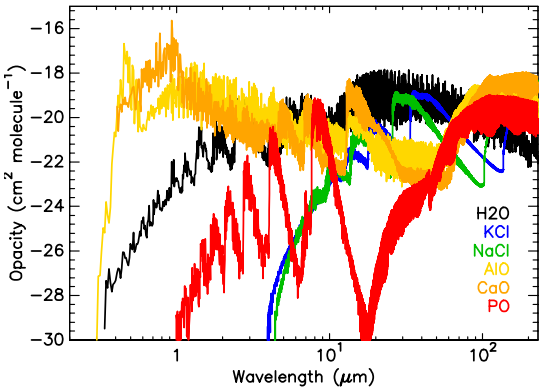

Figure 2: Opacity calculations for several new species. NaCl and KCl are abundant species in our context, and H2O is shown for comparison.

2.Results

2.1 Radiative-Convective Equilibrium Models

Using our well-tested radiative-convective equilibrium code [3],[4],[5] we ran models for these three compositions, at decreasing separation between the planet and the star. We build 1D models for a planet similar to Kepler 78b: g=13 m/s2, around a 5100 K star (BT-settl model with log g=4.5), with surface pressure from 1 to 100 bar. We vary the distance from the star from 0.05 to 0.01 AU to follow the changes in atmospheric structure. These preliminary models do not include clouds and hazes. We calculate the abundance profiles by interpolating the equilibrium chemistry tables on the new pressure-temperature profiles. The solar composition will produce a case similar to a hot Jupiter, up to the surface boundary conditions.

In all cases (for all three compositions) we note a turnover of the pressure-temperature profiles around 0.011 AU from the star. This is similar to the finding for hot Jupiters in [6] (two families , as a function of stellar irradiation). The strong thermal inversion in the upper atmosphere could be due to a new absorber at these temperatures, but this effect might be mitigated by photochemistry. We will address this aspect in future work.

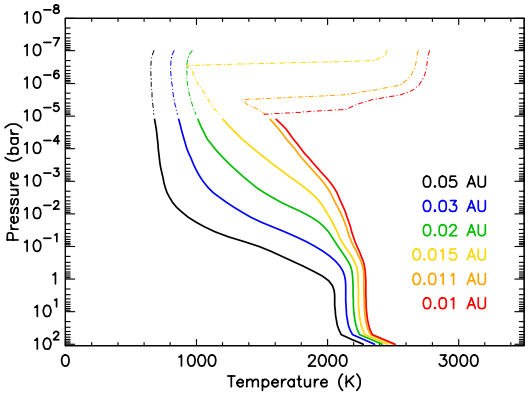

Figure 3: Pressure-temperature profiles for the BSE compositions at various distances from the star.

2.2 Abundances profiles

Using the abundance profiles corresponding to the equilibrium structure, we select the strongest absorbers by multiplying the abundances with the opacities at 2000 K and 0.1 and 1 bar. These will be representative for the hottest planets, closest to the star. Methane will start to dominate as the models approach 1000 K. The first eight highest contributors are selected.

The figures below show a comparison between the vertical molecular abundance profiles for the BSE composition at 0.05 AU and 0.01 AU, respectively. While these atmospheres are dominated mostly by water and CO2, we note other dominant species, such as K, Na, HCl, HF, NaCl, and SO2. These profile will be further affected by vertical mixing and photochemistry.

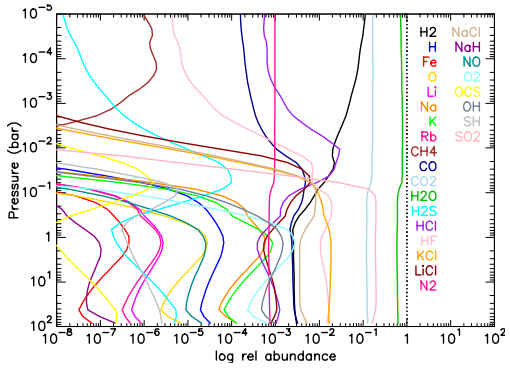

Figure 4: Molecular abundances for the BSE composition at 0.05 AU from the star

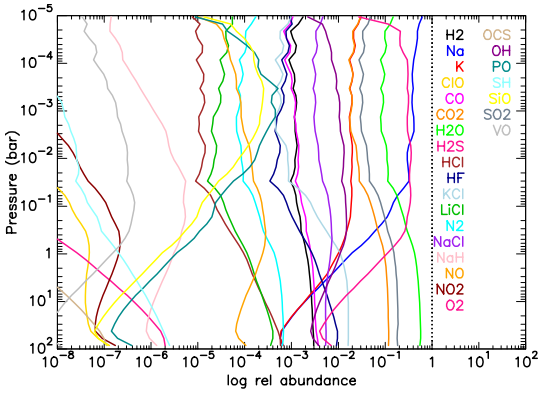

Figure 5: Molecular abundances for the BSE composition at 0.01 AU from the star

2.3 Thermal emission and secondary eclipse spectra

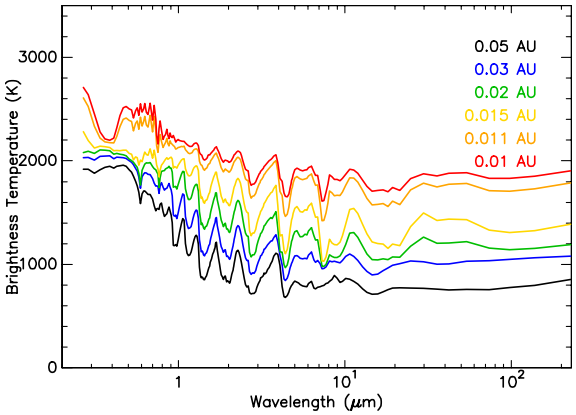

Figure 6: Thermal emission for the Bulk Silicate Earth composition as a function of distance from the host star.

The thermal emission of the planets results as a by-product of our radiative-convective equilibrium model. Due to calculation speed constraints in this iterative code, the radiative transfer treatment uses the correlated-k coefficients method with 196 windows from 0.25 to 200 microns, which results in a low-resolution spectrum. A high resolution version can be calculated using a line-by-line code.

We calculate the secondary eclipse depths assuming the radii for the Kepler 78 system. Work on the transit spectra is in progress.

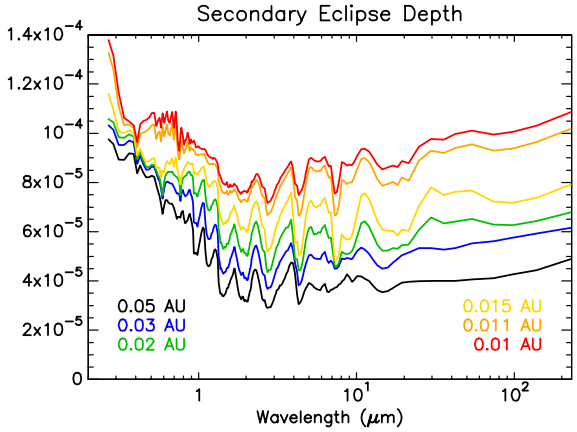

Figure 7: Secondary eclipse spectra for the Bulk Silicate Earth composition as a function of distance from the host star.

3. Summary and Future Work

We present a series of models for volatile-rich hot rocky planets, as a function of distance from the host star. We have investigated three possible compositions, namely solar, bulk silicate earth, and continental crust. The solar composition is taken as a reference case, where we recover the known results for hot Jupiters, with some extra opacity sources. In all cases we wind a turn-over of the pressure-temperature profile when the planet is at 0.011 AU or closer to the star. This change could be due to a new absorber becoming important in the upper atmosphere, and has a detectable signature in both thermal emission and secondary eclipse spectra. we are working on refining these models by taking into account photochemistry, clouds and hazes, and the possibility of disequilibrium chemistry.

Acknowledgements

The authors wish to thank the NASA ROSES XRP program for funding this research. R.L. also thanks Richard Freedman for continuous help with expanding and improving the opacity database.

References

[1] Sanchis-Ojeda R, et al, 2014, ApJ, 787, 47

[2] Lupu, R. E., et al. 2014, ApJ, 784, 27

[3] Marley, M. S., Gelino, C., Stephens, D., Lunine, J. I., & Freedman, R. 1999, ApJ, 513, 879.

[4] Marley, M. S., & McKay, C. P. 1999, Icarus, 138, 268.

[5] McKay, C. P., Pollack, J. B., & Courtin, R. 1989, Icarus, 80, 23

[4] Fortney, J. J., Lodders, K., Marley, M. S., & Freedman, R. S., ApJ, 678, 1419

EPSC Abstracts
Vol. 12, EPSC2018-705, 2018
European Planetary Science Congress 2018

Stellar and Exoplanetary Atmospheres Bayesian Analysis Simultaneous Spectroscopy

Giuseppe Morello (1), Angelos Tsiaras (2), Ian Howarth (2) and Pierre-Olivier Lagage (1)
(1) CEA/Saclay, France, (2) University College London, UK (giuseppe.morello@cea.fr)

Abstract

We present the results of Stellar and Exoplanetary Atmospheres Bayesian Analysis Simultaneous Spectroscopy (SEA BASS) for several systems. SEA BASS is a scheme that enables simultaneous derivation of four-coefficient stellar limb-darkening profiles, transit depths and orbital parameters from exoplanetary transits at multiple wavelengths. The fully empirical approach is recommended to avoid potential biases in transit depth due to the use of limb-darkening coefficients obtained from stellar-atmosphere models. We show that, in some cases, inaccurate limb-darkening parameterisations and/or orbital parameters may impart trends on the derived exoplanetary spectra, therefore leading to erroneous characterisation of the exoplanet atmospheres. We discuss how to minimise the parameter degeneracies that otherwise would significantly inflate the error bars or prevent the convergence of the fit. Finally, we assess the reliability and accuracy of state-of-the-art stellar-atmosphere models for describing the limb-darkening profiles of a range of stellar types.

1. Introduction

Characterisation of the atmospheres of transiting exoplanets relies on accurate measurements of the extent of the optically thick area of the planet at multiple wavelengths with a precision $\lesssim$100 parts per million (ppm). Next-generation instruments onboard the James Webb Space Telescope (JWST) are expected to achieve $\sim$10 ppm precision for several tens of targets. A similar precision can be obtained in modeling only if other astrophysical effects, including the stellar limb-darkening (the radial decrease in specific intensity), are properly accounted for. Stellar-atmosphere models are commonly used to predict the limb-darkening profiles, but empirical estimates are desirable, both to test the stellar models and to reduce potential biases in transit depths due to errors in the theoretical models or to other second-order effects, such as stellar activity, granulation, gravity darkening, etc. Numerous functional forms, so-called limb-darkening laws, have been proposed in the literature to approximate the stellar intensity profile with different numbers of coefficients. While some two-coefficient laws are appropriate for certain stellar types and passbands [Espinoza & Jordan 2016, Morello et al. 2017, Maxted 2018], the Claret's four-coefficients formula is the most robust over all stellar types and passbands [Claret 2000, Morello et al. 2017].

2. The method

The SEA BASS method consists of measuring the "geometric" orbital parameters from infrared transit observations, then implementing the results as informative priors when model-fitting at shorter wavelengths. The impact parameter, b, and central transit duration, T_0, constitute an equivalent set of less correlated parameters than the semi-major axis in units of stellar radius, a/R_*, and inclination, i. The SEA BASS approach is motivated by the smaller limb-darkening effect in the infrared, which mitigates the potential biases due to inaccurate models, and the negligible wavelength-dependence of a/R_* and i. Different variants of the original algorithm, such as using multiple infrared passbands with fixed (four) or free (two) limb-darkening coefficients to derive the geometric priors, will be discussed.

3. Results

3.1. Synthetic datasets

Figure 1 show the results in transit depth of the SEA BASS fit (and others) on synthetic datasets [Morello et al. 2017]. The use of informative priors on a/R_* and i is necessary to enable convergence of the fit with free four-coefficient limb-darkening; the resulting error bars are smaller than those obtained with free two-coefficient limb-darkening and uniform priors on a/R_* and i.

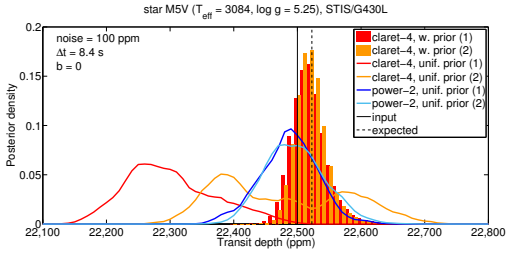

Figure 1: Histograms (red and orange channels) of the MCMC-sampled posterior distributions of the transit depth for a hot-Jupiter in front of a M5 dwarf, *Hubble* STIS/G430L passband, fitting R_p/R_*, a/R_*, i, claret-4 limb-darkening coefficients and the normalization factor, adopting gaussian priors on a/R_* and i. The histogram channels are half-thick and shifted to improve their visualization. The red and orange lines denotes the analogous posterior distributions with non-informative priors for all parameters (the shape and the discrepant results indicate that the chains did not converge, in this case). The blue and light-blue lines are for the case of power-2 limb-darkening and non-informative priors for all parameters.

3.2. Real datasets

Figure 2 compares the empirical limb-darkening profiles obtained for HD209458 over five *HST*/STIS passbands in the range 290–570 nm with some reference models [Morello 2018]. The discrepancies are significant for the three passbands with the highest Signal-to-Noise Ratio (SNR). Figure 3 compares the relevant exoplanet transmission spectra. In this case, no significant biases are obtained when using fixed limb-darkening coefficients from stellar-atmosphere models. However, HD209458 is relatively well-known, because it is a Sun-like star. The preliminary analyses on other systems present larger effects in the exoplanet transmission spectra.

4. Conclusions

We performed self-consistent analyses of infrared to visible exoplanetary transits to obtain accurate transmission spectra of the exoplanet atmospheres and stellar limb-darkening profiles (SEA BASS). The new method is necessary to avoid the potential biases introduced by the stellar-atmosphere models, which, in some cases, may significantly alter the exoplanet spectra. We also assess the reliability and accuracy of state-of-the-art stellar-atmosphere models for describing the limb-darkening profiles of a range of stellar types.

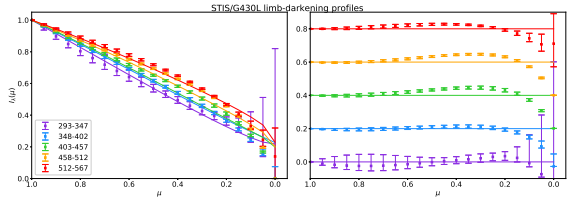

Figure 2: Left panel: empirical limb-darkening profiles obtained from the spectral lightcurve fits (differently coloured squares) and theoretical models computed by [Knutson et al. 2007] (same color lines). Right panels: residuals between the empirical and theoretical profile with vertical offsets.

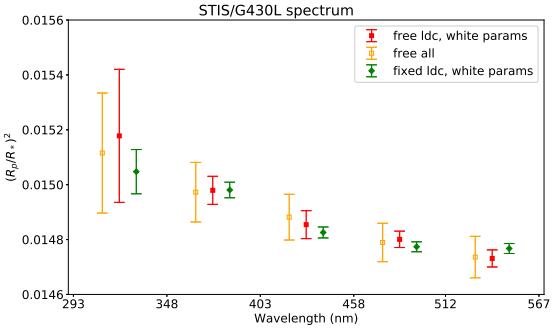

Figure 3: Transit depths for five spectral bins, using: b and T_0 fixed to the Spitzer/IRAC weighted mean values, phase shifts obtained from the white light-curve fit, and free limb-darkening cofficients (red, full squares), or fixed limb-darkening coefficients reported by [Knutson et al. 2007] (green diamonds), all free parameters with Spitzer/IRAC weighted mean priors on b and T_0 (orange, empty squares).

Acknowledgements

The research leading to these results has received funding from the European Union's Horizon 2020 Research and Innovation Programme, under Grant Agreement 776403. G. Morello was also supported by the LabEx P2IO, the French ANR contract 05-BLAN-NT09-573739 and the ERC project ExoLights (617119).

References

[Claret 2000] Claret, A., 2000, A&A, 363, 1081

[Espinoza & Jordan 2016] Espinoza, N., & Jordan, A., 2016, MNRAS, 457, 3573

[Knutson et al. 2007] Knutson, H. A., Charbonneau, D., Allen, L. E., et al., 2007, Nature, 447, 183

[Maxted 2018] Maxted, P. F. L., 2018, arXiv:1804.07943

[Morello et al. 2017] Morello, G., Tsiaras, A., Howarth, I. D., and Homeier, D., 2017, AJ, 154, 111

[Morello 2018] Morello, G., 2018, arXiv:1712.09393

EPSC Abstracts
Vol. 12, EPSC2018-716-2, 2018
European Planetary Science Congress 2018

Mass-Radius Contribution of Sub-Neptunian Atmospheres

Jasmine MacKenzie (1), Philipp Baumeister (1), Mareike Godolt (1), and Nicola Tosi (1,2)
(j.mackenzie@tu-berlin.de)
(1) Zentrum für Astronomie und Astrophysik, Technische Universität Berlin, Berlin, Germany
(2) Institut für Planetenforschung, Deutsches Zentrum für Luft- und- Raumfahrt, Berlin, Germany

Abstract

As the number of discovered exoplanets has increased and the methods used to characterize them have improved, more and more focus has been given to how the atmosphere of a transiting planet affects the observed radius. This is especially true for planets with masses M < $20M_{\oplus}$ and radii R < $4R_{\oplus}$, the so-called sub-Neptunian regime. These planets have densities that can be modeled by a wide variety of interior structures, whose solutions are highly degenerate. Therefore, how one calculates the physical radius of a planet and the contribution by its atmosphere to the measured transiting radius is of great importance to the study and characterization of exoplanets.

For planets that can be modeled with an extended atmosphere, which includes many sub-Neptunes, small differences in atmospheric mass can result in a large contribution to the radius, particularly if the atmosphere mainly consists of hydrogen and helium accreted during its formation. The atmospheric composition affects the measured transit radius, which is defined as where the atmosphere becomes optically thick for a given wavelength. Therefore, the variation in planetary radius at different wavelengths could then be used to infer the atmospheric composition.

In the literature, there are many different approaches for calculating the radius contribution of an atmosphere in interior structure modelling. We will review these approaches and investigate the influence of the paramters used. We will further more compare different approaches used to evaluate the potential atmospheric escape as a first step in determining whether the planets hold a primodial or secondary atmosphere. In particular, the importance of stellar models in the X-ray and EUV regiem, and how the composition of the primoridal atmosphere affects the planetary surface and interior, which in turn will affect the composition of the secondary atmosphere.

Acknowledgements

Jasmine MacKenzie and Philipp Baumeister acknowledges the support of the DFG priority program SPP 1992 "Exploring the Diversity of Extrasolar Planets" (GO 2610/2-1 & TO 704/3-1)

EPSC Abstracts
Vol. 12, EPSC2018-723, 2018
European Planetary Science Congress 2018

Transmission spectroscopy with the ACE-FTS infrared spectral atlas of Earth: A model validation and feasibility study

Franz Schreier (1), Steffen Städt (1), Pascal Hedelt (1), and Mareike Godolt (2)
(1) DLR – German Aerospace Center, Remote Sensing Technology Institute, Oberpfaffenhofen, Germany,
(2) Technische Universität Berlin, Zentrum für Astronomie und Astrophysik (TUB-ZAA), Berlin, Germany

Abstract

For an assessment of the detectability of molecular concentrations from transit spectra of Earth-like exoplanets, occultation spectra observed by the ACE-FTS instrument onboard the Canadian Earth observation satellite "SciSat" mission have been modeled with a line-by-line infrared radiative transfer code. For a quantitative estimate of visibility and detectability the maximum change of the residual spectrum, the relative change of the residual norm, the additional transit depth, and signal-to-noise ratios for a JWST setup are considered.

1. Introduction

With more than 3700 exoplanets known today, including some dozen Earth-likes and super-Earths, the characterization of their atmospheres has come into the focus of current research. Despite the limited quality of currently available exoplanet spectral observations, the methodology developed for Earth and Solar System Planet remote sensing can be readily applied to the analysis of terrestrial extrasolar planet data. For the retrieval of atmospheric composition, transmission spectroscopy analyzing the attenuation of stellar light along its optical path through the planet's atmosphere is particularly suited. In this contribution we use a high resolution line-by-line infrared radiative transfer code to model co-added occultation measurements in order to assess the feasibility to quantify the concentration of atmospheric constituents. (Preliminary results had been reported at EPSC 2017.)

2. Radiative Transfer Modeling

The Generic Atmospheric Radiative Transfer Line-by-Line Infrared Code — GARLIC [1] has been developed with emphasis on efficient and reliable numerical algorithms and a modular approach appropriate for simulation and/or retrieval in a variety of applications (observation geometry, instrumental spectral response and field–of–view). GARLIC has been extensively verified in several intercomparison studies, e.g. [2]. The core of GARLIC's subroutines constitutes the basis of forward models used to implement inversion codes to retrieve atmospheric state parameters from limb and nadir sounding instruments. Furthermore, GARLIC has been used for a variety of exoplanetary atmosphere studies, e.g. [3, 4, 5].

3. Earth Observation Data

Limb sounding in the microwave, infrared, and ultraviolet-visible spectral range is a well-established approach for the characterization of Earth's atmosphere. We take a limb sequence of representative cloud-free infrared (2.2 – 13.3 μm) transmission spectra [6] recorded by the space-borne ACE-FTS Earth observation mission [7] and combine these spectra to the effective height of the atmosphere. These data are compared to spectra modeled with GARLIC to study the impact of individual molecules, spectral resolution, the choice of auxiliary data, and numerical approximations. Moreover, this study can also be considered as a validation of GARLIC.

4. Results

The largest impact on the transit spectra is due to water, carbon dioxide, ozone, methane, nitrous oxide, nitrogen, nitric acid, oxygen, and some chlorofluorocarbons (CFC11 and CFC12). The effect of further molecules considered in the modeling is either marginal or absent. The best matching model with 17 molecules absorbing has a mean residuum of 0.4 km

and a maximum difference of 2 km to the measured effective height. An estimate of the signal-to-noise ratios based on the model by Rauer et al. [3] for an Earth transmission spectrum seen by JWST from 10 pc distance indicates moderately good SNRs for carbon dioxide, water and ozone.

5. Summary and Conclusions

IR transit spectra of Earth's atmosphere observed by the ACE-FTS operational satellite instrument have been modelled by our high resolution code GARLIC [8]. The comparison of modelled and observed spectra clearly indicates the impact of various molecular species as well as continuum-like contributions. Varying the spectral range, spectral resolution, and noise level allows to quantify the detection level for various molecules.

Acknowledgements

Financial support by the Deutsche Forschungsgemeinschaft — DFG (projects SCHR 1125/3-1 and GO 2610/1-1) is gratefully acknowledged.

References

[1] F. Schreier, S. Gimeno García, P. Hedelt, M. Hess, J. Mendrok, M. Vasquez, and J. Xu. GARLIC – a general purpose atmospheric radiative transfer line-by-line infrared-microwave code: Implementation and evaluation. *J. Quant. Spectrosc. & Radiat. Transfer*, 137: pp. 29–50, 2014. doi: 10.1016/j.jqsrt.2013.11.018.

[2] F. Schreier, M. Milz, S.A. Buehler, and T. von Clarmann. Intercomparison of three microwave/infrared high resolution line-by-line radiative transfer codes. *J. Quant. Spectrosc. & Radiat. Transfer*, 211: pp. 64–77, 2018. doi: 10.1016/j.jqsrt.2018.02.032.

[3] H. Rauer, S. Gebauer, P. v. Paris, J. Cabrera, M. Godolt, J.L. Grenfell, A. Belu, F. Selsis, P. Hedelt, and F. Schreier. Potential biosignatures in super-Earth atmospheres — I. Spectral appearance of super-Earths around M dwarfs. *Astron. & Astrophys.*, 529: A8, 2011. doi: 10.1051/0004-6361/201014368.

[4] M. Vasquez, F. Schreier, S. Gimeno García, D. Kitzmann, B. Patzer, H. Rauer, and T. Trautmann. Infrared radiative transfer in atmospheres of Earth-like planets around F, G, K, and M stars. I. Clear-sky thermal emission spectra and weighting functions. *Astron. & Astrophys.*, 549: A26, 2013a. doi: 10.1051/0004-6361/201219898.

[5] M. Vasquez, F. Schreier, S. Gimeno García, D. Kitzmann, B. Patzer, H. Rauer, and T. Trautmann. Infrared radiative transfer in atmospheres of Earth-like planets around F, G, K, and M stars. II. Thermal emission spectra influenced by clouds. *Astron. & Astrophys.*, 557: A46, 2013b. doi: 10.1051/0004-6361/201220566.

[6] R. Hughes, P. Bernath, and C. Boone. ACE infrared spectral atlases of the Earth's atmosphere. *J. Quant. Spectrosc. & Radiat. Transfer*, 148:18 – 21, 2014. doi: 10.1016/j.jqsrt.2014.06.016.

[7] P. F. Bernath. The atmospheric chemistry experiment (ACE). *J. Quant. Spectrosc. & Radiat. Transfer*, 186: 3–16, 2017. doi: 10.1016/j.jqsrt.2016.04.006.

[8] F. Schreier, S. Städt, P. Hedelt, M. Godolt. Transmission spectroscopy with the ACE-FTS infrared spectral atlas of Earth: A model validation and feasibility study. *Molec. Astrophys*, 11: pp. 1-22, 2018. doi: 10.1016/j.molap.2018.02.001.

EPSC Abstracts
Vol. 12, EPSC2018-780, 2018
European Planetary Science Congress 2018

Water build-up on planets orbiting M-Stars via secondary outgassing from the interior

Mareike Godolt (1), Barbara Stracke (2), Nicola Tosi (1,2) and John Lee Grenfell (2)
(1) Zentrum für Astronomie und Astrophysik, Technische Universität Berlin, Berlin, Germany,
(2) Instititut für Planetenforschung, Deutsches Zentrum für Luft und Raumfahrt (DLR), Berlin, Germany
(godolt@tu-berlin.de)

Abstract

Rocky planets residing within the habitable zone of main-sequence M dwarf stars experience high stellar irradiation during their early evolution due to the prolonged pre-main sequence phase of these stars. It has been suggested that this high early irradiation may lead to the desiccation of these planets. However, since this early stage of high luminosity is relatively short compared to the stellar lifetime, and a significant amount of water can be stored in the bulk silicate mantle during planet formation, we study whether a secondary atmosphere and water reservoir may subsequently build up via mantle melting and volcanism.

We have carried out interior evolution calculations of Earth-like stagnant-lid planets (i.e. without plate tectonics) for different interior volatile reservoirs and computed their potential outgassing, as described in Tosi et al. 2017. We use the amounts of CO_2 and H_2O outgassed from the interior to calculate the habitable zone boundaries and their evolution for these planets around M, K, G, and F-type stars.

Assuming that a water reservoir can be preserved in the planetary interior, we show that a surface water reservoir and an atmosphere may build up via secondary outgassing. Taking into account the uncertainty in interior composition we determine minimum and maximum extent of the continuous habitable zone for these stagnant-lid planets.

Acknowledgements

M. Godolt acknowledges support by the DFG (GO 2610/1-1).

References

[1] Tosi, N. , Godolt, M., Stracke, B. et al.: On the Habitability of a Stagnant-Lid Earth, Astronomy and Astrophysics, Vol. 606, A71, 2017.

EPSC Abstracts
Vol. 12, EPSC2018-782, 2018
European Planetary Science Congress 2018

Dynamical deviations from superrotation in hot Jupiters

Ludmila Carone (1), Robin Baeyens (2), Paul Molliere (3),Patrick Barth (1), Paula Sarkis (1,4), Leen Decin (2), Christoph Mordasini (4), Olivia Venot (5) and Thomas Henning (1)
(1) Max Planck Institute for Astronomy, Heidelberg, Germany (carone@mpia), (2) Institute of Astronomy, KU Leuven, Belgium, (3) Leiden Observatory, The Netherlands, (4) University of Bern, Switzerland, (5) Laboratoire Interuniversitaire des Systèmes Atmosphériques (LISA), Paris, France

Abstract

We present as 'proof of concept' a 3D global circulation model for the fast rotating ($P_{orb} = 0.835$ days), high surface gravity ($g = 47.4$ m/s^2) hot Jupiter WASP-43b [1] with anomalous dynamics that at least partly breaks the 'superrotation paradigm'. We will discuss the difference between this model and a 3D model for HD 209458b, the dynamics of which is dominated by unperturbed superrotation. We will show that the anomalous dynamical effect can at the very least explain the reduced east-ward hot spot shift in hot Jupiters and naturally leads to very large day to night side temperature gradients.

Our results suggest that we have to fundamentally question basic assumptions in 3D atmosphere modelling of exoplanets to explain observations of some hot to ultra-hot Jupiter atmospheres. Indeed, there are currently two exoplanets that outright question the paradigm that the hottest spot of a hot Jupiter is always eastward shifted due to superrotation: CoRoT-2b with an apparent westward shift [2] and HAT-P-7b [3], the hot spot of which appears to oscillate between eastward and westward shift with respect to the substellar point.

References

[1] Hellier, C. et al..: WASP-43b: the closest-orbiting hot Jupiter, A& A, Vol. 535, id.L.7, 5 pp. , 2011.

[2] Dang L. et al..: Detection of a westward hotspot offset in the atmosphere of hot gas giant CoRoT-2b, Nature Astronomy, Vol. 2, pp. 220 - 227 , 2018.

[3] Armstrong, D.J. et al..: Variability in the atmosphere of the hot giant planet HAT-P-7 b, Nature Astronomy, Vol. 1, id. 0004 , 2016.

EPSC Abstracts
Vol. 12, EPSC2018-787, 2018
European Planetary Science Congress 2018

Are giant planets good neighbours for habitable worlds?

Nikolaos Georgakarakos (1), Siegfried Eggl (2) and Ian Dobbs-Dixon (1)
(1) New York University Abu Dhabi, Division of Science, P.O. Box 129188, Saadiyat Island, Abu Dhabi, UAE
(2) Jet Propulsion Laboratory, California Institute of Technology, 4800 Oak Grove Drive, CA 91109, USA
(ng53@nyu.edu)

Abstract

The presence of giant planets affects potentially habitable worlds in various ways. Massive planetary neighbours can facilitate the formation of planetary cores and modify the influx of asteroids and comets towards Earth-analogs later on. Moreover, giant planets can indirectly change the climate of terrestrial worlds by gravitationally altering their orbits. In this work we present a method for quantifying how the gravitational perturbations of a giant planet can affect the capacity of a potentially habitable world to sustain liquid water on its surface. Investigating a number of well characterized extrasolar planetary systems known to date to host a main sequence star and a giant planet, we show that the presence of a 'giant neighbour' can reduce a terrestrial planet's chances to remain habitable, even if both planets have stable orbits. By providing constraints on where giant planets cease to have an adverse effect on the habitable zone size, we identify prime targets in the search for habitable worlds.

1. Introduction

The discovery of planets of similar size to that of the Earth has led to numerous interdisciplinary research activities about the potential habitability of other worlds. Previous studies suggest that the presence of a giant planet in the same exosolar planetary system can affect the formation and evolution of potentially habitable planets in various ways. For instance, during the planetary system's formation, a giant planet can act as a dynamical barrier that blocks the inward migration of proto-planetary cores [1] which in turn affects the formation of rocky planets in the inner region of the system. Even after the planetary formation phase giant planets continue to influence habitable conditions on terrestrial neighbors. While the presence of a giant planet close to the habitable zone can mean dynamical chaos and instability for Earth-like planets [2], giant planets residing within the habitable zone can be hosts to habitable Trojan planets [3] or habitable exomoons [4]. In addition, large impacts of minor bodies on terrestrial planets, may be decisive for the existence of liquid water and the evolution of life [5]. The presence of giant planets can increase the impact flux of comets and other minor bodies on terrestrial planets and hence the delivery of life enabling volatiles [6].

This work is concerned with yet another vital piece in the puzzle. The sheer presence of a giant planet in an exoplanetary system alters the orbit of a potentially habitable world over time. This will affect the amount of stellar radiation the latter receives, which is the main energy source that determines the global climate of Earth-like planets on long timescales [7]. Previous studies mainly focused on the orbital stability of the terrestrial planet assuming the habitable zone limits to be independent of the terrestrial planet's orbit. Here, we calculate the actual insolation received by a potentially habitable world by taking into consideration the orbital evolution of the terrestrial planet under the gravitational perturbations of the giant one. Having estimates of the insolation extrema and variability for any given system configuration at our disposal, we are able to determine more realistic habitable zone limits. These zones are named Dynamically Informed Habitable Zones (DIHZs) and they also take into account how the terrestrial planet atmosphere may respond to changes in the incoming radiation.

2. Method

In order to calculate the DIHZs, we combine a globally averaged radiative-convective energy balance model [7], [8], [9] with analytical results for the orbital evolution of planetary systems [10], [11]. The stability of the planetary system is also checked [12] and other dynamical effects than Newtonian gravity between point masses are also taken into consideration when required.

3. Results

We apply our method on 147 systems consisting of a star on the main sequence and a single giant planet with well-determined orbital elements and physical parameters. Assuming the presence of an additional,fictitious Earth-like planet, we investigate the effect of the giant planet on the limits of the classical habitable zone (CHZ) as defined in [7]. We calculate the extent of the CHZ and compare it to the one of the DIHZs. We find that systems with hot Jupiters exhibit the smallest shrinkages, while systems with warm or cold Jupiter show considerable shrinkage (and sometimes complete elimination) of the CHZ.

4. Summary

In this work, we have developed a general method that can assess the level at which planetary systems can sustain habitable conditions on Earth-like planets as we know them and hence provide observers with a tool to select possible targets in search for habitable worlds. More details about this work can be found in [13].

Acknowledgements

This research has received funding from the Jet Propulsion Laboratory through the California Institute of Technology postdoctoral fellowship program, under a contract with the National Aeronautics and Space Administration, USA, as well as the IMCCE Observatoire de Paris, France. The authors have used the NASA Exoplanet Archive, which is operated by the California Institute of Technology, under contract with the National Aeronautics and Space Administration under the Exoplanet Exploration Program. Furthermore, the authors would like to thank the High Performance Computing Resources team at New York University Abu Dhabi and especially Jorge Naranjo for helping us with certain aspects of the evaluation of the habitable zones.

References

[1] Izidoro, A., Raymond, S. N., Morbidelli, A., Hersant, F. and Pierens, A.: Gas giant planets as dynamical barriers to inward-migrating super-Earths, ApJL, Vol. 800, L22, 5 pp., 2015.

[2] Sándor, Z., Süli, Á., Érdi, B., Pilat-Lohinger, E. and Dvorak, R.: A stability catalogue of the habitable zones in extrasolar planetary systems, MNRAS, Vol. 375, 1495-1502, 2007.

[3] Schwarz, R., Pilat-Lohinger, E., Dvorak, R., Érdi, B. and Sándor, Z.: Trojans in habitable zones, Astrobiology, Vol. 5, 579-586, 2005.

[4] Heller, R., Williams, D., Kipping, D., Limbach, M. A., Turner, E., Greenberg, R., Sasaki, T., Bolmont, É, Grasset, O., Lewis, K.,; Barnes, R. and Zuluaga, J. I.: Formation, habitability, and detection of extrasolar moons, Astrobiology, Vol. 14, 798-835, 2014.

[5] Kring, D.A.: Environmental consequences of impact cratering events as a function of ambient conditions on Earth, Astrobiology, Vol. 3, 133-152, 2003.

[6] Grazier, K. R.: Jupiter: cosmic Jekyll and Hyde, Astrobiology, Vol. 16, 23-38, 2016.

[7] Kasting, J.F., Whitmire, D. P. and Reynolds, R. T.: Habitable Zones around Main Sequence Stars, Icarus, Vol. 101, 108-128, 1993.

[8] Kopparapu, R. K., Ramirez, R., Kasting, J. F., Eymet, V., Robinson, T. D., Mahadevan, S., Terrien, R. C., Domagal-Goldman, S., Meadows, V. and Deshpande, R.: Habitable zones around Main-sequence stars: new estimates, ApJ, Vol. 765, 131, 16 pp., 2013.

[9] Kopparapu, R. K., Ramirez, R. M., SchottelKotte, J., Kasting, J. F., Domagal-Goldman, S. and Eymet, V.: Habitable zones around Main-sequence stars: dependence on planetary mass, ApJL, vol. 787, L29, 6 pp., 2014.

[10] Georgakarakos, N. and Eggl, S.: Analytic orbit propagation for transiting circumbinary planets, ApJ, vol. 802, 94, 16 pp., 2015.

[11] Georgakarakos, N., Dobbs-Dixon, I. and Way, M.J.: Long-term evolution of planetary systems with a terrestrial planet and a giant planet, MNRAS, vol. 461, 1512-1528, 2016.

[12] Petrovich, C.: The Stability and fates of hierarchical two-planet systems, ApJ, vol. 808, 120, 15 pp., 2015.

[13] Georgakarakos, N., Eggl, S. and Dobbs-Dixon, I.: Giant Planets: Good Neighbors for Habitable Worlds?, ApJ, vol. 856, 155, 30 pp., 2018.

EPSC Abstracts
Vol. 12, EPSC2018-792, 2018
European Planetary Science Congress 2018

Feasibility study for a retrieval from transit spectra of Earth-like planets in the habitable zone

Steffen Städt (1), Franz Schreier (1), Fabian Wunderlich (2) and Mareike Godolt (2)
(1) DLR - German Aerospace Center, Remote Sensing Technology Institute, Oberpfaffenhofen, Germany (steffen.staedt@dlr.de)
(2) Technische Universität Berlin, Zentrum für Astronomie und Astrophysik (TUB-ZAA), Berlin, Germany

Abstract

Exoplanetary atmosphere retrievals gain more and more importance with every new discovered planet. Due to the lack of prior information, the feasibility of such retrievals is widely unknown and primary limited by the number of transits (noise). With nonlinear least squares fitting and some model atmospheres, we quantitatively investigate the influence of noise, wavelength range, initial guess and resolution to assess the range of possible outcomes.

1. Introduction

The demand for atmospheric retrievals of habitable exoplanets is a rising field and will become more important the more possible candidates are discovered. At the moment there are more than 3700 exoplanets discovered and although the data coverage and/or resolution and noise level is not as good as for the Earth, the possibility to develop a retrieval is granted. The methodology of atmospheric retrievals is a classical inverse problem which is typically ill-posed. The solution of such a problem is obtained by a nonlinear least squares fit. In this contribution we want to asses the performance of our retrieval algorithm for Earth-like exoplanets and future approaches despite of their different start-ups how to retrieve the molecular vertical columns.

2. Method

The retrieval of an exoplanetary atmosphere is done by a series of forward calculations with different starting values to find the best fit of the model spectrum to the real spectrum. We only see the additional transit depth or effective height of an exoplanet, i.e. the integral of individual limb spectra traversing the atmosphere with different tangent heights and therefore we focus on estimating the vertical column densities (VCDs) of every molecule in the spectrum. We parameterize the profile by a single scale factor. For that we consider different initial guesses, noise levels and wavelength intervals to determine some limits of the retrieval. The impact of missing/additional molecules has already been studied previously [5].

2.1. Forward Model

The "Generic Atmospheric Radiation Line-by-line Infrared-microwave Code" [1] is a radiative transfer model with the purpose to simulate spectra. The code has been used for exoplanet studies, e.g. [2, 3] and has been verified by intercomparisons to other radiative transfer models, e.g. [4]. Transmission spectra are calculated with atmospheric information, limb geometry and molecule information. These limb spectra are then combined to an effective height spectrum of the atmosphere.

3. Model atmospheres

As input for the retrieval we used a set of climatological atmospheres, where all of these atmospheres have different attributes, e.g. (surface) temperatures, water content and integrated ozone content, and are provided with some important molecule profiles. The range of the temperatures and pressure levels are representative for the Earth and therefore well suited for an exoplanet retrieval of Earth-like planets in the habitable zone.

4. Results

The overall water content in the atmosphere has a huge impact on the goodness, as well as the shape of the profile. Water should be retrieved at 6.7 microns and then this value should be used as prior for other wavelength intervals. The initial guess should not be too far away otherwise the fit might end in a local minimum and not at the optimum.

5. Summary & Conclusions

A lot of retrieval results have been analyzed which lead to the following conclusions. Nonlinear least squares proved to be a good tool for exoplanet retrievals and might be even better if the prior is near the true value. The noise of Earth-like exoplanets is critical for a reliable retrieval. The wavelength window for a retrieval should be chosen according to the apparent molecules. In future, we expect better retrievals, because of the increasing number of transits and better resolutions provided by the JWST.

Acknowledgements

Financial support by the Deutsche Forschungsgemeinschaft — DFG (project SCHR 1125/3-1) is gratefully acknowledged

References

[1] F. Schreier, S. Gimeno García, P. Hedelt, M. Hess, J. Mendrok, M. Vasquez, and J. Xu. GARLIC – a general purpose atmospheric radiative transfer line-by-line infrared-microwave code: Implementation and evaluation. *J. Quant. Spectrosc. & Radiat. Transfer*, 137: pp. 29–50, 2014. doi: 10.1016/j.jqsrt.2013.11.018.

[2] P. Hedelt, P. von Paris, M. Godolt, S. Gebauer, J. L. Grenfell, H. Rauer, S. Schreier, F. Selsis and T. Trautmann Spectral features of Earth-like planets and their detectability at different orbital distances around F, G, and K-type stars *Astronomy & Astrophysics*, 553: A9, 2013 doi: 10.1051/0004-6361/201117723

[3] M. Vasquez, F. Schreier, S. Gimeno García, D. Kitzmann, B. Patzer, H. Rauer, and T. Trautmann. Infrared radiative transfer in atmospheres of Earth-like planets around F, G, K, and M stars. I. Clear-sky thermal emission spectra and weighting functions. *Astron. & Astrophys.*, 549: A26, 2013a. doi: 10.1051/0004-6361/201219898.

[4] F. Schreier, M. Milz, S.A. Buehler, and T. von Clarmann. Intercomparison of three microwave/infrared high resolution line-by-line radiative transfer codes. *J. Quant. Spectrosc. & Radiat. Transfer*, 211: pp. 64–77, 2018. doi: 10.1016/j.jqsrt.2018.02.032.

[5] F. Schreier, S. Städt, P. Hedelt, M. Godolt. Transmission spectroscopy with the ACE-FTS infrared spectral atlas of Earth: A model validation and feasibility study. *Molec. Astrophys*, 11: pp. 1-22, 2018. doi: 10.1016/j.molap.2018.02.001.

EPSC Abstracts
Vol. 12, EPSC2018-803, 2018
European Planetary Science Congress 2018

Effect of geologically-constrained environmental parameters on the atmosphere and biosphere of early exo-Earths

Stefanie Gebauer (1), John Lee Grenfell (1), Ralph Lehmann (2) and Heike Rauer (1,3)
(1) Institut für Planetenforschung (PF), Abteilung Extrasolare Planeten und Atmosphären (EPA), Deutsches Zentrum für Luft- und Raumfahrt (DLR), Rutherfordstr. 2, 12489 Berlin, Germany, (2) Alfred-Wegener Institut, Helmholtz-Zentrum für Polar- und Meeresforschung, Telegrafenberg A 45, 14473 Potsdam, Germany, (3) Zentrum für Astronomie und Astrophysik (ZAA), Technische Universität Berlin (TUB), Hardenbergstr. 36, 10623 Berlin, Germany (stefanie.gebauer@dlr.de)

Abstract

In this work we address the impact of geologically-constrained environmental parameters such as carbon dioxide (CO_2) content, surface pressure and ocean temperature upon the atmosphere and biosphere of early exo-Earths by applying our updated Coupled Atmosphere Biosphere (CAB) model developed by [1]. We derive atmospheric profiles of ozone and molecular oxygen (O_2) and calculate the corresponding Net Primary Productivity (NPP) of a photosynthesizing biosphere. Furthermore, we investigate the dominant net chemical production and destruction pathways of O_2 by applying the Pathway Analysis Program (PAP) developed by [2].

1. Introduction

The Great Oxidation Event (GOE) about 2.3 Gigayears ago denotes the first major rise of atmospheric molecular oxygen (O_2) - from less than 10^{-5} of the Present Atmospheric Level (PAL) up to at least 0.01 PAL (e.g. [3]) - in Earth's history. As a consequence the planet experienced the emergence of widespread habitability and complex life.

Recently there has been a revolution in improved methods for constraining geological data (for e.g. atmospheric pressure, composition, ocean temperature etc.) of the early Earth. In this study we investigate the effect of this new data upon our understanding of key processes which drove the GOE.

We have updated the Coupled Atmosphere Biosphere (CAB) model to apply it to the constrained environmental conditions of early Earth as a reference for early exo-Earths in order to analyze the effect of CO_2 content, surface pressure and ocean temperature on the atmosphere and productivity of a photosynthesizing biosphere.

2. Summary and Conclusions

In the case of an Archean-like atmosphere increasing CO_2 leads to an increase of O_2 with atmospheric height which is related to its enhanced production via CO_2 photolysis in the upper atmosphere. This is counterbalanced by stronger destruction of O_2 in the lower atmosphere due to higher abundance of CO from CO_2 and NO_x from low OH due to high CO. Therefore, atmospheres having low surface O_2 volume mixing ratios (vmr) such as was the case before the GOE but high amounts of CO_2 could counteract the accumulation of O_2 in the atmosphere from a given photosynthetic whereas moderate CO_2 abundances result in negligible impacts on the Net Primary Productivity (NPP) needed to maintain a specified O_2vmr.

On reducing the surface pressure to 0.5 bar the O_2 concentration profile between 0.5 to 0.005 bar is decreased compared to an early Earth atmosphere with higher surface pressures. This is a result of enhanced O_2 destruction by increased HO_x from enhanced H_2O at a given pressure level below about 0.01 bar and lower O_2 production due to less UV radiation (at a given pressure level due to less backscattering from below) destroying CO_2 in this pressure regime. Lowering the surface pressure to 0.5 bar has a negligible effect on the NPP at 2.7 Gyrs ago. However, shortly before the GOE an approximately 20% lower NPP is sufficient to maintain the same amount of O_2 in the atmosphere as for a 1 bar

atmosphere hence the accumulation of O_2 produced by a photosynthetic biosphere is supported.

We identify production and destruction pathways of O_2 for Archean-like Earth by applying the Pathway Analysis Program (PAP) for high CO_2 atmospheres and low/high surface pressure scenarios. In both cases new O_2 production and destructions pathways emerge due to the presence of NO_x containing species.

On increasing ocean temperatures as proposed by proxy data, results suggest that the NPP from oxygenic photosynthesis is strongly reduced due to lower O_2 solubility before the GOE supporting the accumulation of O_2 in the atmosphere more easily.

Acknowledgements

S. Gebauer acknowledges support by the DFG project GZ: GR 2004/2-1 of the SPP 1833 “Building a Habitable Earth”.

References

[1] Gebauer, S., J. L. Grenfell, J. W. Stock, R. Lehmann, M. Godolt, P. von Paris, and H. Rauer: Evolution of Earth-like Extrasolar Planetary Atmospheres: Assessing the Atmospheres and Biospheres of Early Earth Analog Planets with a Coupled Atmosphere Biogeochemical Model, Astrobiology, 17, pp. 27-54, 2017.

[2] Lehmann, R.: An algorithm for the determination of all significant pathways in chemical reaction systems, Journal of Atmospheric Chemistry, 47, pp. 45-78, 2004.

[3] Catling, D. C., and M. W. Claire: How Earth's atmosphere evolved to an oxic state: A status report, Earth and Planetary Science Letters, 237, pp. 1-20, 2005.

EPSC Abstracts
Vol. 12, EPSC2018-818-2, 2018
European Planetary Science Congress 2018

Coupling the internal and orbital evolution of close-in terrestrial exoplanets

M. Walterová and M. Běhounková
Charles University, Faculty of Mathematics and Physics, Department of Geophysics, Czech Republic
(kanova@karel.troja.mff.cuni.cz)

Abstract

Exoplanets orbiting close to their host star are subject to extreme environments. Their internal dynamics are marked by pronounced tidal heating and high surface temperatures or temperature contrasts. Their orbital evolution, as well as the evolution of the spin rate, is greatly influenced by the tidal interaction with the host star, which could lead the planet into one of the stable spin states (either a spin-orbit resonance or a pseudosynchronous rotation) and – on longer time-scales – even circularize its orbit. The rate and the exact form of such a process depends on the rheological parameters of the planet, which, in turn, are linked to the thermal evolution via their temperature dependencies.

Here, we introduce a semi-analytical model of coupled thermal-orbital evolution of a single terrestrial exoplanet orbiting a single star and present some of its applications on several currently known planetary systems.

1. Model and Methods

In order to describe the long-term evolution of a rocky planet without atmosphere, we combine a tidal evolution model for viscoelastic bodies with parametrized (1D) mantle convection.

The calculation of the orbital evolution is based on the Darwin-Kaula expansion of the tidal potential and Lagrange's planetary equations [3], which, together with the conservation of the total angular momentum, read

$$\frac{\mathrm{d}a}{\mathrm{d}t} = -\sqrt{\frac{a}{\mathcal{G}(M+m)}}\sum_{lmpq} k_l \sin\varepsilon_{lmpq}\,\frac{2r_\mathrm{p}^{2l+1}}{a^{2l+2}} \times B_{lm}G_{lpq}^2F_{lmp}^2(l-2p+q)\,, \tag{1}$$

$$\frac{\mathrm{d}e}{\mathrm{d}t} = -\sqrt{\frac{1-e^2}{a\,\mathcal{G}(M+m)}}\sum_{lmpq} k_l \sin\varepsilon_{lmpq}\,\frac{r_\mathrm{p}^{2l+1}}{ea^{2l+2}} \times B_{lm}G_{lpq}^2F_{lmp}^2[\sqrt{1-e^2}(l-2p+q)-(l-2p)]\,, \tag{2}$$

$$\frac{\mathrm{d}(C\Omega)}{\mathrm{d}t} = -\frac{1}{2}\sqrt{\frac{\mathcal{G}M^2(M+m)}{a}}\sqrt{1-e^2}\,\frac{\mathrm{d}a}{\mathrm{d}t} + \sqrt{a\,\mathcal{G}M^2(M+m)}\,\frac{e}{\sqrt{1-e^2}}\,\frac{\mathrm{d}e}{\mathrm{d}t}\,. \tag{3}$$

Here, a is the semi-major axis, e is the eccentricity, Ω symbolizes the rotational frequency, $\mathcal{G}$ stands for the gravitational constant, m and M are masses of the two bodies, G_{lpq} and F_{lmp} are the eccentricity and the inclination functions, respectively, r_p is the planetary radius and $B_{lm} = \mathcal{G}M\frac{(l-m)!}{(l+m)!}(2-\delta_{0m})$. For the sake of simplicity, we neglect the tides raised on the star due to the planet, set the inclination and the axial tilt of the planet to zero and consider the moment of inertia about its rotation axis C constant. The eccentricity functions G_{lpq} are computed as the Hansen's coefficients $X^{-(l+1),(l-2p)}_{(l-2p+q)}$ either numerically, from their definition, or using recurrent formulae [1].

The internal structure of the planet and its rheological properties are represented by the frequency dependent tidal Love numbers $k_l(\omega_{lmpq})$, describing the change in the external potential due to the planet's tidal deformation, and by the phase lag between the tidal and the disturbing potential $\varepsilon_{lmpq}(\omega_{lmpq})$. We calculate these parameters adopting the method of [5] for a tidally loaded body and considering a layered spherical model planet with solid inner core, liquid outer core and a viscoelastic mantle, whose upper part forms a highly viscous lithosphere.

Together with the evolution of the orbit and the spin rate, we evaluate the average tidal heating and update the internal structure of the planet and the viscosities

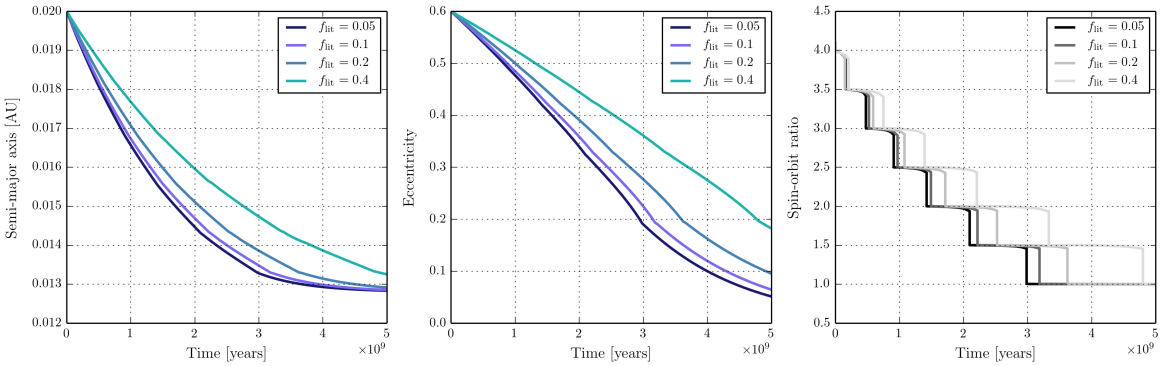

Figure 1: Long-term evolution of the semi-major axis, the eccentricity and the spin rate, computed for an Earth-size planet orbiting a red dwarf ($M = 0.1\,M_{\rm Solar}$). Effect of the thermal lithosphere thickness.

of its layers according to the changes in the thermal structure. Subsolidus convection in the stagnant lid regime is computed using a 1D parametrized model of a mantle heated both volumetrically (due to the tidal dissipation and the decay of radiogenic elements) and from below (e.g., [2]). The viscosity η of the mantle follows an exponential temperature dependence of the form

$$\eta = \eta_0 \exp\left(\frac{E^*}{R}\frac{(T_{\rm ref} - T)}{T_{\rm ref} T}\right) \qquad (4)$$

with $\eta_0 = \eta(T_{\rm ref})$, where $T_{\rm ref} = 1600\,{\rm K}$ is the reference temperature, E^* is the activation energy for viscous deformation and R is the universal gas constant.

2. Preliminary results

For the static model, without mantle convection, we perform several parametric studies concerning the dependence of the Love numbers and the tidal torque on the internal structure and continue with assessing its effect on the orbital evolution. Figure 1 depicts orbital and spin-rate evolution of an Earth-size planet, depending on the ratio $f_{\rm lit}$ between the thickness of its thermal lithosphere and the thickness of the mantle. Average viscosity of the mantle is $10^{16}\,{\rm Pa\,s}$; viscosity of the lithosphere increases logarithmically from its base to the surface, where it reaches its maximum value of $10^{24}\,{\rm Pa\,s}$. Varying thickness of the lithosphere affects the rate of the orbital eccentricity decay and, as a result, determines the stable spin-orbit resonance.

The results of these parametric studies will be compared to the time-evolving, convecting model with tidal heating and applied on several currently known rocky exoplanets. We are also planning to connect the semi-analytical model with numerical computation of Love numbers [4], which would enable us to study moons or planets with heterogeneous mantle viscosity structure.

Acknowledgements

This work was supported by the Charles University grant SVV–2018–260447.

References

[1] Cherniack, J. R. (1972) *SAO Special Report #346*.

[2] Grott, M. and Breuer, D. (2008) *Icarus* 193, pp. 503-515.

[3] Kaula, W. M. (1964) *Rev. Geophys.* 2, pp. 661-685.

[4] Walterová, M. and Běhounková, M. (2017) *Celest. Mech. Dyn. Astron.* 129, pp. 235-256.

[5] Wu, P. and Peltier, W. R. (1982) *Geophys. J.* 70, pp. 435-485.

EPSC Abstracts
Vol. 12, EPSC2018-862, 2018
European Planetary Science Congress 2018

Correcting HIRES radial-velocities for systematic errors

Lev Tal-Or (1,4), Trifon Trifonov (2), Shay Zucker (1), Tsevi Mazeh (3), and Mathias Zechmeister (4)
(1) School of Geosciences, Raymond and Beverly Sackler Faculty of Exact Sciences, Tel-Aviv University, 6997801, Israel
(2) Max-Planck-Institut für Astronomie, Königstuhl 17, D-69117 Heidelberg, Germany
(3) School of Physics and Astronomy, Tel Aviv University, Tel Aviv, Israel
(4) Institut für Astrophysik, Georg-August-Universität, Friedrich-Hund-Platz 1, 37077 Göttingen, Germany
(levtalo@post.tau.ac.il)

Abstract

We use publicly-available radial velocities (RVs) from the HIRES spectrograph to identify and correct for minute (~1 m/s) systematic RV variations. By averaging the RVs of different quiet stars that were observed each night, we calculate instrumental nightly zero-point RVs, and find small but significant variations on three different timescales. In addition, we find an average small intra-night RV drift. We correct the HIRES RVs for the systematic effects, and investigate the impact of the correction. Our findings highlight the importance of observing quiet stars on a nightly basis, even in the era of self-calibrated and stabilized RV spectrographs.

1. Introduction

The HIRES spectrograph on the 10-m Keck telescope in Hawaii belongs to a small family of radial-velocity (RV) instruments that can produce stellar RVs with internal precision and long-term stability down to ~1 m/s. For the last two decades it was extensively used to monitor F, G, K, and M dwarf stars in search for exoplanets. Last year, the HIRES team made public ~65,000 RVs of ~1,700 stars that were collected with HIRES between 1996 and 2014 [1]. In what follows, we use these RVs to identify and correct for minute systematic instrumental RV variations.

2. Four different systmatic effects

To identify the systematic effects, we select a sub-sample of ~800 stars whose RV scatter is < 10 m/s (RV-quiet stars). By averaging the RVs of the different stars that were observed each night, we calculate a nightly zero-point RV (NZP) for ~900 nights in which at least three different RV-quiet stars were observed. Using the NZPs we find that the two most significant systematic effects are a discontinuous jump, which was caused by major modifications of the instrument in Aug 2004, and a slow NZP variation, with a typical timescale of a few years. We find the Aug 2004 jump to be 1.5 ± 0.1 m/s, and the magnitude of the slow variation to be ~1 m/s. Periodogram analysis of the NZPs reveals yet another systematic effect of ~0.5 m/s with a period of ~30 days, which is probably related to the bright-time scheduling of the observations. On top of that, we find a significant correlation between RVs and the time from local midnight, indicative of an average nightly drift of the RVs of 0.049 ± 0.003 m/s/hr.

3. Correcting the RVs

We correct the public HIRES RVs for the systematic effects we find. The night-to-night variations are corrected by subtracting a moving (50-day window) weighted-average filter applied to the NZPs. The intra-night drift is corrected by using the observation's time from local midnight. The median absolute value of the total correction is ~0.7 m/s. The corrected RVs will be soon made public alongside a dedicated publication [3].

The median RV rms scatter per star in the public HIRES data is ~5 m/s, while the most RV-quiet stars have an rms of ~2 m/s. This scatter contains both the intrinsic stellar RV variations, which come from orbital motions and photospheric activity, and the instrumental RV errors, which can be further divided to internal RV precision and systematic errors. Therefore, correcting for ~1 m/s systematic effects does not change significantly each-star's RV rms. However, the correction is important when analyzing low amplitude signals. In particular, it suppresses spurious signals of a few planet candidates that were listed by [1]. Moreover, the correction makes the HIRES data slightly more self-consistent over timescales of years, which can facilitate combining it with data from other precision RV instruments in search for low-amplitude long-period orbital signatures of low mass planets.

4. Figures

Figure 1 demonstrates our NZP correction method of HIRES RVs. The NZPs have an STD of ~1.3 m/s and a median uncertainty of ~0.9 m/s, which shows that the NZPs reveal an additional source of systematic RV scatter, on top of the internal RV uncertainties. The Aug 2004 jump can be seen at JD~2453225.

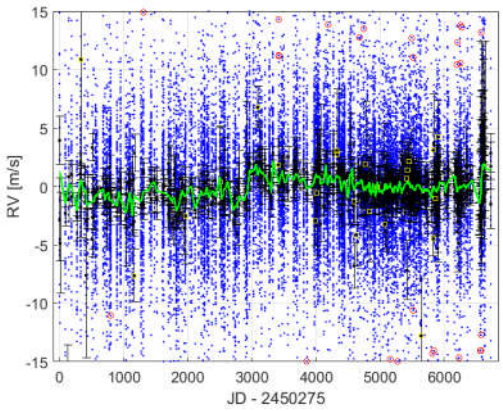

Figure 1: HIRES NZP correction. RV-quiet star RVs are shown as blue points. Black errorbars show the NZPs, while NZPs that were derived from less than three RVs are marked with yellow boxes. Outliers are marked in red. The green line shows our adopted NZP model: a moving (50-day window) weighted-average filter. Aug 2004 is at JD ~ 2453225.

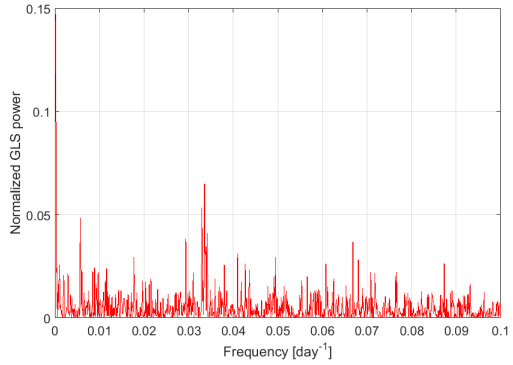

Figure 2: GLS periodogram of the HIRES NZPs.

Figure 2 shows a GLS periodogram of the NZPs. The two highest peaks belong to periods of ~6000 and ~30 days. The low frequency peak originates from the Aug 2004 jump, combined with a slow decay of the NZPs back to their median value. The 30-day peak naturally emerges from the bright-time scheduling of HIRES observations.

Figure 3 shows the small intra-night drift of HIRES RVs. The linear correlation has a p(F_{test})-value of ~$5 \cdot 10^{-7}$, which shows that it is significant.

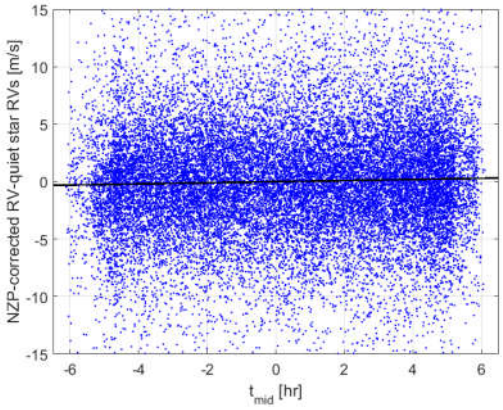

Figure 3: HIRES RVs of RV-quiet stars versus the time from local midnight.

5. Conclusions

Observing RV standard stars to correct for systematic errors is a technique that was in use ever since the RV method was invented. However, in the era of self-calibrated and stabilized RV spectrographs it was largely abandoned, while sophisticated calibration methods were adopted instead. We show here that repeated observations of RV-quiet stars is still important, and can reveal systematic errors well below the noise level of the instrument. As more and more precision RV instruments become operational, and as the precision is being pushed to the ~0.1 m/s limit [2], we urge the observatories to keep observing RV-quiet stars on a nightly basis, in order to identify and correct for instrumental systematic RV errors.

References

[1] Butler, R. P., et al.: The LCES HIRES/Keck Precision Radial Velocity Exoplanet Survey, AJ, Vol. 153, 208B, 2017.

[2] Fischer, D. A., et al.: State of the Field: Extreme Precision Radial Velocities, PASP, Vol. 128, f6001F, 2016.

[3] Tal-Or, L., et al.: in preparation, 2018.

EPSC Abstracts
Vol. 12, EPSC2018-887, 2018
European Planetary Science Congress 2018

The controls of planetary bulk composition and tectonic style on the long-term evolution of outgassed atmospheres

Robert J. Spaargaren (1), Maxim D. Ballmer (1), Caroline Dorn (2), Daniel J. Bower (1,3) and Paul J. Tackley (1)
(1) Institute of Geophysics, ETH Zürich, Switzerland
(2) Center for Theoretical Astrophysics and Cosmology, Institute of Computational Sciences, Universität Zürich, Switzerland
(3) Center for Space and Habitability, Universität Bern, Switzerland
(sprobert@student.ethz.ch)

Abstract

Observations of super-Earth atmospheres have revealed information regarding the surface conditions of these exoplanets. More advanced instruments will allow future missions to observe atmospheres of exoplanets down to Earth size. Atmospheres of terrestrial planets form under interaction with their rocky interiors, by degassing from the magma ocean during the early life of the planet and by interaction with the solid rocky interior during the remainder of the planets life. Therefore, characterising an atmosphere and its composition based on observations may provide us with clues about the interior of a planet.

We have constructed a simplified model describing the simultaneous evolution of the planetary interior and its atmosphere. It is used to investigate possible evolutionary tracks of the atmosphere based on variations in planetary bulk composition, interior structure and tectonic setting, where only the end-members stagnant lid and plate tectonics are considered. Identifying separate tracks allows observations of planetary atmospheres to place first-order constraints on the planets interior.

1 Introduction

So far, the only properties that can be used to constrain interior conditions of Earth-sized planets are the planetary mass and radius, and the host star bulk composition. There is an ambiguity in investigating the interior based on the planetary mass and radius alone [1]. The bulk composition of the host star can be determined through stellar spectrography, and provides constraints on the bulk planetary composition in terms of heavier, rock-forming elements [2]. However, additional information is needed to accurately determine bulk planetary composition.

Since atmospheres form and develop in equilibrium with the rocky interior for terrestrial planets, atmospheric data provides more constraints on the interior composition and evolution. New technological developments will allow future instruments, such as the James Webb Space Telescope (JWST), to observe atmospheres of Earth-sized planets and provide these constraints. In this study, we link the bulk composition of planetary mantles in terms of Mg/Si and Fe/Mg to the coupled interior-atmospheric evolution in a parametrized model. We use this model to investigate whether the composition and interior evolution leave a measurable signature in the atmospheric size and composition.

2 Models

The model describes the coupled interior-atmospheric evolution of an Earth-like exoplanet around a Sun-like star in two phases: a primary phase during which a Magma Ocean (MO) crystallises and an atmosphere degasses, and a secondary phase, in which long-term processes govern the interaction between the solid rocky interior and the atmosphere. Model parameters involve both planetary composition and dynamic regime, which describes the interaction between the mantle and the surface. The planetary composition parameters are based on the host star bulk composition for the major rock-forming elements Fe, Mg and Si, where stellar bulk composition data is retreived from the Hypatia catalog [3]. The model only includes the most important greenhouse gases, H_2O and CO_2. In terms of dynamical regimes, we only consider stagnant lid and plate tectonics.

2.1 Primary evolution

During the first phase, the model describes bottom-up fractional crystallisation of a MO. The crystallisation sequence is determined based on thermodynamic data of the FeO-MgO-SiO_2 system at lower mantle conditions, published by Boukaré et al. [4]. The data shows that three stable phase fields are present at these conditions, crystallising ferropericlase (fp), bridgmanite (bm) and stishovite (st). At each step, the stable phase(s) given the current pressure and composition are determined and removed, after which the liquid composition is adjusted accordingly. Solubility of volatiles is also recalculated and volatiles are degassed accordingly.

The crystallising phases fp and bm are solid solutions between Mg- and Fe-end members, and both preferentially incorporate MgO over FeO. The remaining liquid MO becomes progressively more enriched in FeO, until the material crystallising at the top of the mantle has become so enriched that it becomes negatively buoyant. This development of the liquid MO composition is showsn in Figure 1, which shows the compositional pathway of the liquid MO for a range of compositions. At this point of the evolution, an overturn of the solid mantle occurs [5], where the compositional and density profiles of the mantle are inverted. We consider that subsequent mantle convection occurs across a single layer (whole mantle convection, blue dots in Figure 1), unless a threshold criterion (i.e., density difference of >200) is exceeded, and mantle convection collapses into two layers (red dots).

2.2 Secondary evolution

After the overturn is complete, the subsequent long-term evolution of the coupled interior-atmospheric planetary system can be modelled based on the degassed atmosphere and the properties of the solidified mantle. A 1D parametrized convection code based on Mixing Length Theory [6] is applied to model the thermal evolution of the mantle and the long-term in-/outgassing of the atmosphere. The tectonic regime and related mantle melting are considered to calculate volatile fluxes. In the stagnant lid regime, melt produced in the mantle is added to the crust, of which around 10% will reach the surface through extrusive volcanism and degas [7]. Volatiles preferentially partition into the melt, progressively moving volatiles from the mantle into the crust and atmosphere. In the plate tectonics regime, melting exclusively occurs at the very top of the mantle at plate boundaries. Complete

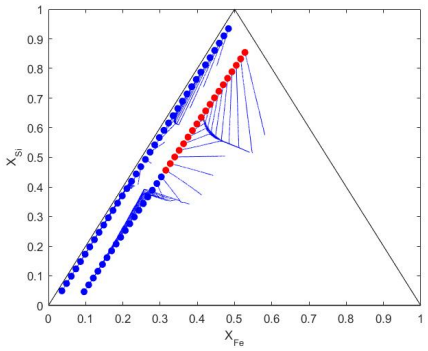

Figure 1: An overview of compositional pathways of the liquid MO during crystallisation, shown in the FeO-MgO-SiO2 triangle. The bulk compositions vary for molar MgO/(MgO+SiO_2) ratios between 0.05 and 0.95, and for FeO contents of 2 and 12 weight percent. Each starting composition has a coloured dot indicating the number of stable layers formed after overturn (blue: 1 layer; red: 2 layers).

degassing is assumed to occur here. In turn, regassing occurs at subduction zones. Since the goal is to use a simplified model, no atmospheric processes except for atmospheric escape are considered [8].

3 Summary and Discussion

A simplified model describing the simultaneous evolution of a planetary interior and its atmosphere is constructed to study the way interior conditions affect the atmosphere. The goal was to find distinct atmospheric evolutionary tracts, so atmospheric observations can be used to constrain interior conditions. Since the three phases in the FeO-MgO-SiO_2 diagram that are stable throughout most of the mantle have different volatile solubilities, retaining varying amounts of volatiles in the solidified mantle. Since outgassing of H_2O is limited for high atmospheric pressures while outgassing of CO_2 is affected by atmospheric pressure to a much lesser extent [9], retention of volatiles in the liquid MO and solidified mantle affects the final H_2O/CO_2 ratio of the atmosphere.

References

[1] Rogers, L.A., Seager, S.: A framework for quantifying the degeneracies of exoplanet interior compositions, the Astrophysical Journal, 712, pp. 974-991, 2010.

[2] Bond, J.C., O'Brien, D.P., Lauretta, D.S.: The compositional diversity of extrasolar terrestrial planets: I. In situ simulations, the Astrophysical Journal, 715, pp. 1050-1070, 2010.

[3] Hinkel, N.R., Timmes, F.X., Young, P.A. et al.: Stellar abundances in the Solar neighbourhood: The Hypatia catalog, the Astrophysical Journal, 148, pp. 33, 2014.

[4] Boukaré, C.E., Ricard, Y., Fiquet, G.: Thermodynamics of the MgO-FeO-SiO2 system up to 140 GPa: Application to the crystallisation of Earth's magma ocean, Journal of Geophysical Research: Solid Earth, 120, pp. 6085-6101, 2015.

[5] Ballmer, M.D., Lourenço, D.L., Hirose, K. et al.: Reconciling magma-ocean crystallization models with the present-day structure of the Earth, Geochemistry, Geophysics, Geosystems, 18, 22 pp., 2017.

[6] Bower, D.J., Sanan, P., Wolf, A.S.: Numerical solution of a non-linear conservation law applicable to the interior dynamics of partially molten planets, Physics of the Earth and Planetary Interiors, 274, pp. 49-62, 2018.

[7] White, S.M., Crisp, J.A., Spera, F.J.: Long-term volumetric eruption rates and magma budgets. Geochemistry, Geophysics, Geosystems, 7, 20 pp, 2006.

[8] Johnson, R.E., Oza, A., Young, L.A. et al.: Volatile loss and classification of Kuiper Belt objects, the Astrophysical Journal, 809, 9 pp, 2015.

[9] Tosi, N., Godolt, M., Stracke, B. et al.: The habitability of a stagnant-lid Earth, Astronomy and Astrophysics, 605, 21 pp., 2017.

EPSC Abstracts
Vol. 12, EPSC2018-980, 2018
European Planetary Science Congress 2018

Mapping exoplanet clouds with high-dispersion spectro-polarimetry

A. García Muñoz (1)

(1) Technische Universität Berlin, Berlin, Germany

Abstract

Polarization is an under-exploited technique in the investigation of exoplanet atmospheres. A polarization detection, particularly if extended over a broad spectral range, will set valuable constraints on the gas and clouds in an exoplanet atmosphere that are impossible through brightness-only observations. In this presentation, I will describe simulations that show that the polarization of a spatially unresolved exoplanet may be detected by cross-correlating high-dispersion linear polarization and brightness spectra of the planet-star system [1]. In this approach, the Doppler shift of the planet-reflected starlight facilitates the separation of the signal from other polarization sources, including the star, the interstellar medium and the terrestrial atmosphere. I will elaborate on the case of close-in giant exoplanets with non-uniform cloud coverage, in which cases the hemispheres east and west of the sub-stellar point will produce different polarizations. The simulations show that high-dispersion spectro-polarimetry can rule out some of the proposed cloud scenarios and, in particular, set additional constraints on the cloud particles' optical properties.

1. Introduction

Whole-disk polarization measurements of reflected sunlight have a long history in the remote sensing of the solar system bodies, their surfaces and atmospheres. Linear polarimetry is potentially more sensitive than brightness measurements to the composition, size, and shape of the scattering particles. The two approaches complement each other in the characterization of the condensate–gas envelope of an atmosphere [2].

The potential and current status of polarimetry for the detection of exoplanets and the characterization of their atmospheres and orbits has been discussed at length [3]. Since polarimetry is a photon-starved technique, most efforts to date have focused on broadband measurements from bright star systems (55 Cancri, τ Boötes, HD 189733). Broadband polarimetry ensures that a large number of photons are collected, which is essential for reaching the required sensitivities of tens of ppms or better. On the other hand, broadband polarimetry also requires the removal of systematics introduced by the telescope-instrument optical system, and the subtraction of the polarization arising in the interaction of the starlight with the ISM or with the terrestrial atmosphere. In practice, the non-planet components of the measured polarization signal may easily bury the polarization attributable to the planet.

2. HDSP: High-dispersion spectro-polarimetry

An alternative to broadband polarimetry is the use of high-dispersion spectro-polarimetry (HDSP) together with some form of cross-correlation. In recent years, the HDS technique (without polarimetry) has become established as a powerful tool in the investigation of exoplanet atmospheres [e.g. 4]. The technique benefits from the spectral separation of the planet and the star due to their relative Doppler shifts. The same idea, i.e. the separation of the starlight from the planet signal due to their different Doppler shifts, can also be used to investigate the planet polarization. The distinct velocity of the planet signal should facilitate its identification against other polarization sources such as the star, the ISM, the terrestrial atmosphere or the telescope.

3. Simulations of Kepler-7b's atmosphere

Figure 1 presents synthetic phase curves for brightness and polarization based on the best fits by Ref. [5] to the brightness measurements of Kepler-7b. Three condensate compositions plausibly explain the measurements, namely: silicate, perovskite and silica. Small changes in the optical properties of the condensates (e.g. the particle size) have no apparent impact on the simulated brightness phase curves. These small changes, however, affect the polarization phase curves significantly. The simulations show the unique

diagnostic potential of polarimetry to confirm some of the proposed cloud scenarios.

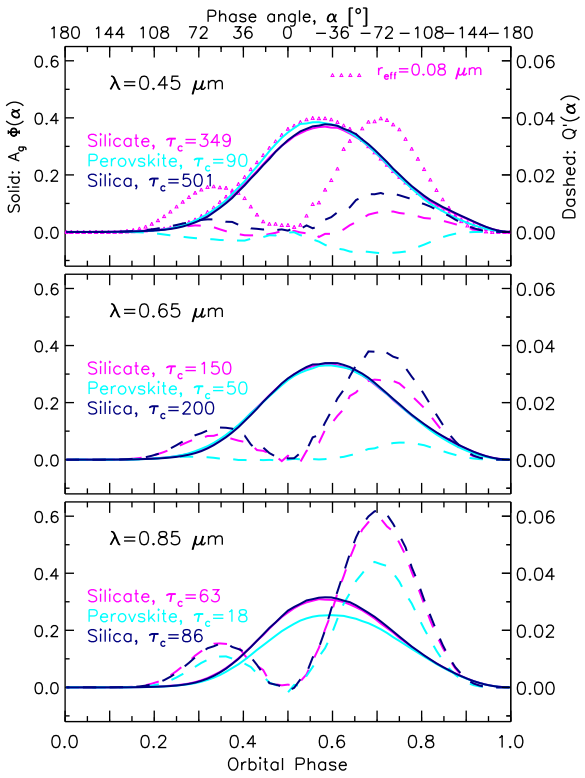

Figure 1. Simulated phase curves (brightness and polarization) for Kepler-7b at three wavelengths. Polarization is much more sensitive than brightness to the optical properties of the condensates in this hot Jupiter's atmosphere. Figure from Ref. [1].

4. The Cross-Correlation Function

Cross-correlating the linear-polarization spectrum of the planet-star system with the measured brightness spectrum of the star reveals the planet signal at the corresponding planet Doppler shift. Figure 2 shows an example of a CCF simulation for Kepler-7b. The planet signal is Doppler-shifted by about 130 km/s with respect to the star for a phase angle of ~70 deg.

5. Summary

Polarimetry is a valuable complement to photometric and spectroscopic measurements in the characterization of exoplanet atmospheres. The HDSP-CC technique offers a built-in way to separate polarization contributions originating with different radial velocities. This feature may be of great advantage to prevent the spurious identification of exoplanet polarization signals. The technique can be tested on a number of targets (e.g. 51 Peg b) orbiting bright stars with currently existing telescopes and instruments.

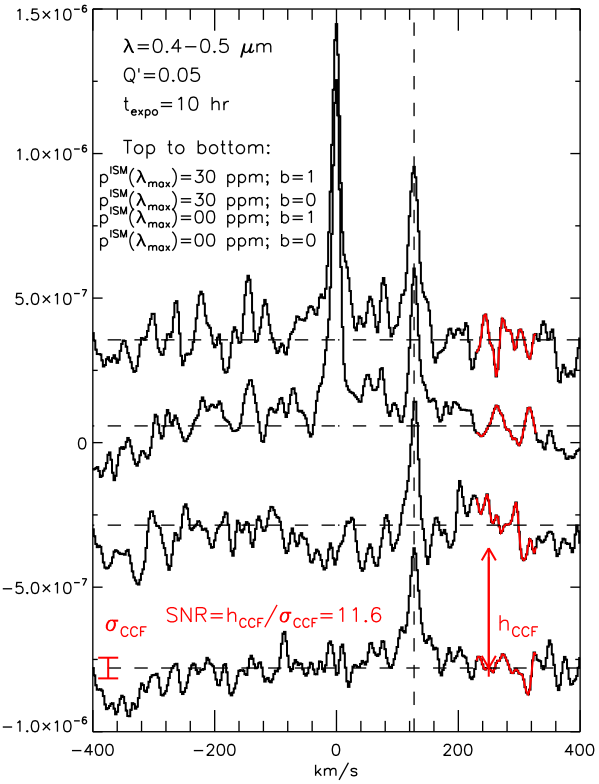

Figure 2. Simulated CCF for Kepler-7b. The planet signal is well-separated in the velocity space from the signal introduced by the star and the ISM. Figure from Ref. [1].

References

[1] García Muñoz, A. On mapping exoplanet atmospheres with high-dispersion spectro-polarimetry: Some Model predictions. The Astrophysical Journal, 854:108, 2018.

[2] Hansen, J.E. & Travis, L.D. Light scattering in planetary atmospheres. Space Science Reviews, 16, 527-610, 1974.

[3] Wiktorowicz, S.J. & Stam, D.M. Exoplanets. In Polarimetry of stars and planetary systems. Cambrige University Press, 2015.

[4] Snellen, I. High-dispersion spectroscopy of extrasolar planets: from CO in hot Jupiters to O_2 in exo-Earths. Phil. Trans Royal Society A: Mathematical, Physical and Engineering Sciences, 372, 20130075-20130075, 2014.

[5] García Muñoz, A. & Isaak, K.G. Probing exoplanet clouds with optical phase curves. PNAS, 112, 13461-13466, 2015.

EPSC Abstracts
Vol. 12, EPSC2018-987, 2018
European Planetary Science Congress 2018

Water detection in the near infrared in HD 189733 b with CARMENES

A. Sánchez-López (1), F. J. Alonso-Floriano (2), I. A. G. Snellen (2), M. López-Puertas (1), E. Nagel (4), H. J. Hoeijmakers (2), F. Bauer (1), P. J. Amado (1), J. A. Caballero (3), A. Quirrenbach (5), I. Ribas (6), A. Reiners (7) and the CARMENES Consortium
(1) Instituto de Astrofísica de Andalucía (CSIC), Granada, Spain, (2) Leiden Observatory - Leiden University, Leiden, The Netherlands, (3) Centro de Astrobiología (CSIC/INTA), Madrid, Spain, (4) Hamburger Sternwarte, Hamburg, Germany, (5) Zentrum für Astronomie der Universtät Heidelberg, Landessternwarte, Heidelberg, Germany, (6) Institut de Ciències de l'Espai (CSIC-IEEC), Barcelona, Spain, (7) Institut für Astrophysik, Georg-August-Universität, Göttingen, Germany

Abstract

The current scientific interest on radial velocity surveys around M type stars has pushed the development of high-resolution high-stabilized spectrographs in 4-m class telescopes. Such is the case of the Calar Alto high-Resolution search for M dwarfs with Exoearths with Near-infrared and optical Échelle Spectrographs (CARMENES, [1]). The capabilities of CARMENES provide us with the opportunity of extending the scientific exploitation of the instrument to the field of exo-atmospheres. Therefore, we have used CARMENES to detect the water vapour signature in the atmosphere of the Hot Jupiter HD 189733 b using tranmission spectroscopy in the primary transit. To do so, we have used the Cross-correlation (CC) technique for high-resolution spectra as in [2], [3], [4].

1. Cross-Correlation Technique applied to CARMENES

We observed one of the transits of HD 189733 b with the near-infrared (NIR) channel of CARMENES. The spectra were reduced by the CARMENES pipeline. After properly removing hot pixels and cosmic rays, we normalized the spectra and masked the strongest tellluric absorption and emission lines. For the removal of the telluric and stellar variations during the observations we used an iterative Principal Component Analysis algorithm called SYSREM ([5], [6]), succesfully applied in [4]. The spectra were then cross-correlated with H_2O transmission models that were created with the Karlsruhe Optimized and Precise Radiative Transfer Algorithm (KOPRA, [7]). An example can be seen in Fig. 1.

2. Water vapour detection with CARMENES

We detect the H_2O signature in the atmosphere of HD 189733 b using the NIR wavelength coverage of CARMENES (0.96–1.71 μm) with a signal-to-noise ratio, SNR > 6 (Fig. 2) at a significance level > 6σ. The signal was found to be slightly blueshifted, hence indicating the presence of winds in the terminator region flowing from the day to the night-side. We tested several templates for the CC with two different pressure-Temperature profiles and two possible H_2O abundances (VMR= 10^{-4}, 10^{-5}). We found that their effect in the model (e.g. line shapes and depths) does not translate in significantly different SNRs nor significances (Fig. 3).

We explored the possibility of individually detecting H_2O in the two stronger bands at wavelength ranges $1.06 - 1.23\,\mu m$ and $1.29 - 1.54\,\mu m$, and in the combination of the other weaker bands in the covered region (see Fig. 1). We found the H_2O signal individually for each of them with SNR$\sim$4.

Acknowledgements

A. S.-L. and M. L.-P. have been supported by the Spanish MINECO through grant ESP2014-54362-P and EC FEDER funds. F.J. A.-F. and I. S. acknowledge funding from the ERC under the EU's Horizon 2020 research and innovation programme under grant agreement No 694513. CARMENES is funded by the German MPG, the Spanish CSIC, the European Union through FEDER/ERF, the Spanish MINECO, the state of Baden-Württemberg, the German DFG, and the Junta de Andalucía, with additional contributions by

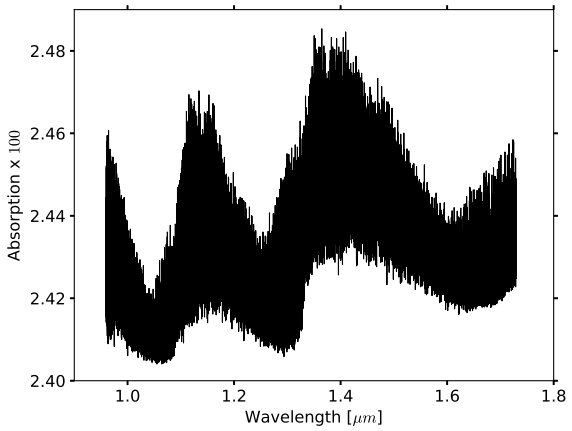

Figure 1: Example of absorption model calculated with KOPRA for HD 189733 b in the CARMENES NIR spectral range. The contribution of the solid planetary disk (i.e., opaque at all wavelengths) has been included.

the members of the CARMENES Consortium (MPIA, IAA, LSW, ICE, IAG, UCM, TLS, IAC, HS, CAB, and CAHA). Financial support also provided by the UCM, the C. A. de Madrid, the Spanish Ministerios de Ciencia e Innovación and MINECO, and the FEDER/ERF funds under grants AYA2011-30147-C03-01, -02, and -03, AYA2012-39612-C03-01, and ESP2013-48391-C4-1-R. Based on observations collected at CAHA, operated jointly by the MPIA and the IAA-CSIC.

References

[1] Quirrenbach, A., Amado, P. J., Caballero, J. A., et al., 2016, Proc. SPIE, 9908, 990812

[2] Snellen, I. A. G., de Kok, R. J., de Mooij, E. J. W. and Albrecht, S., 2010, Nature, 465, 1049

[3] Brogi, M., Giacobbe, P., Guilluy, G., et al., 2018, arXiv:1801.09569

[4] Birkby, J. L., de Kok, R. J., Brogi, M., Schwarz, H., and Snellen, I. A. G., 2017, AJ, 153, 138

[5] Tamuz, O., Mazeh, T., and Zucker, S., 2005, MNRAS, 356, 1466

[6] Mazeh, T., Tamuz, O., and Zucker, S., 2007, Transiting Extrapolar Planets Workshop, 366, 119

[7] Stiller, G. P., von Clarmann, T., Funke, B., et al., 2002, Journal of Quantitative Spectroscopy and Radiative Transfer, 72, 249

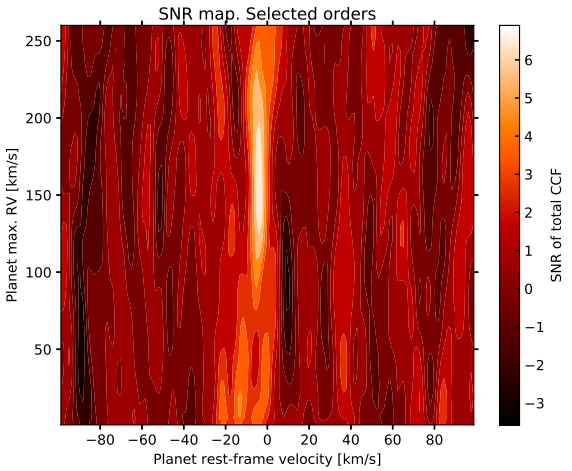

Figure 2: Signal-to-noise ratio as a function of the planet rest frame velocity and radial velocity semi-amplitude (K_p). The strongest SNR is found at the expected K_p and rest velocity intervals of the exoplanet.

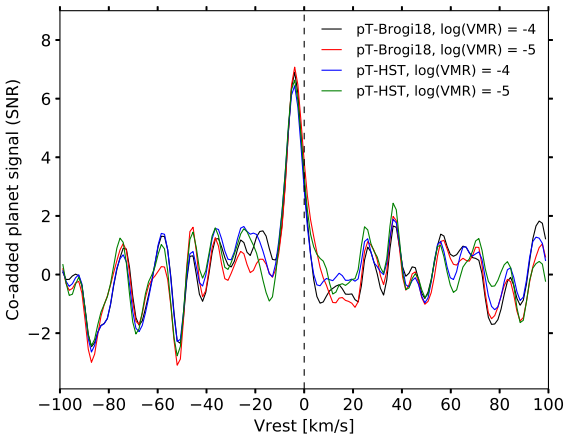

Figure 3: CCF, plotted as SNR, as a function of the planet rest frame velocity for all the models tested and for the maximum SNR-K_p pair. All models allow us to detect H_2O, but a degeneracy between p-T profiles and abundances is shown.

EPSC Abstracts
Vol. 12, EPSC2018-1008, 2018
European Planetary Science Congress 2018

The legacy of HST/WFC3: a prototype for future population studies of exoplanets

Angelos Tsiaras
UCL, London, UK, (angelos.tsiaras.14@ucl.ack.uk)

Abstract

Today, more that 3500 exoplanets have been detected and, despite the significant progress in the field of atmospheric characterisation in the last decade, we still have a limited understanding for a small number of planets. Similarly to the field of exoplanetary detection, atmospheric population studies are the way forward in constraining, which is the current condition of planets, how did they form, and how have they evolved. One of the most successful instruments for observing exoplanetary atmospheres is the *Wide Field Camera 3* (WFC3) on-board the *Hubble Space Telescope*. In particular, the use of the spatial scanning technique has given the opportunity for even more efficient observations of the brightest targets, achieving the necessary precision of 10 to 100 ppm to the flux of the star.

In this presentation, I will discuss the main characteristics of the WFC3/IR instrument, the process followed to develop an automatic analysis pipeline, and the lessons learnt from this process, focusing on the parallel development of both data analysis and simulation software. I will also present the result of this study: an extended catalogue of consistently analysed spectra from HST/WFC3 for cases ranging from super-Earth to Jupiter sizes, from warm to hot temperatures, from clear to cloudy atmospheres. The collective behaviour of these planets with respect to their atmospheric conditions, as well as exceptional cases, such as the super-Earths in the Trappist-1 and 55-Cancri systems will be discussed in more detail. Following a scalable approach is vital for observation planning and data processing in the future, as more dedicated instruments will provide a large number of observations.

EPSC Abstracts
Vol. 12, EPSC2018-1011, 2018
European Planetary Science Congress 2018

Validation of an exoplanetary atmospheric model for high resolution spectroscopy for remote sensing

Denis Shulyak (1), Miriam Rengel (1), Ansgar Reiners (2)
(1) Max Planck Institute for Solar System Research, Justus-von-Liebig-Weg 3, 37077 Göttingen (denis.shulyak@gmail.com)
(2) Institute for Astrophysics, Friedrich-Hund-Platz 1, 37077 Göttingen

Abstract

The discovery of first planets orbiting other stars opened a new era of (exo)planetary research with a potential to find many planets similar to our own home. Thanks to the great success of the *Kepler* mission, but also other photometric and spectroscopic surveys, we learned that there are many other planets that span a wide range of masses from several Jupiter masses to very small rocky Mercury-size objects. These exoplanets are expected to have very different chemical and physical structures, and studying their atmospheres provides an insight into origin, evolution, composition, temperature stratification, dynamics, and habitability. Present and future observing facilities will make it possible to address these important questions in more detail and will shape the exoplanetary science for decades to come. The aim of our work is to test theoretical models and approach against a model observations in near-infrared wavelengths at very high spectral resolution as provided by, e.g., soon expected CRIRES$^+$ instrument (ESO, Chile). We will apply available and develop a methodology to assess our ability for remote sensing of exoplanetary atmospheres from individual spectral features. We will also present suggestions for the improvements of existing models and analysis techniques in the framework of future observing facilities.

1. Introduction and objectives

Retrieval of atmospheric features from transmission and emission spectroscopy is a powerful method to constrain chemical and physical conditions in atmospheres of exoplanets. Using dedicated inversion techniques and predictions from forward models we can study a variety of physical phenomena originated in planetary atmospheres [1, 2]. Because of obvious limitations of modern instruments for exoplanet research in terms of efficiency, integration time, wavelength coverage, and sources of uncertainties, only a very small group of large planets in close-in orbits (known as hot-Jupiters) were accessible for observations. But already these limited observations were proven to bear an essential information about temperature-pressure atmospheric structure and composition of main absorbing species[3]. It is clear that future instruments and missions will allow us to detect and explore features from even smaller planets.

Until now, some available retrieval methods have been tested against low resolution observations. While providing obvious improvements in terms of, e.g., integration time needed to achieve a required signal-to-noise ratio, there are other physical processes that are difficult or impossible to capture with low resolution (atmospheric winds and circulations, abundances of trace gases, etc.). Therefore, our main goal here is to explore our ability to measure atmospheric properties of extrasolar planets from high-resolution observations. This work is grossly motivated (but not limited to) the soon available CRIRES$^+$ spectrograph mounted at the 8-m VLT telescope of the European South Observatory (ESO, Chile). CRIRES$^+$ will have unique characteristics essential for the exoplanetary research. In particular, it will be able to cover an entire near-infrared range between $0.93-5.3$ μm in only a few exposures and with very high resolving power of R$=$ $50\,000-100\,000$ essential to resolve individual spectral lines and track them simultaneously [4]. Also, it will have a polarimetric module that will open a whole new way to study morphology of planetary atmospheres via the analysis of the linear polarization originated from, e.g., the scattering on particles and condensates presented in, e.g., planetary clouds and hazes.

Thus we want to push the limits of present models and observing facilities to high spectral resolution. Future observation facilities will no doubt provide new, more accurate and robust information about planetary atmospheres, which will also help to better validate and improve our theoretical models.

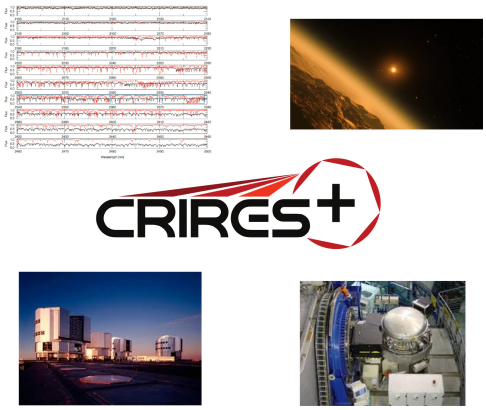

Figure 1: CRIRES$^+$ exoplanet research. Image credits: ESO.

2. Analysis methods

In our approach we combine both forward and inverse models. Exoplanet science has benefited tremendously from the decades of work on Solar System planets. We plan to adopt the retrieval technique based on optimal estimator and, e.g., dedicated radiative transfer model [5]. We adapt this model to the observations delivered by modern instruments that are used for exoplanet research. The essential part of our analysis is to predict the amount of information that we can derive by applying our algorithms to different sets of spectral lines. For instance, by studying CO lines at 2.3 μm and their time variability it is possible to constrain the global wind pattern in atmospheres of distant planets [6]. Similar, strong potassium lines in the H-band as well as the lines of molecules like, e.g., H_2O, HCN, NH_3, and CH_4 can be used to probe the atmospheric structure and composition, etc. We plan to investigate the limitations of modern approaches arising from the wavelength range and instrument's resolving power used, and address possible not yet included physics in our forward models. Our final result here is the list of suggestions and improvements that need to be done both in models and retrieval techniques essential for the future research with high resolution instruments.

3. Discussion

In spite of the current very fast progress in exoplanetary science from both theoretical and observation points of view, we still lack instruments capable of catching signatures from atmospheres of planet smaller than Jupiter size giants. Moreover, the spectroscopic observations are too sparse, often suffer from instrument systematics, low SNR, etc. However, future facilities will greatly improve towards better performance and wavelength coverage thus allowing us to address new questions about structure of exoplanetary atmospheres. Increasing the spectral resolution is a promising way to learn more detailed physics and test our models. There are many codes and tools designed for the retrieval and forward modelling of exoplanet atmosphere, but little attention has been paid so far to model individual spectral lines with an efforts in accurate predictions and at near-infrared domain. Because there are a number of new instruments coming to operation exactly at this wavelength range, we find it important to improve the model, make more accurate predictions, and apply our approach to real data.

Acknowledgements

This research is supported by the DFG priority program SPP 1992 "Exploring the Diversity of Extrasolar Planets"

References

[1] Gandhi, S., & Madhusudhan, N.: Retrieval of exoplanet emission spectra with HyDRA, MNRAS, 474, 271, 2018

[2] Waldmann, I. P., Tinetti, G., Rocchetto, M., et al.: TauREx I: A Next Generation Retrieval Code for Exoplanetary Atmospheres, ApJ, 802, 107, 2015

[3] Tinetti, G., Encrenaz, T., & Coustenis, A.: Spectroscopy of planetary atmospheres in our Galaxy, A&ARev, 21, 63, 2013

[4] Dorn, R. J., Anglada-Escude, G., Baade, D., et al.: CRIRES+: Exploring the Cold Universe at High Spectral Resolution, The Messenger, 156, 7, 2014

[5] Rengel, M., Hartogh, P., & Jarchow, C.: Mesospheric vertical thermal structure and winds on Venus from HHSMT CO spectral-line observations, P&SS, 56, 1368, 2008

[6] Snellen, I. A. G., de Kok, R. J., de Mooij, E. J. W., & Albrecht, S.: The orbital motion, absolute mass and high-altitude winds of exoplanet HD209458b, Nature, 465, 1049, 2010

EPSC Abstracts
Vol. 12, EPSC2018-1026-1, 2018
European Planetary Science Congress 2018

Global Chemistry and Thermal Structure Models for the Hot Jupiter WASP-43b and Predictions for JWST

Olivia Venot (1), Nicolas Crouzet (2,3), Ludmila Carone (4), Pascal Tremblin (5), Vivien Parmentier (6), Julianne Moses (7), Patricio Cubillos (8), Jasmina Blecic (9), Paul Mollière (10), Laura Kreidberg (11) and Kevin B. Stevenson (12)
(1) Laboratoire Interuniversitaire des Systèmes Atmosphériques, UMR CNRS 7583, Université Paris Est Créteil (UPEC) et Université Paris Diderot (UPD), Institut Pierre Simon Laplace (IPSL), Créteil, France (olivia.venot@lisa.u-pec.fr), (2) Instituto de Astrofísica de Canarias, C. Vía Láctea s/n, E-38205 La Laguna, Tenerife, Spain, (3) Universidad de La Laguna, Dept. de Astrofísica, E-38206 La Laguna, Tenerife, Spain, (4) Max Planck Institute for Astronomy, Koenigsstuhl 17, D-69117 Heidelberg, Germany, (5) Maison de la Simulation, CEA-CNRS-INRIA-UPS-UVSQ, USR 3441, Centre d'Étude de Saclay, 91191 Gif-Sur-Yvette, France, (6) Aix Marseille Univ, CNRS, CNES, LAM, Marseille, France, (7) Space Science Institute, Boulder, CO, USA, (8) Space Research Institute, Austrian Academy of Sciences, Schmiedlstr. 6, 8042, Graz, Austria, (9) NYU Abu Dhabi, Abu Dhabi, UAE, (10) Leiden Observatory, Leiden University, Postbus 9513, 2300 RA Leiden, The Netherlands, (11) Harvard-Smithsonian Center for Astrophysics, 60 Garden Street, Cambridge, MA 02138, USA, (12) Space Telescope Science Institute, Baltimore, MD, 21218, USA

Abstract

With its broad wavelength coverage (visible to mid-infrared) and high sensitivity of its instruments, the *James Webb Space Telescope* (JWST) is expected to revolutionise the field of exoplanet characterization. In order that the scientific community rapidly learns how to benefit from the full science potential of the telescope, the STScI developed the Director's Discretionary Early Release Science program (ERS). All the data acquired during this program will immediately be in open access.
In response to this call, the Transiting Exoplanet Community, gathering researchers who are leaders in exoplanet studies and experts for the JWST instruments, proposed an ERS program [1] to test all the instruments of the JWST in different available modes while observing three exoplanets targets, one of which is WASP-43b [2].

We will observe a full phase curve of WASP-43b using MIRI/LRS (5-12 μm). WASP-43b is a target of prime interest: despite it is one of the best-characterised transiting exoplanets, many questions remain uncertain concerning the atmospheric circulation and the longitudinal variation of chemical composition and cloud coverage [3, 4, 5]. The full-orbit phase curve of WASP-43b obtained in this ERS program will greatly improve our understanding of this planet.

To support this proposal and prepare the future observations of this planet, an important modelling work has been carried out using various 1D, 2D, and/or 3D tools: radiative transfer models, chemical models, forward models, JWST data simulator, retrieval models [6].

We will review the scientific objectives of this work, the results we obtained, and the information we expect to learn from the future JWST observations.

References

[1] Batalha, N. M., Bean, J., Stevenson, K., Sing, D., Crossfield, I., Knutson, H. et al.: The Transiting Exoplanet Community Early Release Science Program for JWST, American Astronomical Society Meeting Abstracts, Vol. 231, 2018.

[2] Bean, J. L., Stevenson, K. B., Batalha, N. M., Berta-Thompson, Z., Kreidberg, L., Crouzet, N. et al.: The Transiting Exoplanet Community Early Release Science Program for JWST, arXiv preprint arXiv:1803.04985, 2018.

[3] Stevenson, K. B., Désert, J. M., Line, M. R., Bean, J. L., Fortney, J. J., Showman, A. P., et al.: Thermal structure of an exoplanet atmosphere from phase-resolved emission spectroscopy. Science, 1256758, 2014.

[4] Stevenson, K. B., Line, M. R., Bean, J. L., Désert, J. M., Fortney, J. J., Showman, A. P., et al.: Spitzer phase curve constraints for WASP-43b at 3.6 and 4.5 μm. The Astronomical Journal, 153(2), 68, 2017.

[5] Kataria, T., Showman, A. P., Fortney, J. J., Stevenson, K. B., Line, M. R., Kreidberg, L.,et al.: The atmospheric circulation of the hot jupiter WASP-43b: Comparing three-dimensional models to spectrophotometric data. The Astrophysical Journal, 801(2), 86, 2015.

[6] Venot, O., Carone, L., Crouzet, N., Tremblin, P., Parmentier, V., Moses et al.: Global Chemistry and Thermal Structure Models for the Hot Jupiter WASP-43b and Predictions for JWST. in prep.

EPSC Abstracts
Vol. 12, EPSC2018-1083, 2018
European Planetary Science Congress 2018

Atmospheric Characterisation of Exoplanets with Broadband Color Filters on the PLATO 2.0 Mission

John Lee Grenfell (1), Mareike Godolt (2), Juan Cabrera (1), Ludmila Carone (3), Antonio Garcia Munoz (2), Daniel Kitzmann (4) and Heike Rauer (1)

(1) Dept. Extrasolar Planets and Atmospheres (EPA), Inst. Planetary Research, German Aerospace Centre (DLR), Berlin, Germany (lee.grenfell@dlr.de)

(2) Centre for Astronomy and Astrophysics (ZAA), Berlin Inst. Technology (TUB), Berlin, Germany

(3) Max Planck Inst. for Astronomy, Heidelberg, Germany

(4) Centre for Space and Habitability (CSH), Uni. Bern, Switzerland

Abstract

We assess broadband color filters for the two fast cameras on the PLATO 2.0 space mission with respect to atmospheric characterization via Rayleigh absorption, haze and geometric albedo on Hot Jupiters and Low Mass Low Density planets for different atmospheric composition and cloud scenarios for planets placed at 25pc and 100pc.

EPSC Abstracts
Vol. 12, EPSC2018-1115-2, 2018
European Planetary Science Congress 2018

Ultra-short Period Rocky Super-Earths

Luca Malavolta (1,2) , Andrew W. Mayo (3,4) , Tom Louden (5) , Vinesh M. Rajpaul (6) , Aldo S. Bonomo (7) , Lars A. Buchhave (4) , Laura Kreidberg (3,8) , Martti H. Kristiansen (9,10), Mercedes Lopez-Morales (3) , Annelies Mortier (11) , Andrew Vanderburg (3,12) , Adrien Coffinet (13), David Ehrenreich (13) , Christophe Lovis (13), Francois Bouchy (13), David Charbonneau (3) , David R. Ciardi (14), Andrew Collier Cameron (11) , Rosario Cosentino (15), Ian J. M. Crossfield (16,17), Mario Damasso (7) , Courtney D. Dressing (18) , Xavier Dumusque(13) , Mark E. Everett (19) , Pedro Figueira (20), Aldo F. M. Fiorenzano (15), Erica J. Gonzales (16,28), Raphaëlle D. Haywood (3,27) , Avet Harutyunyan (15), Lea Hirsch (18) , Steve B. Howell (21) , John Asher Johnson (3) , David W. Latham (3) , Eric Lopez (22), Michel Mayor (13), Giusi Micela (23), Emilio Molinari (15,24) , Valerio Nascimbeni (1,2) , Francesco Pepe (13), David F. Phillips (3) , Giampaolo Piotto (1,2) , Ken Rice (25), Dimitar Sasselov (3) , Damien Ségransan (13) , Alessandro Sozzetti (7) , Stéphane Udry (13), and Chris Watson (26)
(1) Dipartimento di Fisica e Astronomia “Galileo Galilei,” Università di Padova, Italy (luca.malavolta@unipd.it) (2) INAF—Osservatorio Astronomico di Padova, Italy (3) Harvard-Smithsonian Center for Astrophysics, USA (4) Centre for Star and Planet Formation, Denmark (5) Department of Physics, University of Warwick, UK (6) University of Cambridge, UK (7) INAF—Osservatorio Astrofisico di Torino, Italy (8) The Harvard Society of Fellows, USA (9) DTU Space, National Space Institute, Denmark (10) Brorfelde Observatory, Denmark (11) Centre for Exoplanet Science, SUPA, UK (12) Department of Astronomy, The University of Texas at Austin, USA (13) Observatoire Astronomique de l’Université de Genève, Switzerland (14) Caltech/IPAC-NExScI, USA (15) INAF—Fundación Galileo Galilei, Spain (16) Department of Astronomy and Astrophysics, University of California (17) Department of Physics, Massachusetts Institute of Technology, USA (18) Astronomy Department, University of California Berkeley, USA (19) National Optical Astronomy Observatory, USA (20) Instituto de Astrofísica e Ciências do Espaço, Universidade do Porto, Portugal (21) NASA Ames Research Center, USA (22) NASA Goddard Space Flight Center, USA (23) INAF—Osservatorio Astronomico di Palermo, Italy (24) INAF—Osservatorio Astronomico di Cagliari, Italy (25) SUPA, Institute for Astronomy, UK (26) Astrophysics Research Centre, Queen’s University Belfast, UK

Abstract

Ultra-short period (USP) planets are a class of low-mass planets with periods shorter than one day and radii smaller than 2 R_E. An early hypothesis suggested that USP planets and small planets in general were originally Hot Jupiters (HJs) that underwent strong photo-evaporation due to the high insolation flux, (e.g., thousands of times that of Earth, Lecavelier des Etangs et al. 2004) ending up with the complete removal of their gaseous envelope and their solid core exposed. Recent studies determined that the metallicity distributions of HJs and USP planets are significantly different, supporting instead a similar hypothesis in which the progenitors of USP planets are not the HJs but the so-called mini-Neptunes, i.e., planets with rocky cores and hydrogen–helium envelopes, typically with radii between 1.7 and 3.9 R_E and masses lower than ~10 M_E. Alternatively, USP planets may represent the short-period tail of the distribution of close-in rocky planets migrated inwards from more distant orbits (e.g., Lee & Chiang 2017) or formed in situ (e.g., Chiang & Laughlin 2013). It appears clear that only a systematic study of the internal and atmospheric composition of USP planets, in conjunction with the amount of irradiation to which they are subjected and the presence of other companions in the system, can shed light on their origin. In order to do so, we need precise and accurate measurements of both their radius and mass.

So far only a handful of USP planets have reliable density estimates, and only for two of them have the secondary eclipse and phase variations have been detected, namely Kepler-10b (Batalha et al. 2011) and Kepler-78b (Sanchis-Ojeda et al. 2013). Formation scenarios differ radically in the predicted composition of USP planets, and it is therefore extremely important to increase the still limited sample of USP planets with precise and accurate mass and density measurements.

We report here the characterization of a USP planet with a period of 0.28 days around K2-141 (EPIC 246393474), and the validation of an outer planet with a period of 7.7 days in a grazing transit configuration. We derived the radii of the planets from the K2 light curve and used high-precision radial velocities gathered with the HARPS-N spectrograph for mass measurements. For K2-141b, we thus inferred a radius of 1.51 ± 0.05 R_E and a mass of 5.08 ± 0.41 M_E, consistent with a rocky composition and lack of a thick atmosphere. We also report the detection of secondary eclipses and phase curve variations for K2-141b. The phase variation can be modeled either by a planet with a geometric albedo of 0.30 ± 0.06 in the Kepler bandpass, or by thermal emission from the surface of the planet at ~3000 K. Follow-up observations at longer wavelengths will allow us to distinguish between these two scenarios. If USP planets were really lava-ocean worlds, their atmospheres would be likely made of heavy-element vapors with a very low pressure and, being tidally locked, would experience extremely high day-night contrasts (Léger et al. 2011). The discovery of an outer planet with a period of 7.7 days in a grazing transit configuration, K2-141c, corroborates the previously observed trend that USP planets are often found in multi-planet systems (Sanchis-Ojeda et al. 2014).

We conclude discussing future perspectives in USP planet detection with *TESS* and *PLATO* and the characterization of their atmosphere and surface properties with the *CHEOPS*, the *Hubble Space Telescope* and the *James Webb Space Telescope*

1. Figures

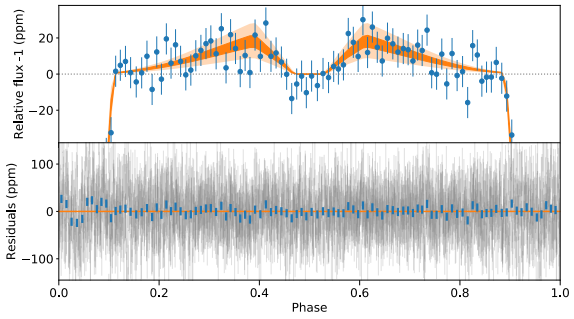

Figure 1: *Top*: The detrended data phase-folded on the period of planet b with the transits of planet c removed, the data have been binned by a factor of thirty for clarity. The 1 and 3 σ credible intervals calculated from the posterior are overplotted in dark and light orange respectively. *Bottom*: The residuals to the best fitting model, the binned data are plotted as thick blue lines and the unbinned data is plotted as thin grey lines.

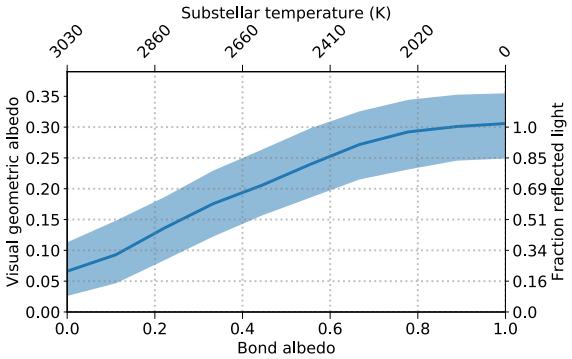

Figure 1: The best fitting visual geometric albedo as a function of the Bond albedo. The shaded area is the 68% credible region for the geometric albedo. The corresponding substellar temperature for the planet is plotted on the top axis, and the fraction of the occultation depth from the reflected light alone is calculated using the best fitting Bond albedo for the corresponding visual albedo.

EPSC Abstracts
Vol. 12, EPSC2018-1149, 2018
European Planetary Science Congress 2018

On the exospheres of the rocky planets HD219134b and c

H. Lichtenegger (1), A. Vidotto (2), L. Fossati (1), C. P. Folsom (3), B. E. Wood (4), E. Alecian (5), P. E. Cubillos (1), V. Girish (6), J. Murthy (7), P. Petit (3), A. G. Sreejith (1), and G. Valyavin (8)
(1) Space Research Institute, Austrian Academy of Sciences, Schmiedlstrasse 6, A-8042 Graz, Austria, (2) School of Physics, Trinity College Dublin, the University of Dublin, Dublin-2, Ireland, (3) Universit_e de Toulouse, UPS-OMP, IRAP, F-31400 Toulouse, France, (4) Naval Research Laboratory, Space Science Division, Washington, DC 20375, USA, (5) Universit_e Grenoble Alpes, IPAG, 38000, Grenoble, France, (6) Space Astronomy Group, ISRO Satellite Centre, Airport Road Bangalore, 560017 India, (7) Indian Institute of Astrophysics, Bangalore 560 034, India, (8) Special Astrophysical Observatory, Laboratory of Stellar Magnetism, Nizhnii Arkhyz, Karachai-Cherkessian Republic, 369167, Russia

Abstract

We simulate the formation of exospheres around the rocky planets HD219134 b and c. The exospheres are formed by surface particles that have been sputtered by the wind of the host star. The stellar wind properties are derived from 3D simulations driven by observationally-derived stellar magnetic field maps; our simulations are con strained by Ly-α observations of wind mass-loss rates. The interaction between the wind particles and the planets' crust makes the surfaces of planets b and c sputter, similarly to what occurs at Mercury. Due to the proximity of the planets to their host stars and, therefore, the high kinetic energy of the incident stellar wind particles, the sputtering process is sufficiently energetic to build up relatively dense metal-rich exospheres. We show that sputtering is expected to release refractory elements from the dayside surface of the planet, with elements such as oxygen and magnesium creating an extended neutral exosphere with densities larger than 10 cm^{-3}, within several planetary radii. By integrating the particle densities along the line-of-sight, we derive column densities of up to $\sim 10^{14}$ cm^{-2} for O and $\sim 10^{13}$ cm^{-2} for Mg, with higher column densities found ahead of the orbital motion of planets b and c.

1. Introduction

For planets similar to Mercury (i.e., weakly-magnetised and without a thick atmosphere), the stellar wind interacts directly with either their atmosphere or solid surface. Although lacking a substantial atmosphere, bodies like Mercury may hold a tenuous (i.e., non-collisional) gaseous envelope, forming their exospheres. This exosphere is made up of particles sputtered from the surface by precipitating solar wind protons and following ballistic orbits around the planet. Photoionisation of these neutral particles creates an ion population in addition to the ions directly ejected from the surface. Among the interaction processes, sputtering is considered to be the most energetic mechanism, leading to particles with energies of up to several hundreds of eV, distinctly exceeding the escape energies of many species at Earth-like planets. In this work, we start from the assumption that both planets have lost their CO2-dominated atmosphere and do not host a significant magnetic field. We use state-of-the-art models of stellar wind and wind-induced sputtering to investigate the effects that the wind of HD219134 has on building up an exosphere on the two inner-most planets and how the wind interacts with it.

2. Discussion and Conlusion

Our stellar wind model is possibly the most well constrained to date after that of the Sun. We used observationally-derived maps of the stellar surface magnetic field for the inner boundary of our 3D wind model. Additionally, the mass-loss rate derived in our wind model is constrained by Ly-α observations of the stellar astrosphere. We then used the results of our stellar wind model to quantify surface sputtering for the two planets and estimate the density and structure of the planetary exospheres.

Our results can be summarised as follows. The large-scale magnetic field of the planet-hosting star HD219134 can be described as a dipole whose axis is roughly perpendicular to the stellar rotation axis. As a consequence, the stellar wind of HD219134 is highly non-axisymmetric, which implies that planets orbiting in the equatorial plane of the star interact with low and high speed winds in a very short timescale.

The simulations show that sputtering processes release refractory elements from the entire dayside surface with velocities sufficiently high to allow for elongated trajectories of the sputtered particles. In particular, we find that oxygen and magnesium are expected to form an extended neutral exosphere with densities larger than 10 cm^{-3}, within several planetary radii. Because of the close proximity of both planets to the host star, a substantial amount of the neutral atoms will quickly be ionised and picked up by the stellar wind. The simulations suggest the column density of oxygen to be on average up to $\sim 10^{13}$ cm^{-2} close to the day-side of planet b and an order of magnitude smaller for planet c. Further, the column densities are not symmetric, with enhanced densities ahead of the planets' orbits.

3. Equations

Below, you will find examples of two equations. You should use an equation editor of your word-processing program in order to include your equation(s). The equation number should be placed at the right side of the column and all equations should be consecutively numbered.

$$a^2 + b^2 = c^2 \quad (1)$$

$$E = m \cdot c^2 \quad (2)$$

4. Summary and Conclusions

After having finished your paper in your word-processing program, please create a respective pdf file out of the document. The correct page settings of 237 (height) x 180 (width) mm are included in the template document. **Please make sure that the generated pdf file actually has a page size of 237 x 180 mm.** This is the only way to guarantee the proper inclusion of your paper in the Copernicus Office database. Please note that you are asked to upload a pdf file during the abstract submission in Copernicus Office. No other file type than .pdf is accepted for the file upload. The actual citation header will be added automatically!

Acknowledgements

The Acknowledgements section should not be numbered. Here, you may include all persons or institutions which you would like to thank. We recommend that the abstract is carefully compiled and thoroughly checked, in particular with regard to the list of authors, **before** submission.

References

[1] Author, A., Author, B., and Author, C.: First example of a cited article title, First Example Journal, Vol. 1, pp. 1-100, 1999.

[2] Author, D. and Author, E.: Second example of a cited book, Example Publishing House, 2000.

[3] Author, F.: Third example of a cited conference paper, The Great Science Conference, 1–7 February 2001, Sciencetown, Sciencecountry, 2001.

EPSC Abstracts
Vol. 12, EPSC2018-1191, 2018
European Planetary Science Congress 2018

Transits in the Solar System and the Composition of the Exoplanet Atmospheres

Pauli Laine

University of Jyväskylä, Finland (pauli.e.laine@jyu.fi)

Abstract

Our knowledge about exoplanets depends on very limited measurements and resolution. Atmospheric compositions are limited only to hot Jupiters and Neptunes. Detection of possible biosignatures on Earth-sized planets is not possible today. However, upcoming space missions, e.g. TESS, JWST, CHEOPS, and PLATO will give us unprecedented access to exoplanet light curves and other observations. Before the new results arrive, it could be useful to collect the only known living planet's and other well-known planet's light curves and spectra for the future comparison and habitability modeling. For this, we need to seek possibilities to measure Earth's and other terrestrial planet's transits, occultations, and reflections from different locations in the Solar System. This paper will present some past events and experiments, potential locations and events, probes, and their instruments that could be used, as well some limitations and challenges.

1. Introduction

In a board view, there are three different worlds within the habitable zone of our Solar System: Venus, Earth and Mars. However, only Earth is capable of maintaining life as we know it. Our three terrestrial planets can reveal a lot of what makes planet habitable, and help us to distinguish habitable terrestrial exoplanet apart from e.g. exo-Venus with future observations.

Planetary transits are phenomena where planet appears to move across the disk of system's parent star. Transit method is the most used exoplanet detection method. For example the Kepler space telescope has discovered over 2800 confirmed exoplanets with transit method [1]. The dimming of star's light during the transit is called the light curve. From the photometric light curve, we can measure planet's size. On the other hand, the spectroscopic measurement of light curve can reveal atmospheric composition. However, transmission spectra are extremely weak.

2. Exoplanet Light Curves

Earth-size exoplanet has a very weak transit depth, magnitude in ppm scale (c.f. hot-Jupiters around 1%) and the atmospheric signal of exoplanet is even weaker ($\Delta\delta$ 0.1-1 ppm). Terrestrial planet transits in the Solar System have similar magnitude in atmospheric signal ($\Delta\delta$ 1-10 ppm, slightly bigger due to geometrical effect), which makes them interesting for exoplanet comparison.

With the transits of Venus, Earth and Mars we can mimic Earth-like exoplanet atmosphere detection and help habitability assessment. Moreover, detecting transits of our terrestrial planets serve as technique validation for future exoplanet detection missions.

3. Future Transits

There will be transits of all terrestrial planets in the near future. None of them will be visible from Earth, but could be observed from the outer Solar System, with some ongoing or planned planetary missions. These transits include transit of Earth from Jupiter in 2026, transit of Venus from Jupiter in 2024 and 2030 and from Mars in 2030 and 2032.

4. Spacecrafts

Cassini spacecraft ended its Saturn mission in 2017, and there currently no plans for new one. There will be transit of Venus from Jupiter in 2024, but NASA's Jupiter spacecraft Juno will end its primary mission in 2018. There is a hypothetical possibility of observing the transit of Earth in 2026 and the transit of Venus in 2030 with ESA's JUICE spacecraft (or Joint Europa Mission) on its way to Jupiter. According to ESA, the possibilities of observing these Earth transits in 2026 and the transit of Venus in 2030 from Jupiter will be looked at after the launch, and will be depending on the launch date (currently envisaged in 2022 or 2023), the cruise trajectory (7.6 years interplanetary transfer), and the instrument capabilities. There are several possible interplanetary trajectories for JUICE mission depending the launch date, and it now seems that the transit of Earth in 2026 is not favored in any of the them [2]. On the other hand, the transit of Venus in

November 2030 is favored with the 2022 launch window.

The transits of Venus from Mars in 2030 and 2032 are interesting since there are many current and planned Mars orbiters and rovers. If we put 15 years lifetime limit to orbiter and 10 years to rover, then potential instruments are in ESA's ExoMars Trace Gas Orbiter (TGO) (launched in March 2016) and NASA's Mars 2020 missions. However, at least TGO's camera would be destroyed if we pointed it directly to the Sun, since it has no filters for this.

5. Summary and Conclusions

Transits of the terrestrial planets in the Solar System can help us to identify habitable Earth-like exoplanets in the future. Transit spectrum of Venus has already been obtained. Earthshine and eclipses have been used to get Earth transit spectrum. Next potential transits are: Earth 2026 (Jupiter), Venus 2030 (Jupiter), Venus 2030 and 2032 (Mars).

Among the all currently operational and planned deep space missions, potentially only the transits of Venus in 2030 and 2032 could be observed. By those years, we should have more sensitive exoplanet observing space telescopes in the orbit. So, at least we should have good comparison between Venus and potential exo-Venuses.

Instead of looking for very limited spacecraft opportunities for transit observations, we could observe reflected sun light from planets with space-bound or earth-bound telescopes. This is similar technique as used for earthshine observations, where Sun's light, dimmed by transiting terrestrial planet, is reflected from the current viewpoint planet

Acknowledgements

Jay Pasachoff/Williams College, Cassini, Jorge Vago/ESA, ExoMars TGO, Olivier Witasse/ESA, JUICE.

References

[1] https://www.nasa.gov/kepler/discoveries.

[2] ESA: JUICE Red Book. JUpiter ICy moon explorer. Exploring the emergence of habitable worlds around gas giants. European Space Agency, 2014.

EPSC Abstracts
Vol. 12, EPSC2018-1199-2, 2018
European Planetary Science Congress 2018

Exogenic Volatiles in the Extended Exospheres of Extrasolar Giant Planets

Apurva V. Oza (1), Robert E. Johnson (2), Phil Arras (3), Nicolas Thomas (1), Carl Schmidt (4), Brice Olivier Demory (5), Christoph Mordasini (1), Aurelien Wyttenbach (6), Nick Schneider (7), Vincent Bourrier (6), David Ehrenreich (6), Romain Allart (6), David Dubois (8,9), Prabal Saxena (10)
(1) University of Bern, Physikalisches Institut, Switzerland (apurva.oza@space.unibe.ch) (2) University of Virginia, Department of Engineering Physics, USA (3) University of Virginia, Department of Astronomy, USA (4) Boston University, Center for Space Physics, USA (5) University of Bern, Center for Space and Habitability, Switzerland (6) University of Geneva, Geneva Observatory, Switzerland (7) University of Colorado at Boulder, Laboratory for Atmospheric & Space Physics, USA (8) University of Versailles Saint Quentin, LATMOS, France (9) California Institute of Technology, Jet Propulsion Laboratory, USA (10) NASA Goddard Space Flight Center

Abstract

Our understanding of the observations of volatiles in extrasolar giant planet (EGP) exospheres is quite incomplete at the present. The volatiles, water products, alkalis, or other trace gases detected in transmission spectra are assumed to emanate from the gas giant itself (endogenic) and are typically modeled using hydrostatic atmospheric escape models to fit observations. Here, we examine the possibility of an exogenic source, such as a stable, orbiting satellite [1,2], and its influence on the geometry and spectral line of the observed feature. The gas distribution then, rather than being spherically symmetric about the gas giant, can be influenced by transient clouds or rapidly rotating gas tori. By analogy, we present a simple geometrical model for EGPs with relatively long orbital periods able to host an active satellite capable of sourcing an extended exosphere on Gyr timescales. Our model takes into account possible source rates from such a putative satellite, and estimates optical depth and column density for expected species. Our analysis finds that the expected exogenic Na column densities can be of the same order of magnitude of Na observed at an EGP by high resolution spectrographs [3]. Moreover, we describe how to spectrally differentiate between an endogenic and an exogenic source.

References

[1] Johnson, R.E & Huggins, P. Toroidal Atmospheres Around Extrasolar Giant Planets. Publications of the Astronomical Society of the Pacific, 118: 1136–1143, 2006.

[2] Cassidy, T. et al. Massive Satellites of Close-in Gas Giant Exoplanets. The Astrophysical Journal, 704:1341–1348, 2009 October 20.

[3] Wyttenbach et al. Spectrally resolved detection of sodium in the atmosphere of HD189733b with the HARPS spectrograph. A&A 577, A62 (2015)

EPSC Abstracts
Vol. 12, EPSC2018-1204, 2018
European Planetary Science Congress 2018

The ExoMol project: progress and perspectives

Sergei N. Yurchenko, Jonathan Tennyson, Katy L. Chubb, Barry Mant, Phillip A. Coles, Alec Owens, Oleg N. Polyansky, Pawel Jagoda and the ExoMol Team
Department of Physics and Astronomy, University College London, Gower Street, London WC1E 6BT, UK
(s.yurchenko@ucl.ac.uk)

Abstract

The ExoMol project aims to provide molecular line lists for exoplanets and other atmosphere with a particular emphasis on those atmospheres which are significantly hotter than the Earth's. ExoMol has now computed line lists for about 40 molecules including, in most cases, isotopologues. These are available at WWW.EXOMOL.COM. Key new line lists include ones for H_3^+, NO, C_2H_4 and a significantly improved one for hot water, as well as for a range closed and open shell diatomic molecules.

The ExoMol database underwent a major reformat and upgrade in 2016; it now provides information on a variety of topics including, of course, line lists, cross sections (generated from the same line lists), lifetimes and Landé g-factors. It now comprises 52 molecules (130 isotopologues). Our new flexible code ExoCross can rapidly generate cross sections even from huge line lists. ExoCross also allows facile conversion between ExoMol and HITRAN formats.

1. ExoMol data 2018

The need for extensive, high temperature spectroscopic data on molecules, many of whom do not occur in the Earth's atmosphere, has led to a number of systematic efforts to generate the molecular line lists required [1]. In particular, a number of groups have been progressively generating line lists for key molecules. These includes the TheoReTS [2] group (Reims/Tomsk), the NASA Ames team and our own ExoMol activity based in University College London, all of which used similar theoretical procedures discussed below, and an experimental initiative led by Bernath [3]. These activities have been significantly enhanced by the discovery of exoplanets and the requirement of extensive line lists to be used in exoplanet models and characterization [4, 5].

The ExoMol database comprises line lists for 52 molecules (130 isotopologues). Table 1 summarises the molecules for which line lists have been provided as part of the ExoMol project. Sources for line lists of other key species are also provided, many based on line lists from Bernath and co-workers, see [6].

Table 1: Datasets created by the ExoMol project and included in the ExoMol database [7].

Paper	Molecule	$N_{\rm iso}$	$T_{\rm max}$	$N_{\rm elec}$	$N_{\rm lines}$	DSName
I	BeH	1	2000	1	16,400	Yadin
I	MgH	3	2000	1	10,354	Yadin
I	CaH	1	2000	1	15,278	Yadin
II	SiO	5	9000	1	254,675	EJBT
III	HCN/HNC	1	4000	1	399,000,000	Harris
IV	CH_4	1	1500	1	9,819,605,160	YT10to10
V	NaCl	2	3000	1	702,271	Barton
V	KCl	4	3000	1	1,326,765	Barton
VI	PN	2	5000	1	142,512	YYLT
VII	PH_3	1	1500	1	16,803,703,395	SAITY
VIII	H_2CO	1	1500	1	10,000,000,000	AYTY
IX	AlO	4	8000	3	4,945,580	ATP
X	NaH	2	7000	2	79,898	Rivlin
XI	HNO_3	1	500	1	6,722,136,109	AIJS
XII	CS	8	3000	1	548,312	JnK
XIII	CaO	1	5000	5	21,279,299	VBATHY
XIV	SO_2	1	2000	1	1,300,000,000	ExoAmes
XV	H_2O_2	1	1250	1	20,000,000,000	APTY
XIV	H_2S	1	2000	1	115,530,3730	AYT2
XV	SO_3	1	800	1	21,000,000,000	UYT2
XVI	VO	1	2000	13	277,131,624	VOMYT
XIX	$H_2{}^{17,18}O$	2	3000	1	519,461,789	HotWat78
XX	H_3^+	1	3000	1	11,500,000,000	MiZATeP
XXI	NO	6	5000	2	2,281,042	NOName
XXII	SiH_4	1	1200	1	62,690,449,078	OY2T
XXIII	PO	1	5000	1	2,096,289	POPS
XXIII	PS	1	5000	3	30,394,544	POPS
XXIV	SiH	4	5000	3	1,724,841	SiGHTLY
XXV	SiS	12	5000	1	91,715	UCTY
XXVI	HS	6	5000	1	219,463	SNaSH
XXVI	NS	6	5000	1	3,479,067	SNaSH
XXVII	C_2H_4	1	700	1	49,841,085,051	MaYTY
XXVIII	AlH	3	5000	3	40,000	AlHambra
XXIX	CH_3Cl	2	1200	1	166,279,593,333	OYT
XXX	$H_2{}^{16}O$	1	5000	1	1,500,000,000	POPKAZATEL
XXXI	C_2	3	5000	8	6,080,920	8State
XXXII	MgO	3	5000	4	22,579,054	LiPTY

$N_{\rm iso}$: Number of isotopologues considered; $T_{\rm max}$: Maximum temperature for which the line list is complete; $N_{\rm elec}$: Number of electronic states considered; $N_{\rm lines}$: Number of lines, value is for the main isotopologue; DSName: Name of line list and of data set in ExoMol database [7].

Data for all these species, including cross sections, are available on the ExoMol website. A comprehensive status review of the molecular line lists in the ExoMol database in a form of an atlas of opacities, illustrating their spectroscopic coverage, main spectroscopic signatures as well as temperature dependence of the molecular opacities relevant for atmospheric studies of hot exoplanets and stars can be found in [6].

Figure 1 presents an example of temperature-dependent cross sections for three isotopologues of water computed using ExoMol line lists. The opaci-

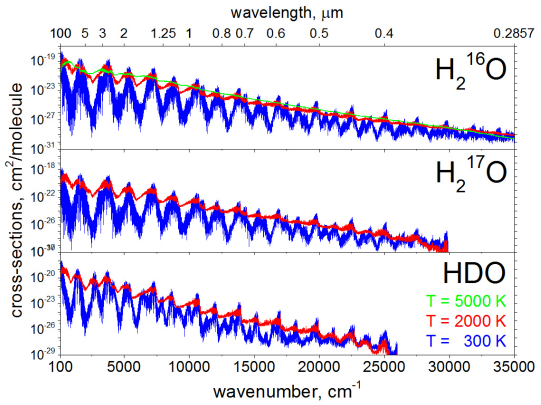

Figure 1: Cross sections for $H_2{}^{16}O$ from the POKAZATEL line list [9], $H_2{}^{17}O$ from the HotWat78 line list [10] and HDO from the VTT line list [11]. All cross sections are for 100% abundance, see [6].

ties are given for two reference temperatures, 300 K, 2000 K and 5000 K. For simplicity, we use a Doppler profile on a wavenumber grid of 1 cm^{-1}. A full atlas of ExoMol opacities can be found in [6]. The cross sections can be also obtained at higher resolutions (up to 0.01 $^{-1}$) using the cross sections App at www.exomol.com. The cross sections have been generated using the methodology by Hill et al. [8].

Compiling molecular opacity functions requires a large range of spectroscopic data on a large range of molecules. For many key species, there are now extensive line lists available that can be used to compute temperature-dependent opacity functions. This is a process of constant improvement and immediate improvements are indeed identified for several species discussed above. Recent observations have identified a whole new class of exoplanets with masses somewhat larger than the Earth's and orbits close to their host stars. These hot rocky super-Earths, lava planets or magma planets as they are variously known as are just beginning to be characterized [12], for which opacities are missing or incomplete [13].

Acknowledgements

The ExoMol project was funded by the ERC Advanced Investigator Project 267219 and is currently supported by UK STFC under grant ST/M001334/1, and has been supported under COST action MOLIM No. CM1405.

References

[1] J. Tennyson, S. N. Yurchenko, *Mon. Not. R. Astron. Soc.*, 2012, **425**, 21–33.

[2] M. Rey, A. V. Nikitin, Y. L. Babikov, V. G. Tyuterev, *J. Mol. Spectrosc.*, 2016, **327**, 138–158.

[3] P. F. Bernath, *Int. Rev. Phys. Chem.*, 2009, **28**, 681–709.

[4] G. Tinetti, A. Vidal-Madjar, M.-C. Liang, J.-P. Beaulieu, Y. Yung, S. Carey, R. J. Barber, J. Tennyson, I. Ribas, N. Allard, G. E. Ballester, D. K. Sing, F. Selsis, *Nature*, 2007, **448**, 169–171.

[5] G. Tinetti, T. Encrenaz, A. Coustenis, *Astron. Astrophys. Rev.*, 2013, **21**, 1–65.

[6] J. Tennyson, S. N. Yurchenko, *Atoms*, 2018, **6**, 26.

[7] J. Tennyson, S. N. Yurchenko, A. F. Al-Refaie, E. J. Barton, K. L. Chubb, P. A. Coles, S. Diamantopoulou, M. N. Gorman, C. Hill, A. Z. Lam, L. Lodi, L. K. McKemmish, Y. Na, A. Owens, O. L. Polyansky, T. Rivlin, C. Sousa-Silva, D. S. Underwood, A. Yachmenev, E. Zak, *J. Mol. Spectrosc.*, 2016, **327**, 73–94.

[8] C. Hill, S. N. Yurchenko, J. Tennyson, *Icarus*, 2013, **226**, 1673–1677.

[9] O. L. Polyansky, A. A. Kyuberis, N. F. Zobov, J. Tennyson, S. N. Yurchenko, L. Lodi, *Mon. Not. R. Astron. Soc.*, 2018.

[10] O. L. Polyansky, A. A. Kyuberis, L. Lodi, J. Tennyson, R. I. Ovsyannikov, N. Zobov, *Mon. Not. R. Astron. Soc.*, 2017, **466**, 1363–1371.

[11] B. A. Voronin, J. Tennyson, R. N. Tolchenov, A. A. Lugovskoy, S. N. Yurchenko, *Mon. Not. R. Astron. Soc.*, 2010, **402**, 492–496.

[12] A. Tsiaras, M. Rocchetto, I. P. Waldmann, G. Tinetti, R. Varley, G. Morello, E. J. Barton, S. N. Yurchenko, J. Tennyson, *Astrophys. J.*, 2016, **820**, 99.

[13] J. Tennyson, S. N. Yurchenko, *Mol. Astrophys.*, 2017, **8**, 1–18.

EPSC Abstracts
Vol. 12, EPSC2018-1217, 2018
European Planetary Science Congress 2018

A GIANO@TNG view of the atmosphere of transiting Hot Jupiters

Paolo Giacobbe, Aldo Bonomo, Alessandro Sozzetti, Gloria Guilluy and the GAPS team

(1)Astrophysical Observatory of Turin (INAF), Pino Torinese, ITALY (paolo.giacobbe@inaf.it)

Abstract

We present near-infrared transmission spectroscopy of a sample of transiting hot Jupiters with the GIANO spectrograph on the Telescopio Nazionale Galileo (TNG). GIANO offers the opportunity to probe at high spectral resolution the planet's atmosphere simultaneously over the Y-H-J-K bands, a 21-fold increase in wavelength coverage with respect to the existing studies, e.g. based on CRIRES data. We use the high-dispersion spectroscopy technique described in Brogi, Giacobbe et al. (2018 for the GIANO data and we carry out a cross-correlation analysis with different models of planetary spectra looking for the presence at high confidence of different molecular species. We discuss the prospects for detection of the individual contributions of the molecular species (e.g., water, methane, carbon dioxide, hydrogen cyanide) and for constraining the planet C/O ratio with the GIANO data, ultimately gauging the prospects for establishing GIANO among the leading instruments for characterizing exoplanet atmospheres.